

https://dspace.org/

Miniaturisation of an isothermal nucleic acid amplification system for HIV-1 viral load evaluation at point of care in low resource areas

Cunningham, Bradford Edwin

2012-02-01
http://hdl.handle.net/10539/11232

Downloaded from a DSpace repository. https://dspace.org/

Miniaturisation of an Isothermal Nucleic Acid Amplification System for HIV-1 Viral Load Evaluation at Point of Care in Low Resource Areas

Bradford Edwin Cunningham

A dissertation submitted to the Faculty of Engineering and the Built Environment, University of the Witwatersrand, Johannesburg, in fulfilment of the requirements for the degree of Master of Science in Engineering.

Johannesburg, 2011

Contents

1. INTRODUCTION 10
   1.1 Collaborators 11
   1.2 Scope 12
   1.3 Methodology 12
      1.3.1 Thermal Controller 12
      1.3.2 Evaluation of PDMS 13
      1.3.3 Objectives and impact 13
      1.3.4 Factors influencing results 14
   1.4 Introduction to the Document 14
      1.4.1 Chapter 1 – Introduction 14
      1.4.2 Chapter 2 – Viral Load Testing 15
      1.4.3 Chapter 3 – Introduction to Microfluidics 15
      1.4.4 Chapter 4 – Temperature Controller and Transducer 15
      1.4.5 Chapter 5 – Miniaturized Nucleic Acid Amplification System 15
      1.4.6 Chapter 6 – Thermal Characterization of PDMS 15
      1.4.7 Chapter 7 – Thermal Controller 15
      1.4.8 Chapter 8 – Thermal Simulations 15
      1.4.9 Chapter 9 – Results 16
      1.4.10 Chapter 10 – Future Recommendations 16
      1.4.11 Chapter 11 – Conclusion 16
2. VIRAL LOAD TESTING 17
   2.1 DNA Amplification 18
      2.1.1 Traditional PCR 19
      2.1.2 DNA Amplification 19
   2.2 Lab on a Chip and micro-Total Analysis Systems 21
   2.3 Continuous Flow Systems 22
      2.3.1 Channel Blockage 23
      2.3.2 Protein Fouling 23
   2.4 Isothermal Nucleic Acid Amplification System 24
   2.5 Advantages of a Miniaturized System 24
   2.6 POC Device Functional Requirements 25

2.7 NucliSENS EasyQ HIV-1 v2.0 26
3. MICROFLUIDICS 27
3.1 Overview of PDMS 28
3.2 Protein fouling 28
3.2.1 Effects of Protein Fouling 28
3.2.2 Minimization of Protein Fouling 29
3.2.3 Contact Angle 29
3.2.4 Sample Bubbling 30
3.3 Microfluidic Chip Design 30
3.3.1 Construction of the Microfluidic Amplification Chamber 30
3.3.2 Reaction Chamber 31
3.3.3 Glass vs PDMS 31
3.4 µTAS Design Beginnings 32
3.4.1 Fabrication of the Device 33
3.4.2 Design Constraints 35
3.4.3 Temperature Sensors 36
3.4.4 Pneumatic Valves (Sieve Valves) 36
3.4.5 Effects of Laminar Flow 37
3.4.6 Mixing Fluids 38
3.4.7 Non-Uniform Chamber Fill 39
3.4.8 Detection Chamber/Channel 41
3.4.9 Evaluation of µTAS Chip 41
4. TEMPERATURE CONTROLLER AND TRANSDUCER 43
4.1 Selected Hardware 44
4.1.1 PIC18F452 Microprocessor 44
4.1.2 Thermocouple Transducer 45
4.1.3 Thermocouple Amplifier 45
4.2 Development Criteria 46
4.3 Implemented Solution 46
4.3.1 PCB Breakdown 47
4.4 DC Bus Noise Minimization 48
4.5 Capacitive Decoupling 49
4.5.1 Noise Reduction using Discrete Component Decoupling 49
4.5.2 Choosing the Decoupling Capacitor 49

4.5.3 Guidelines for Placing Decoupling Capacitors 49
4.5.4 Determining the Decoupling Capacitor Value 50
4.5.5 Embedded Capacitance Decoupling 51
4.6 DC-Bus Impedance and Noise Relationship 51
4.7 Reducing Noise Using Power Islands 51
4.8 Separating Ground Planes 52
4.9 Low-Pass Filter Implementation 54
4.10 Noise Characterization of Developed PCB 55
4.10.1 Methodology: Characterizing the DC Bus 55
4.10.2 Equivalent Circuit Model 55
4.10.3 Connecting the Function Generator to the IC Power 56
4.10.4 Essential Equations 56
4.10.5 Calculating the path inductance 56
4.10.6 Calculating the path capacitance 58
4.10.7 Calculating the path impedance 59
4.11 DC-BUS Characterization Results 59
4.11.1 Measurement of the path Inductance 59
4.11.2 Measurement of the Impedance 61
4.11.3 Measurement of the path Capacitance 61
4.11.4 Evaluation 62
4.11.5 PICDEM2 Plus 63
4.11.6 Custom Developed Temperature Sensing Board 64
4.11.7 Conclusion 64
5. MINIATURIZED NUCLEIC ACID AMPLIFICATION SYSTEM 66
5.1 System Overview 67
5.1.1 Temperature Sensors 68
5.1.2 A/D Converters 68
5.1.3 Control Algorithm 68
5.1.4 PWM Control 69
5.1.5 Peltier Heating / Cooling 69
5.1.6 RS-232 Interface 69
5.2 System Calibration 69
5.2.1 Calibration Procedure 69
5.2.2 Calibration Results 70

5.2.3 Thermal Drift Errors 71
5.3 Performance Evaluation and Conclusion 73
6. THERMAL CHARACTERIZATION OF PDMS 74
6.1 PCR and Microfluidics 75
6.2 Background to Thermal Conduction and Conductivity 76
6.2.1 Thermal Conductivity of Materials 76
6.2.2 Thermal Conduction 76
6.2.3 Heat Transfer Coefficient 77
6.2.4 Heat Power Calculation 78
6.2.5 Biot Number 79
6.3 Calculations and Methodology 79
6.3.1 Thermal Conductivity 80
6.3.2 Thermal Impedance 81
6.3.3 Heat Transfer Coefficient 81
6.3.4 Biot Number 81
6.4 Conclusion 82
7. THERMAL CONTROLLER 83
7.1 Switching Circuit 84
7.1.1 H-Bridge Implementation 84
7.1.2 Functional Overview of H-Bridge 85
7.2 Controller Design 86
7.2.1 Hysteresis Control Algorithm 86
7.2.2 Proportional Control Algorithm 87
7.2.3 Proportional and Integral Control Algorithm 88
7.3 Implementation 89
7.3.1 Simple Hysteresis 89
7.3.2 Proportional Control 91
7.3.3 Proportional and Integral Control 91
7.4 Evaluation and Assumptions 92
7.5 Conclusion 93
8. THERMAL SIMULATIONS 95
8.1 Finite Difference Model Glass-PDMS 96
8.2 Thermal Profile Simulations 96
8.2.1 Thermal Profile – Top View 96

8.2.2 Thermal Profile – Lateral View 98
8.3 Thermal Contours and Cross Sections 99
8.3.1 Thermal Cross Section – Glass Face 100
8.3.2 Thermal Contour – Glass Face 100
8.3.3 Thermal Contour - Lateral Cross Section 101
8.3.4 Thermal Contour – The Reaction Chamber 102
8.4 Conclusion 103
9. RESULTS 104
9.1 Evaporation 105
9.1.1 Initial Quantitative Evaluation 105
9.1.2 Factors Affecting Evaporative Rates 105
9.1.3 Flow Rate of Air 106
9.1.4 Pressure within the Chamber 106
9.1.5 Surface Area of the Fluid within the Chamber 106
9.1.6 Temperature of the Fluid 106
9.2 Evaporation Testing 106
9.2.1 Evaporative Evaluation 107
9.2.2 Design Alternatives to Prevent Evaporation 108
9.2.3 Hot Lids 109
9.2.4 PCR Mineral Oil 109
9.2.5 Dilution of Contents 109
9.3 Implemented Evaporative Solution 109
9.3.1 Evaporative Evaluation – Maximum Capacity 110
9.3.2 Evaporation Testing – PCR Buffer 111
9.4 Final Test 112
10. FUTURE RECOMMENDATIONS 114
10.1 Reaction Chamber Dimensions 115
10.2 ..... TAS Prototype 115
10.3 Evaluation of Isothermal Assay 115
10.4 PCB Developments 115
10.5 Fluorescent Detection Incorporation 116
11. CONCLUSION 117
12. Acknowledgements 120

13. References 121

Figure 1 - DNA Amplification 19
Figure 2 - PCR Mathematical Simulation 21
Figure 3 - Continuous Flow Systems 22
Figure 4 - Temperature Ramp Cycle 23
Figure 5 - POC Device Stages 25
Figure 6 - Droplet Contact Angle 30
Figure 7 - Single Chamber Microfluidic Prototype 31
Figure 8 - µTAS Prototype Schematic 33
Figure 9 - Microfluidic Pneumatic Actuation 33
Figure 10 - Substrate Development Process 34
Figure 11 - 3 Layer Substrate Casting 35
Figure 12 - Reaction Chamber Support Structures 36
Figure 13 - Push Up/Down Valves 37
Figure 14 - Laminar Flow Demonstration 38
Figure 15 - Tesla Mixer Implementation 38
Figure 16 - Confocal Laser Scan of Tesla Mixer 39
Figure 17 - Non-Uniform Chamber Fill 40
Figure 18 - Maximum Chamber Capacity 40
Figure 19 - Immobilized Surface Capture Probes 41
Figure 20 - Low Noise PCB Development 47
Figure 21- CMOS Model 50
Figure 22 - Ground bridge loop currents 52
Figure 23 - PCB with power bus (bright yellow), ground plane (blue) and return current paths (red) 53
Figure 24 - Altered PCB with power bus (bright yellow), ground plane (blue) and return current paths (red) 54
Figure 25 - RC Filter 54
Figure 26 - Equivalent RLC Bus Model 55
Figure 27 - Current Source Waveform 56
Figure 28 - Expected voltage waveform showing inductive spikes 57
Figure 29 - Measurement connection taken as close the to the surface of the pins as possible 58
Figure 30 - Gradient of the voltage waveform 58
Figure 31 - Voltage level shift indicative of bus resistance 59
Figure 32 - Current waveform rise time and gradient 60
Figure 33 - Inductive voltage spike 60
Figure 34 - Level shift in voltages 61
Figure 35 - Gradient of the voltage waveform (4kHz) 61
Figure 36 - PICDEM2 Plus - Recorded Voltages 63
Figure 37 – Custom Developed PCB – Recorded Voltages 64
Figure 38 - System Flow Diagram 67
Figure 39 - Sensor Calibration Performance 70
Figure 40 – Adapted from Analogue Devices Datasheet (AD595C) 72

Figure 41 - Measurement Drift Experiment 72
Figure 42 - Temperature Drift Evaluation 73
Figure 43 - Example of a continuous flow (CF) microfluidic PCR design 75
Figure 44 - Application of Fourier's Law 77
Figure 45 - Measuring the thermal conductivity 78
Figure 46 - Experimental Setup for Conductivity Verification 79
Figure 47 - H Bridge Implementation 85
Figure 48 - Thermal Plant to be Controlled 86
Figure 49 - ON/OFF Algorithm with a set point of 50°C 90
Figure 50 - Proportional Control Algorithm 91
Figure 51 - Proportional and Integral Control Algorithm 92
Figure 52 - Thermal Profile, Top View 97
Figure 53 - Thermal Profile, Top View (increased) 98
Figure 54 - Thermal Profile, Lateral View 99
Figure 55 - Cross Sectional Thermal Gradient 100
Figure 56 - Slice Angle 100
Figure 57 - Thermal Contour - Glass Face 101
Figure 58 - Slice View. Cross Section 101
Figure 59 - Cross Sectional Thermal Contour 102
Figure 60 - Cross Sectional Gradient and Contour 103
Figure 61 - Evaporative Evaluation - Non-Uniform Chamber Fill 107
Figure 62 - Evaporative Evaluation - Air Pockets 108
Figure 63 - Evaporative Evaluation - Condensation 108
Figure 64 - Evaporative Evaluation - Maximum Capacity 110
Figure 65 - Evaporative Evaluation - Maximum Capacity, Condensation 110
Figure 66 - Evaporative Equilibrium - Maximum Capacity, 4 Hours 111
Figure 67 - Evaporative Evaluation; (a) 80µl of Water, (b) 80µl of PCR buffer 111
Figure 68 - Extracted PCR Buffer 112
Figure 69 - Roche Light Cycler Test Result 113
Figure 70 - Liposome Based detection 116

ABSTRACT

The purpose of this project is the design and evaluation of a miniaturized isothermal nucleic acid amplification system making use of readily-available and affordable technologies in order to amplify a given vRNA (viral-RNA) sample to detectable levels. The developed solution made use of low cost, simple thermocouple transducers along with a custom developed PCB which, when calibrated, was found to have a tolerance within 1°C, which is required for most nucleic acid based platforms. A PI controller was found to be sufficient to maintain the reagents in the developed microfluidic cassettes to the desired temperature. The nucleic acid amplification system chosen was the bioMerieux NucliSENS EasyQ HIV-1 v2.0 (bioMerieux, Lyon, France) since this was an isothermal amplification system with built in FRET (Fluorescence Resonance Energy Transfer) probe fluorescence capabilities combining both amplification and detection. This assay, however, was found to be unreliable with null results on all but one test limiting the evaluation of the developed microfluidic and temperature controller performances.

Table of Abbreviations

Abbreviation	Meaning
µTAS	micro Total Analysis System
A/D	Analogue to Digital
CMOS	Complementary Metal-Oxide Semiconductor
CSIR	Council for Scientific and Industrial Research
DC	Direct Current
DNA	Deoxyribonucleic Acid
HAART	Highly Active Anti-Retroviral Treatment
HIV	Human Immunodeficiency Virus
PCB	Printed Circuit Board
PCR	Polymerase Chain Reaction
PDMS	Polydimethylsiloxane
POC	Point of Care
RC	Resistor-Capacitor
RLC	Resistor-Inductor-Capacitor
RNA	Ribonucleic Acid
RT-LDA	Reverse Transcriptase Lood Dependent Amplification
SNR	Signal to Noise Ratio
ssDNA	single-stranded DNA
vRNA	viral-RNA

1. INTRODUCTION

Viral load medical equipment used for the detection of HIV-1 RNA viral loads exists and several are currently licensed by international bodies such as the US FDA (Food and Drug Administration). The main issue to be addressed with these systems is that they are highly resource intensive [1]. Not only do they require highly trained personnel spending many man-hours processing the assays, but the equipment itself is highly expensive. Even if the issue of equipment cost could be addressed and personnel trained to acceptable levels, these devices also need accurately controlled temperatures and stable conditions such as electricity and cooling which introduces a challenge into implementing these devices in low resource areas where the availability of these resources is unpredictable at best.

Regional facilities are available to the public whereby the complicated and sensitive processing can be done and even though this is highly beneficial, it is far from ideal. Regional clinics are often situated great distances from the very patients they are treating. The patients do not have readily available transportation (in general) which decreases the number of return (follow up) visits to a clinic a patient can make, coupled with the fact that tests may take weeks to be processed simply due to the processing time and sheer volume of patients, often results in patient data being lost, patients not returning for their results or even patients receiving results at a point where their conditions have significantly changed. This situation brings about the need for a more effective solution to provide adequate monitoring facilities to patients receiving treatment in low resource areas so that they are not kept on failing treatments to the point whereby drug resistance is accumulated or switched to different regimens too soon.

The detection of HIV has a very important and distinct window period (3-6 weeks) which is the time from initial infection until the time the body produces sufficient antibodies which can be detected. One of the advantages of implementing a system based on nucleic acid techniques is that the virus can be detected in these early stages (the window period) so that adequate treatment and medical care can be organised and initiated as early as possible. This is not only advantageous to adults infected with HIV but also in early infant diagnosis which can typically be done within days of birth by confirmed, repeated detections of HIV-1 DNA [1].

The main hindrance at this point in time is the complexity and cost of nucleic acid tests - which is the fundamental basis of all Polymerase Chain Reaction (PCR) testing and analysis procedures as discussed in *Chapter 2*. There are a few POC prototype assays which make use of PCR technology and concepts but have yet to receive FDA approval and a limited number of papers have been published describing their possible POC applications [1]. These key factors are recognized by the WHO (World Health Organisation) who strongly encourage the development of this technology alongside a large drive in the medical industry detailing the need for early diagnosis in infancy which is key in both treatment and prevention of the HIV/AIDS pandemic. The WHO outlines the ideal guide to clinical patient management would be a simple device which could identify viral load thresholds in a qualitative or semi-quantitative way [2].

The purpose of this research was to investigate the development of a physical test platform which could be used in conjunction with a novel isothermal amplification - Reverse Transcriptase Loop Dependent Amplification (RT-LDA) - developed by the Department of Molecular Medicine and Haematology. This testing platform was then to be evaluated using a proven, commercially available isothermal amplification platform.

1.1 Collaborators

The development of a POC device is truly an interdisciplinary effort. Expert knowledge is required in molecular biology, chemical engineering, electrical and electronic engineering and microfluidic manufacturing. It is for this reason that a collaboration was established between the Department of Molecular Medicine and Haematology and the School of Electrical and Information Engineering at the University of the Witwatersrand, Johannesburg alongside the Council for Scientific and Industrial Research's (CSIR) Material Science Manufacturing (MSM) group.

1.2 Scope

The intended output of this research is not to develop a fully functional, marketable device rather the development of a prototype system which can be used as proof of concept for functionality for further development and implementation in an extended capacity.

The outputs of this research are two-fold:

1. Development of a thermal heating element and controller sensitive to within 1°C,
2. The evaluation of PDMS* (Polydimethylsiloxane) as a microfluidic substrate for use with an isothermal nucleic acid amplification system.

* Discussed in more detail in *Chapter 3 – Microfluidics* and *Chapter 6 – Thermal Characterization of PDMS*

1.3 Methodology

The successful development of a thermal controller for a custom developed microfluidic substrate requires a number of successive and progressive milestones to be reached before the components can be integrated into a single functional device.

The requirements imposed on the thermal control module are not only strict on sensitivity but also in physical dimensions. The isothermal nucleic acid amplification assay chosen (BioMerieux NucliSENS EasyQ HIV-1 v2.0) requires a strictly controlled, uniform, temperature held at 41°C and accurate to within 1°C. The chosen temperature transducers would also need to be small enough to allow for accurate, non-evasive monitoring of the temperature at a given point on the microfluidic substrate without interfering with the fluid flow or functioning of the chip.

The constraints imposed on the development of the microfluidic chip are far less strict since there is no known ideal solution. However, practical interfacing to the substrate is vital. The development of the microfluidic cassettes requires a level of interfacing to the heating element and temperature transducers in such a way which does not require permanent bonding. The use of the microfluidic assays in conjunction with the isothermal amplification dictate that the microfluidic chips will only be single use and will need to be disposed of after each use.

1.3.1 Thermal Controller

The heating element chosen as the microfluidic heater was a peltier device. The use of a peltier device allows for both dynamic heating and cooling of a microfluidic substrate at a high enough conductive heat rates to overcome the slow thermal responses typical of these types of microfluidic systems. The peltier device functions on the reverse Seebeck effect. The Seebeck effect states that a temperature difference across two points of a conductor (or semiconductor) creates a potential difference between these points [3]. The peltier device is based on the Peltier effect, which (as previously stated) is the reverse effect of the Seebeck phenomenon – a potential difference applied across the semiconductor (in this case) creates a temperature difference between the two points. This allows for the option to implement a thermal cycler by being able to 'drive' the heat away from or into the system in a strictly controlled manner.

The development of the thermal controller was subject to a number of constraints for use on the lab-on-a-chip style implementation:

a) The thermal sensors must be small enough to be able to measure the temperature of the reaction chamber.
b) The placement of the thermal sensor/s should not interfere in any way with the operation of the nucleic acid amplification system or heating element.
c) The thermal controller must be able to hold the fluidic chamber, without fluctuation, at 41°C.
d) The accuracy of the thermal controller should be within 1°C.

One of the indirect objectives of this research is to contribute towards the development of low-cost devices.

1.3.2 Evaluation of PDMS

The evaluation of the PDMS as a microfluidic substrate for use with an isothermal nucleic acid amplification system will be subject to the results of:

a) The power required to heat the substrate and maintain the reaction chamber at the required temperature.
b) A comparison of the yield between a standard, bench-top isothermal amplification assay and the custom developed chip using the same vRNA (viral-RNA) samples and isothermal amplification system.
c) An evaluation of the extent of protein fouling present in the static-fluid reaction chamber.

1.3.3 Objectives and impact

- **Develop a microfluidic cassette**:
  - Design, printing, etching and casting the PDMS
  - Design verification (functional testing, performance evaluation)
- **Develop a thermal control system**:
  - Integration of a heating element (specifically a peltier device) into the microfluidic substrate.
  - Develop a low-noise temperature logging circuit capable of capturing the output from a thermocouple amplifier.
  - Development of a thermal control system (PID or similar controller).
- **Optimizing the isothermal amplification on the microfluidic platform:**
  - Determine compatibility of the isothermal amplification on the PDMS substrate.
  - Perform the isothermal amplification on the PDMS in parallel with standard laboratory reaction tubes.
  - Externally detect both products using the Light Cycler with FRET (Fluorescence Resonance Energy Transfer) probes.
- **Perform a laboratory evaluation (method comparison)**
  - Compare the microfluidic peltier chip generated isothermal amplification HIV viral load result against an existing commercial isothermal amplification platform.

The outputs of the project will take the form of tangible prototypes capable of proof-of-concept functionality of the system as well as the performance evaluation of the device as a whole against existing commercial, laboratory based systems on clinical samples.

Table 1 - Project Breakdown

Project Objective	Indicators of Success	Monitoring & Evaluation
Development a microfluidic cassette	Functional microfluidic lab-on-a-chip platform for testing and evaluation	Collaborator (CSIR) will provide the manufacturing, assembly and testing on silicon/PDMS substrates
Develop a thermal control system	Thermally stable, responsive temperature kept at 41˚C with a tolerance within 1˚C.	Stable, stand-alone system with controlled performance data logging capabilities.
Adapting the isothermal amplification on the microfluidic platform:	Successful amplification of nucleic acid using an isothermal amplification system on the microfluidic substrate.	Comparison of lab-on-chip performance against standard, bench-top procedure.

1.3.4 Factors influencing results

As with any engineering development, a number of different factors must be considered which may adversely affect the output. The main factors which will affect the results of these various developments are:

Table 2 - Key Factors

Influencing Factor	Description
Exceptionally poor thermal conductivity of PDMS (0.2 W/m°K)	The fact that PDMS behaves more like a thermal insulator than a thermal conductor significantly influences the heating strategies which can be employed.
Hydrophobicity of PDMS and the prevalence of protein fouling	The hydrophobic nature of PDMS causes exceptionally high levels of protein fouling and may hinder a good DNA amplification yield.
Physical dimensions of the temperature transducers	The temperature transducers need to be small enough to be able to interface into microfluidic channel dimensions in the sub millimetre range.
Accuracy of the temperature transducers	The temperature transducers need to be accurate enough to ensure a 1°C sensitivity during functioning otherwise the isothermal amplification will not function optimally.
Induced, erroneous readings (noise)	Background noise levels are exceptionally important – especially when making use of low-voltage transducers.
Response time of the controller	The response time of the thermal controller must be fast enough to act upon rapid changes in the system.
Response time of the heating element	The heating element's response time to the thermal controller will determine whether or not a stable temperature will be obtained.

1.4 Introduction to the Document

A brief introduction to the subsequent chapters presented in this document outlining the content, structure and purpose is presented below. This is intended to give the reader a quick overview of what to expect in the presented chapters and allow for easier navigation throughout the document.

No formal literature study is presented in this document as a single chapter. Due to the fact that the investigation covers such a broad range of topics (molecular medicine, control theory, electronics and microfluidics) it would seem disjointed to include all of the relevant theory in a single chapter. Instead, each chapter is presented with its own introduction which includes all of the relevant background and theory pertinent to the discussions and developments in the chapter.

1.4.1 Chapter 1 – Introduction

Chapter 1 provides an overview of the problem statement and introduces the field into which the primary investigation falls. This chapter also outlines the current technological deficits faced in the current state of medical developments and the need for the development of POC instrumentation as well as the immense benefits which they would be able to provide – especially in the developing world.

The key collaborators in the project are identified as well as the scope and methodology with which the investigation will be conducted. The development criteria are outlined and briefly discussed including the evaluation methods alongside the indicators of success. Potential factors which would influence the result of the investigation are also briefly outlined.

1.4.2 Chapter 2 – Viral Load Testing

This chapter provides the basic background and theory to the process of how important nucleic acid tests (NATs) are to the medical sciences and how these tests have benefitted from and contributed to the development of PCR systems. This chapter aims to provide a basic understanding of the functioning of the PCR process from a scientific and engineering perspective. A basic mathematical model is introduced to simulate the typical performance of a standard three cycle PCR.

Furthermore this chapter outlines the advantages this technology may benefit from miniaturized systems as well as discussing some promising miniaturized techniques and their current status as well as introducing an overview of the development criteria required for the implementation of a POC device.

1.4.3 Chapter 3 – Introduction to Microfluidics

The introduction to microfluidics serves to give a broad overview of the microfluidics field as well as a brief outline of the substrate chosen for prototyping. The focus of this chapter, however, is more the inherent issues introduced with the use of PDMS as a substrate for use with nucleic acid assays and more importantly the hindrance of the reaction by protein interaction and surface adsorption.

Focus in the chapter then shifts towards the development of the initial prototype chips and the various aspects which need to be considered and reviewed in their design. The two prototyped platforms viz. the single chamber and the micro Total Analysis System (µTAS) prototype are presented and evaluated.

1.4.4 Chapter 4 – Temperature Controller and Transducer

The custom developed PCB for use in this investigation is presented in Chapter 4. The PCB was developed with the key design feature being the attempt at noise minimization on the signal and power bus lines. Noise minimization aspects such as selection of decoupling capacitors, separation of ground planes and embedded capacitive decoupling are discussed in detail and en evaluation of the performance of the board is presented.

1.4.5 Chapter 5 – Miniaturized Nucleic Acid Amplification System

The various hardware aspects of the device are presented separately with the required functionality which would need to be obtained from each system as well as the interfacing between the components. A flow diagram of the intended functional and process flow of the system is presented and discussed.

1.4.6 Chapter 6 – Thermal Characterization of PDMS

This chapter gives a theoretical background on Fourier's Laws of thermodynamics as well as their application in the verification of the thermal conductivity of materials. The mixing and curing process of PDMS can alter the expected thermal conductivity if the process is carried out incorrectly. The thermal conductivity of the PDMS is tested and compared against previously measured values in the literature to ensure that no erroneous values are assumed of the material.

1.4.7 Chapter 7 – Thermal Controller

The thermal controller problem is presented in Chapter 7. This chapter describes the selected hardware and software implementation for the chosen solution to the thermal control issue. A comparison of the tested algorithms is presented with a brief discussion on the performance of each with more detail focused on the performance and implementation of the final solution.

1.4.8 Chapter 8 – Thermal Simulations

A 3-dimensional, finite element model of the microfluidic substrate and heating element is presented and the results are compared to those physically measured with reference to any assumptions that were initially made about the thermal plant and heat flow distribution.

1.4.9 Chapter 9 – Results

The results for the overall functioning of the components and the device as a whole are presented here and discussed in detail. Initial testing results are presented alongside any amendments and alterations made to the system in order to improve the performance.

1.4.10 Chapter 10 – Future Recommendations

Future recommendations for the system are presented and their likely implications on the overall performance of the device (or various components thereof) are discussed.

1.4.11 Chapter 11 – Conclusion

The conclusion to the POC isothermal amplification investigation is presented and discussed. The major componential results are separated into their respective sections as well a discussion of the performance of the fully integrated device as a whole and its success in application.

2. VIRAL LOAD TESTING

Despite numerous AIDS awareness campaigns and aggressive treatment with ARV's (AntiRetroViral Drugs) employed world-wide, it is estimated that in 2007 [4]:

- 33,200,000 people worldwide were infected with HIV/AIDS
- 2,500,000 of the infected people were under 15 years of age
- A further 2,500,000 people were newly infected, of which approximately 420,000 were children.

The most affected region still remains that of Sub-Saharan Africa with 68% of the global HIV/AIDS population along with 76% of all AIDS related deaths [5]. Life expectancy has fallen dramatically in these regions with reported estimates of life expectancy dropping by at least 6 to 7 years on average in the African nations with the highest HIV/AIDS prevalence [6].

Highly Active ARV Treatment (HAART) of patients has been known to increase life expectancy anywhere between 5 to 16 times the expected life median of those without access to ARV's. In the absence of ARV therapies, the average survival time of a patient once the HIV virus has progressed to AIDS in low-resource areas where treatment is scarcely available is estimated to be between 6 and 19 months [7]. Without treatment, death normally occurs within a year due to opportunistic infections resulting from failure of the immune system [8].

Being able not only to administer HAART to HIV infected patients, but also being able to monitor the effectiveness or ineffectiveness of the treatment and being able to switch patients to different regimens at the correct stages greatly increases the potential life span of the patient. As previously discussed, the infrastructure, equipment, skilled personnel and transportation facilities in low-resource areas are far too sparse to be able to cater for individual patient's needs. Introducing a device which can be used by individuals (or families or even small communities) which can aid medical professionals in making informed decisions regarding a patient's treatment progression holds great potential for effective HAART deployment programs and future HIV/AIDS prevention.

Clinical patient management for HIV at this point involves both CD4 counts and viral load monitoring. The problem, however, is that CD4 counts do not accurately reflect the progression of the HIV virus in the patient nor can these routine tests be used for the diagnosis of the infection in infants - unlike nucleic acid testing for viral loads. The viral load of a patient is a quantitation of the severity of a viral infection within an individual and is calculated by estimating the amount of virus in a bodily fluid. Viral load determination is used in the therapy and monitoring of a patient suffering from a chronic viral infection. Routine testing is available for monitoring viral loads in HIV-1 infections.

2.1 DNA Amplification

The Polymerase Chain Reaction (PCR) is an indispensable laboratory technique used in present day molecular biology. PCR systems are used in fields ranging from genetic manipulation to forensic sciences (DNA fingerprinting, paternal/maternal testing). The application of PCR systems is based on the ability to amplify DNA samples which can then be used for further genetic analysis. With PCR, it is possible to amplify a single strand of DNA across several orders magnitude producing millions of copies of the single, original strand [9].

Complementary DNA sequences are defined as two nucleotides connected on opposite single DNA strands via hydrogen bonds and are called nucleotide base pairs. Base pairs are comprised of nucleotide molecules which are joined together to form the structural units of RNA and DNA. The nucleotides abbreviations of A, T, C, G are adenine, cytosine, guanine, and thymine respectively. In the nucleotide pairing A bonds only to T and similarly C to G. An example of a complementary DNA sequence is given below:

- Primary strand: ATCGAT
- Complementary: TAGCTA

Since there is only one complementary base for any of the bases found in DNA/RNA it is possible to construct a complementary sequence to any possible strand - this is the foundation for DNA amplification.

2.1.1 Traditional PCR

Traditional PCR systems require a thermal cycling unit which allows for a rapid change in temperature in order to successfully amplify DNA. PCR – when broken down – is a fairly simple process which requires the basic understanding of a few terms:

DNA Polymerase

DNA polymerase is an enzyme which is used in DNA replication. This enzyme reads a (partially) intact DNA sequence as a template and synthesizes a new strand based on complementary base pairs to the template. DNA polymerase, however, cannot simply synthesize a new DNA strand without a primer – the polymerase enzyme needs a place to start. Thus primers (see below) for specifically known sequences are used to first mark/bind to their respective sites before the polymerase can begin functioning.

DNA Primers

DNA primers are lab created nucleic acid sequences which form the starting point for DNA replication. These sequences are generated complementary to the known genetic sequence which is being quantified or tested for in a given DNA sample. Primers also serve as the focal point for the activation of DNA polymerase which adds new nucleotides only to an existing strand of DNA, which the primer being bound to a portion of the ssDNA (single stranded DNA) sequence has now formed.

2.1.2 DNA Amplification

The Polymerase Chain Reaction process is a three-stage system which must be completed in order to amplify the given DNA sample. The three distinct stages all generally occur at different temperatures in the process - unless an isothermal amplification technique is used, whereby all three stages occur at the same temperature which eliminates the need for a temperature cycling system.

The three stages in the PCR process are:

1. **Denaturing**: The DNA strand is heated to a point where it acquires enough energy to split into two single strands of DNA (ssDNA). This takes place between 94 ˚C to 98 ˚C.
2. **Annealing**: The temperature is lowered significantly (50 ˚C to 65 ˚C) to allow for the annealing of the primers to their respective sites on the ssDNA sequences. It is at this point that the polymerase also binds to the incomplete, partial double stranded sequences.
3. **Extension**: The temperature is again increased (75 ˚C to 80 ˚C) to allow for an increase in polymerase activity in which DNA polymerase is used to extend the newly bound primers to the ssDNA strands.



Figure 1 - DNA Amplification

At each cycle the amount of product generated is doubled with each double stranded sequence being the template for two new double stranded sequences. When dealing with vRNA (such as HIV) which is used for viral load testing, a reverse transcriptase step is added to transcribe the RNA to DNA for the initial stage. DNA is used for qualitative testing such as infant diagnosis.

Mathematically we can model a cyclical PCR system with a simple exponential function of $yield = 2^n$, however, to be more concise the equation below is substituted:

$$yield = (1 + X)^n \quad [1]$$

Where *X* is the overall efficiency of the process which can have a value between 0 (0%) and 1 (100%) and *n* is the number of cycles. Evaluating this model begins with a single strand, and assuming 100% efficiency, for the first cycle (*n = 1*) and $yield = 2^n$:

- n = 1 -> 2 strands
- n = 2 -> 4 strands
- n = 3 -> 8 strands
- n = 4 -> 16 strands and so on

The resulting error in assuming 100% efficiency is that the loss of reagents in each cycle which have been used is ignored. This assumption eventuates to an infinite yield assuming all reagents are not consumed in the process. Another (slightly less significant assumption) is assuming that all reagents are available for the reaction and are not lost due to contamination or incorrect / unwanted binding to surface of the reagent housing (protein fouling).

The one way to obtain a more accurate model preserving the exponential equation (2) is by factoring a cumulative efficiency loss per cycle into the equation and assuming an overall efficiency of slightly less than perfect. The cumulative efficiency loss per cycle takes into account the loss of reagents in each cycle which have been consumed and turned into useful product. This is represented by:

$$yield = (1 + ((X - e(n)))^n \quad [2]$$

Where *e(n)* is the cumulative efficiency loss per cycle.

Simulating the above equation making the following assumptions:

- *X* = 90%
- *n* = 100 cycles
- *e* = 2% efficiency loss per cycle

The following results for the yield of the PCR system (Fig. 1).

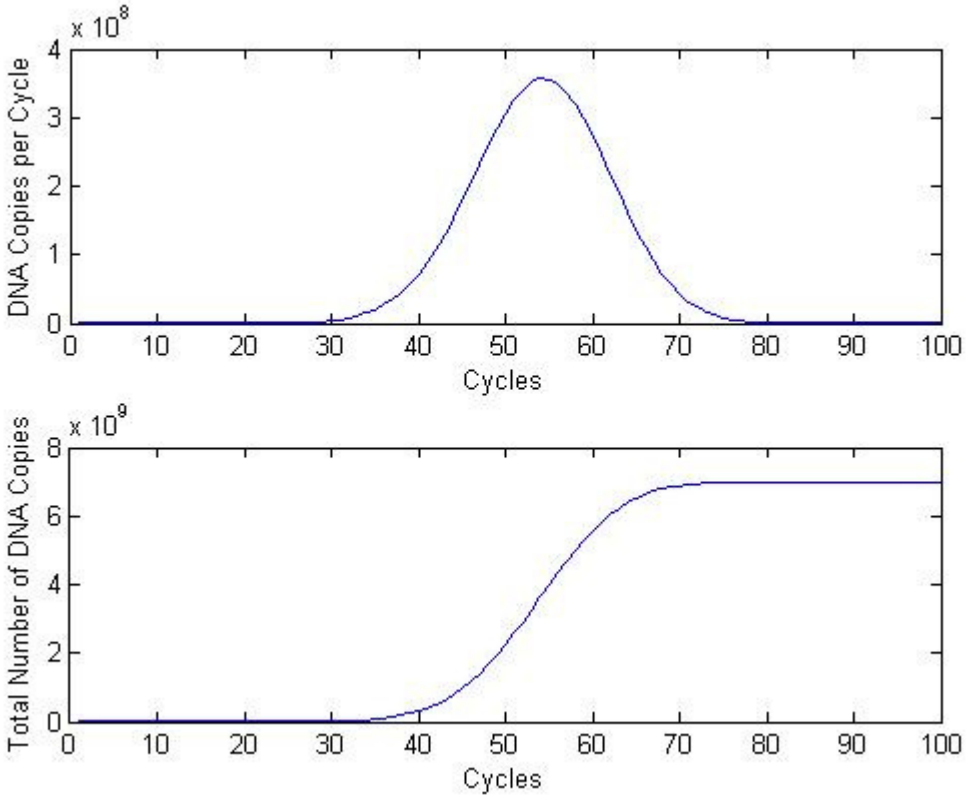

Figure 2 - PCR Mathematical Simulation

The above graphs are representative of a typical cyclical PCR curve. From these results – even for a fairly inefficient PCR system – at roughly 40 cycles there are already 100million copies of the single, original DNA strand of interest. This illustrates the true power of the PCR technique demonstrating its ability to amplify even a single strand of DNA/vRNA/RNA to significantly higher orders of magnitude for use in further testing.

2.2 Lab on a Chip and micro-Total Analysis Systems

Lab on a chip (LOC) and micro-Total Analysis Systems (µTAS) are miniature devices which are able to perform sensitive and complex laboratory procedures such as PCR without the substantial requirements placed on resources and trained personnel. These miniaturized devices attempt to replicate the functionality (some even with improvement on existing technologies) of a number of different expensive laboratory based devices and apply these techniques at POC (point of care). The terms lab on a chip (LOC) and µTAS were coined from the fact that an entire diagnostic (or equivalent) procedure is shrunken down and implemented on a single, autonomous substrate at physical dimensions within or below the micro-meter range. One of the ideals described in the implementation of POC diagnostics is that any instrumentation developed should be low maintenance, low cost, automated and battery operated. High throughput, automated robotic systems cannot be successfully applied in third world countries which do not have adequate laboratory infrastructure.

Thanks to breakthroughs in the fields of nanotechnology and microfluidics a number of publications have emerged in the last 6 years describing early technologies attempting to overcome the hurdles of introducing diagnostics to the developing world [10]. One of the problems which have emerged in the modern world is the strict application of location specific technologies. The technological requirement's on patient diagnosis is dependent on the location and income levels in those areas. This has led to the development of location specific technologies which meet the immediate environmental requirements of turn-around time and cost and limit the applicability of these technologies in harsher, lower resourced environments [10]

In a recent study conducted by international scientists familiar with public health programs of developing countries, it was found that the highest overall priority was the development of "molecular technologies for affordable, simple diagnostics of infectious diseases" [11]. Third world design constraints for LOC devices successful implementation have been documented as:

- Low cost devices
- A need to perform reliably with the absence of trained personnel
- Function in environments without readily available electricity
- Operate in poorly equipped laboratories
- Survive transportation and storage in unrefrigerated environments.

2.3 Continuous Flow Systems

One of the more popular methods of on-chip-PCR developments such as Lab-on-a-chip and micro total analysis systems (µTAS) are continuous flow systems. These chips have had limited success in application, however, they have managed to overcome the slow thermal responses of typical materials used in microfluidics. The most significant drawback using plastic-based substances such as PDMS, PTFE (Polytetrafluoroethylene), Polypropylene etc. is the fact that these materials have exceptionally low thermal conductivities (0.1-0.2 W/mK) which is virtually identical to that of hardwoods such as oak and maple.

The overall efficiency of the process is highly dependent on the temperature ramp times which are needed to transition from the current temperature to the next stage in the PCR cycle. The faster the temperature transition the more efficient the process [12,13]. In order to decrease the temperature ramp times of PDMS, some groups have attempted to mix metallic powders and copper flakes into the PDMS pre-mix in an attempt to increase the overall thermal conductivity of the material [14].

The main advantage of continuous flow systems (Fig. 2) is that they negate the slow thermal response times of these materials by incorporating three different sections in the chip design which are pre-heated to the correct temperatures. The fluid is then passed through these zones continuously (hence the name continuous flow) and then routed back again to the beginning to allow for another 'cycle' of flow. The flow of fluids from one temperature zone to the next allows for a virtually instantaneous heat transfer (since the exceptionally small volumes of fluid have virtually no thermal mass) to the fluid improving the overall efficiency.

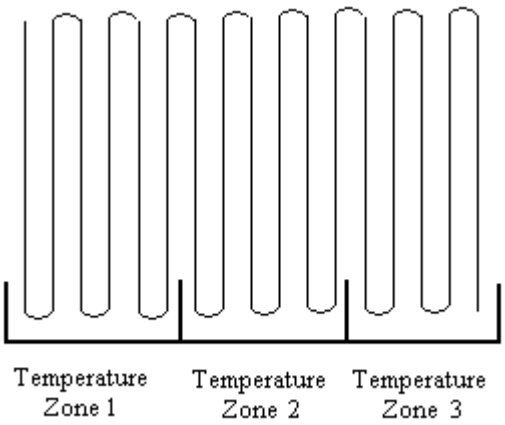

Figure 3 - Continuous Flow Systems

The fluid volumes used at this scale are generally a few hundred picolitres up to a few microlitres which means that the fluid has a minimal thermal mass and it takes very little energy (and time) to change the temperature

of the fluid. The graph below (Fig. 3) shows a more intuitive comparison of the fluid temperatures (and the temperature ramp times) in traditional, cyclical PCR systems and continuous flow systems.

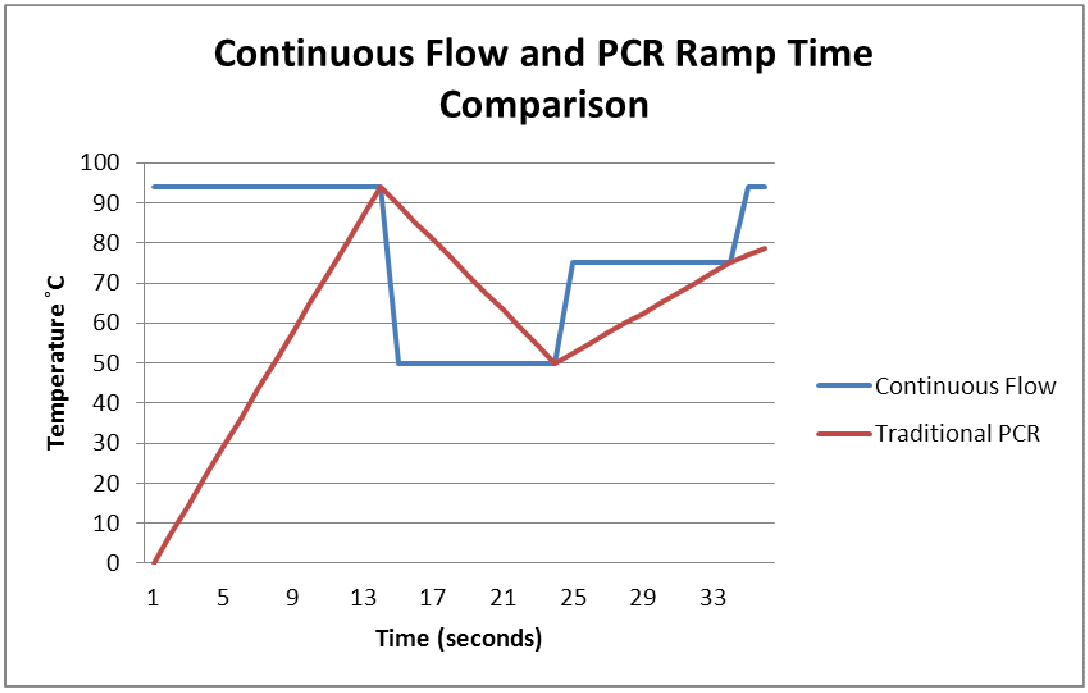

Figure 4 - Temperature Ramp Cycle

As previously stated, this is a popular technique which has been applied with limited success and often exhibits higher efficiencies, sensitivities and shorter run-times than conventional PCR systems [15]. The two main limiting factors are:

a) Channel Blockage
b) Protein Fouling

These two factors are often thought of a single phenomenon since protein fouling eventuates to channel blockage, however, a number of different factors can contribute to channel blockage.

2.3.1 Channel Blockage

Channel blockage occurs when impurities or other potential contaminants get 'trapped' in the channel. Typical channel widths for these applications vary from a few hundred pico-meters up to around 1µm which is comparable to actual cell sizes (100nm for HIV) on the lower pico-meter scale. A downfall of the continuous flow system is that any blockage is crippling. A blockage anywhere on the chip will cause the entire system to stop functioning which makes it a less-reliable technique for commercial implementation in low cost POC devices.

2.3.2 Protein Fouling

The second limiting factor is that of protein fouling. Protein fouling is the binding of reagent enzymes (generally the polymerase enzyme) to the housing / structural surface rather than being used up in the reaction [13].

Not only does this cause a significant loss in reaction enzymes lowering the efficiency of the process but can also be a cause of channel blockage in microfluidic systems. Protein fouling in continuous flow systems is more pronounced than in normal, static-fluid PCR based systems. This is due to the high surface area to volume ratio present in continuous flow systems. In these systems a small volume of fluid is exposed to a large surface area

which significantly increases the exposure to the hydrophobic surface of the PDMS which promotes higher extents of protein fouling.

2.4 Isothermal Nucleic Acid Amplification System

The English Collins Dictionary defines *isothermal* as *"of a process or change taking place at a constant temperature"*.

Isothermal nucleic acid amplification systems achieve the same output as traditional PCR processes without the need for temperature changes to alter the state of the DNA. The denaturing, annealing and extension processes are achieved enzymatically with enzymes which are active at the specified, single, temperature. The NucliSENS EasyQ HIV01 v2.0 isothermal amplification kit requires a stable (within 1°C) temperature of 41°C to successfully amplify the target. Having such a low run-time temperature yields numerous advantages not only to the functioning of the chip but also to the design.

Since there is no requirement for temperature changing, temperature cycling is irrelevant and no fluidic actuation is required to move the sample and reagents between distinct temperature zones provided by continuous flow systems. This allows the process to be completed with static fluid which eliminates the large surface-area to volume ratio present in continuous flow systems which, in turn, minimizes the contact area with the surface and promotes less overall protein absorption (fouling).

Lower heat requirements means lower overall power required in the system. This is generally overlooked in the design and implementation of expensive, laboratory based equipment, however, is important when attempting to design a functional POC device. Ideally, POC devices should be able to operate in conditions and environments which do not necessarily provide day-to-day power sockets where equipment can simply be plugged in and alternative sources such as batteries need to be kept in mind.

The fact that the isothermal amplification, by definition, only requires a single temperature makes the design of the thermal controller much simpler than one which requires fast thermal ramp times between temperatures (especially on poor conductors). Unlike traditional, cyclical PCR's, the efficiency of an isothermal amplification is *not* dependent on temperature ramp times (since there are none). Isothermal system efficiency is dependent on temperature stability, selection of materials and effective use of reagents with minimal losses.

Lower temperatures also minimize the effects of bubbling in porous substrates such as PDMS. Sample bubbling is known to occur at temperatures in the range of 70°C and above [13].

2.5 Advantages of a Miniaturized System

POC diagnostic equipment has the ability to provide timely and critical information where it is needed most.

The overall benefits of developing a POC device for HIV-1 viral load monitoring are:

a) Testing can be completed at the point at which the patient is being cared for (i.e. at the patient's bedside).
b) Quicker turnaround time to result since no samples need to be transported to equipped testing facilities.
c) No need for repeat visits by patients to collect results in areas where transportation for the patients (often chronically ill) is not readily available.
d) The need for highly trained personnel is reduced since the nucleic acid procedure is automated.
e) The device can be operated in non-laboratory environments.
f) The overall process is far less resource intensive in terms of personnel, time and materials.
g) Smaller reagent volumes allow for faster reaction times and faster process results.

h) Less reagent usage saves costs on the expensive biological assays.
i) Miniaturized devices are much lower cost than their bench-top equivalents.

"Any fool can make things bigger, more complex, and more violent. It takes a touch of genius - and a lot of courage - to move in the opposite direction." – Albert Einstein

In order to successfully develop a point of care device for HIV-1 viral load monitoring, 3 distinct stages are necessary for implementation in the device.

2.6 POC Device Functional Requirements

The development of a functional POC to perform viral load evaluation would require, at least, 3 distinct stages of functionality (Fig. 4):

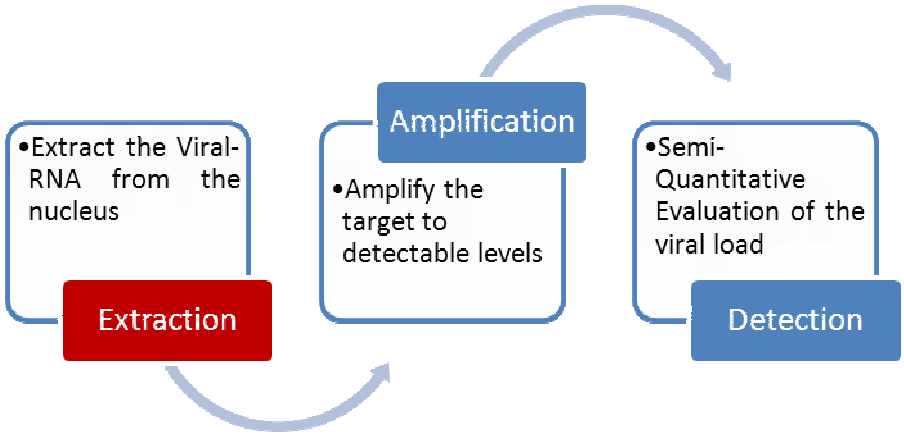

Figure 5 - POC Device Stages

The three stages in the process (Fig. 4) are:

i. Extraction: The viral nucleic acid (vRNA) must be extracted from the whole blood sample.
ii. The target (being the vRNA) is amplified to detectable levels by making use of the isothermal amplification system.
iii. Semi-Quantitative detection of the target occurs in the final stage in order to determine the viral load present in the sample.

To date, there exists no extraction method for nucleic acid testing (NAT) which is readily adaptable to POC devices and testing [16]. Current technologies require complex extraction methods and highly skilled personnel. The focus of this research is *not* on the development of an extraction technique and focuses rather on the amplification phase and the evaluation of the NucliSENS isothermal amplification system on PDMS substrates.

Nucleic acid extraction remains a bottle neck for miniaturization because of the current state of the technology – both the relatively 'young' age of microfluidics in POC diagnostics and the fact that currently there is no nucleic acid extraction technology available which enables non-instrumented RNA or DNA extraction [16]. The process is highly labour intensive and requires sophisticated instrumentation on the macro scale – which impedes the success to which it can be miniaturized. Due to this fact, most evolving micro-scale technologies stray away from attempting to clone and miniaturize sophisticated laboratory extraction techniques and are attempting to take advantage of new techniques (such as capillary-suction forces in porous substrates) which are inherent in microfluidics as new and novel approaches for nucleic acid extraction.

An amplification system (including microfluidic design and heating element) was developed for this system as well as proposing designs for possible semi-quantitative detection systems. The detection system chosen is said to be 'semi'-quantitative which means that the viral load count will be an approximate range of values estimating the actual number of copies of the virus, say between 1,000 and 10,000 copies/ml.

The exact number of copies of the virus, although useful, is just as indicative of the success of administered ARV's as a range approximation as indicated by the WHO [3]. Viral load monitoring is an evaluation of the increase, decrease or stability of the viral load. If the viral load is increasing it is indicative that the ARV's are not preventing the spread of the virus and a difference regiment should be considered. A decreasing or stable viral load indicates that the administered ARV's are, indeed, preventing the spread of the virus in the patient.

2.7 NucliSENS EasyQ HIV-1 v2.0

The chosen isothermal amplification system used in the evaluation of PDMS as a microfluidic substrate for nucleic acid replication was the BioMerieux NucliSENS EasyQ HIV-1 v2.0. This is globally proven assay used for the quantitative determination of HIV-1 RNA in human EDTA (Ethylenediaminetetraacetic acid) plasma and whole blood spotted cards. This assay has not been proven, nor is it recommended as a screening test for HIV-1 or as a diagnostic tool to confirm the presence of an HIV-1 infection in a patient on a commercial or clinical basis.

One of the advantages of using this assay is that it combines a nucleic acid amplification step as well as a combined detection phase. This assay required the use of isolated HIV-1 RNA. The nucleic acid isolation process is not intended to be covered in the design of this prototype and was performed independently for use with the amplification system by Natasha Gous [17] in the Department of Molecular Medicine and Haematology.

The enzymes used in this assay are highly temperature sensitive and require the system to be **pre-heated** to the specified temperature (41°C) before the introduction of the reagents into the microfluidic cassette. The isothermal amplification kit chosen requires a constant temperature of 41°C which is well below the documented reagent bubbling levels of above 70°C.

The detection process of this assay uses target-specific molecular beacons, which are DNA oligonucleotide sequences that recognise a particular RNA target sequence coupled to a fluorophore and target quenching moiety. In the absence of target RNA, the molecular structure will cause the fluorophore molecule to be close enough to the quencher which will result in no signal. In a positive sample the molecular beacon would open causing fluorescence. In the assay used, two molecular beacons are present, one specific to the target HIV-1 amplicons and one for the internal control [69].

An introduction into microfluidics and the cassettes designed to be used with this amplification system are described in the following chapter.

3. MICROFLUIDICS

Microfluidics is seen to be the heartbeat of POC technology developments and has been recognized as a growing field with much potential. The ability for microfluidics to incorporate entire laboratory functions onto a single substrate makes it a field of research of critically high value. There are very few if any POC prototypes being developed which do not take advantage of the microfluidics field. Microfluidics is a multidisciplinary field dealing with the behavior, control and manipulation of fluids which are restricted to geometries within the sub-millimeter range. Typical fluid quantities in this field are in the low picolitres to microlitres range.

The microfluidics field encompasses many different disciplines:

- Engineering
- Physics
- Chemistry
- Biotechnology
- Micro/Nanotechnology

The most common example (and the claim to fame for early microfluidics) was the development of the inkjet printer. Inkjet printers make use of nozzles which eject picolitres of fluid at precisely controlled velocities, trajectories and quantities.

The evolution of microfluidic technology has been spawned, in part, by the developments in Micro Electro-Mechanical Systems (MEMS). Microfluidics owes a significant amount of development contributions from this field to their own contributions, one of which has been the successful developments of photolithographic etching applied in this field.

In order to take advantage of this emerging field, playing a major role in Lab-on-a-chip developments and Micro Total Analysis Systems (μTAS), collaboration was setup with the Centre for Scientific and Industrial Research (CSIR) research group in the Micro Systems Manufacturing (MSM) division. The CSIR-MSM division has recently established a clean room facility for the manufacture of silicon wafer moulds used in the production of microfluidic devices making both technologies in photolithography and PDMS substrate casting available.

3.1 Overview of PDMS

PDMS is commonly used as the development standard for initial prototypes since it is an inexpensive substrate and good testing platform, it is biocompatible and exhibits no autofluorescence [12]. Moulding of PDMS is easily performed and widely used. The PDMS pre-polymer is mixed with a crosslinking agent in a 1:10 ratio (base : curing agent), degassed and then poured over the moulding surface. The PDMS is then cured in a curing oven to prevent demoulding [18].

3.2 Protein fouling

Even though PDMS is a good prototyping platform, the merits of price and ease of use are not without drawbacks. PDMS is known to be a highly hydrophobic substance. Hydrophobic substances promote much higher levels of enzyme surface absorption known as protein fouling. Protein fouling is the binding of proteins to the surface of the reaction chamber. This unwanted effect is a significant impeding factor in the development of efficient POC technologies and is the focus of much research across the globe [19-27].

3.2.1 Effects of Protein Fouling

Protein fouling is caused by intermolecular interactions between proteins and the containing surfaces [28]. Hydrophilic surfaces absorb fewer proteins than hydrophobic ones and the extent to which the protein fouling

occurs is dependent on the size of the surface area of the hydrophobic substrate to which the reagents are exposed.

Proteins tend to bind to hydrophobic surfaces which minimize the available amount to be used up in the reaction. This becomes a crippling factor in the development of nucleic acid systems which make use of the proteins such as Taq-polymerase and other such enzyme reagents. When there are only a few hundred picolitres of expensive reagents available, effective use of the enzymes becomes crucial in order to obtain good specific yields from the reaction.

Protein fouling becomes critical in continuous flow systems for two main reasons:

1. The high surface area to volume ratio to which the proteins are exposed, and
2. Any partial or complete channel blockage cripples the reaction since the fluid can no longer flow at the intended rate (based on the required cycle time), if at all.

PDMS glass hybrid chips were developed in order to reduce the levels to which the sensitive reaction proteins are exposed to hydrophobic surfaces. The slow thermal response of PDMS to temperature ramping dictated that an isothermal amplification system was preferred over a standard 3 cycle PCR process. In order to achieve high temperature ramp times a continuous flow system would most likely need to be implemented. An isothermal amplification system also allows the fluid to be kept static in order to minimize the total surface area to volume ratio of the reagents to the hydrophobic surface of the PDMS as opposed to implementing a continuous flow PCR.

3.2.2 Minimization of Protein Fouling

A number of different techniques and substances exist in an attempt to improve the overall performance of PDMS as a microfluidic substrate for DNA amplification by coating the surface with a combination of substances such as Parlyene, Bovine Serum Albumin (BSA), and Plasma treatment of the surface. Several groups worldwide have made use of these techniques with significant improvement of the reaction performances [12,13,19-22,24,27].

Surface modifications to fluidic substrates can be split into two broad categories [28]:

1. Altering the atoms and molecules in the existing surface using chemical or physical means (such as plasma treatments and laser ablation), and
2. Using a material with a different chemical composition to coat the surface.

This technology, however, was not used in the evaluation of PDMS as a microfluidic substrate since the overall evaluation was to be conducted on ‘raw’, uncoated, untreated PDMS which would allow for a baseline characterization of the yield from which improvements could be made.

3.2.3 Contact Angle

The contact angle of the droplet to the surface of the container is indicative of the nature of the surface being either hydrophobic of hydrophilic. This is also known as the degree of wetting of the surface [28]. The contact angle is measured from the horizontal of the surface at the point where the droplet curvature comes in contact with the surface to the edge of the curvature of the droplet (Fig. 5; below).

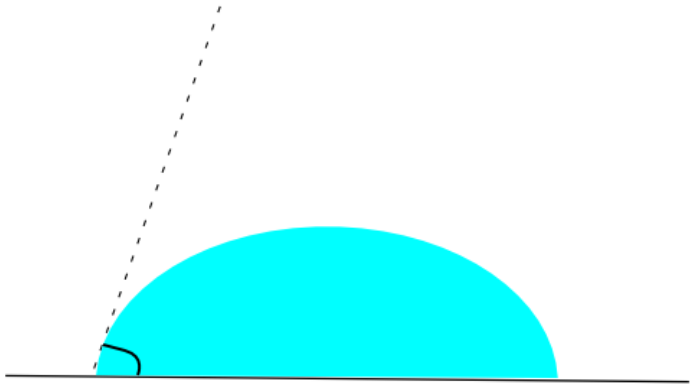

Figure 6 - Droplet Contact Angle

The higher the contact angle, the lower the wetting. Poor wetting is generally considered a contact angle greater than 90° with good wetting less than 90° and complete wetting being an angle of close to 0°. If a surface has a high surface energy the droplet will spread out and wet the surface. A low surface energy is indicated by the clear formation of a droplet on the surface [28]. The contact angle is the angle measured at this junction.

For hydrophobic surfaces larger contact angles are expected producing noticeable droplet formation on the surface. Hydrophilic surfaces promote low contact angles and a much higher spread of the droplet across the surface. It is, however, important to note that *hydrophobic* substances promote *higher* levels of protein fouling than their hydrophilic counterparts since the absorption of proteins is *not* proportional to the contact area with the surface. If this were the case then hydrophilic surfaces would promote higher levels of fouling since they expose the most fluid to the surface – which is not the case. Protein fouling is due to the surface molecular interactions and not the total contact area with the surface.

3.2.4 Sample Bubbling

Sample bubbling in porous substrates causes a number of issues when attempting to control the temperature of the cavity. The air bubbles form thin layers of insulation (thermal conductivity of 0.02W/mK) which destroy the uniform temperature profile within the cavity. These bubbles also tend to grow larger and eventually expel the fluid from the chamber – even in sealed systems [13].

Sample bubbling with fluid expulsion is generally observed at higher temperatures in the PCR cycle – typically above 70°C. Even though PDMS is a porous substrate sample bubbling was not expected to play a negligible role when making use of an isothermal system requiring an operational temperature of 41°C which is well below the documented bubbling zones. Bubble formation may still be observed (as indicated in *Chapter 9 – Results*) however, fluid expulsion due to the bubbling effect is not predicted.

3.3 Microfluidic Chip Design

The first prototype developed for the evaluation of the isothermal amplification system on PDMS was a simple, single-chamber design. The purpose of this chip was not to serve as a functional device to perform a total analysis on the sample. These chips allowed for a simple reaction to be completed (at 40µl) and have the yield externally evaluated and compared against that of a reference bench-top equivalent system.

3.3.1 Construction of the Microfluidic Amplification Chamber

The initial design of the chip for the evaluation of the PDMS as a microfluidic substrate for use in conjunction with an isothermal amplification system was designed as a single chamber microfluidic chip. This chip was used

to conduct all of the compatibility testing and yield evaluation of the isothermal nucleic acid amplification system (Fig. 6).

The single chamber has a volume of between 80µl-100 µl and was cast over a mould which was laser cut from Perspex, baked for an hour to cure, peeled off and then sealed to either the glass or PDMS bases using an oxygen plasma cleaner. The substrate sealed to the glass base is then baked again to ensure a good seal.

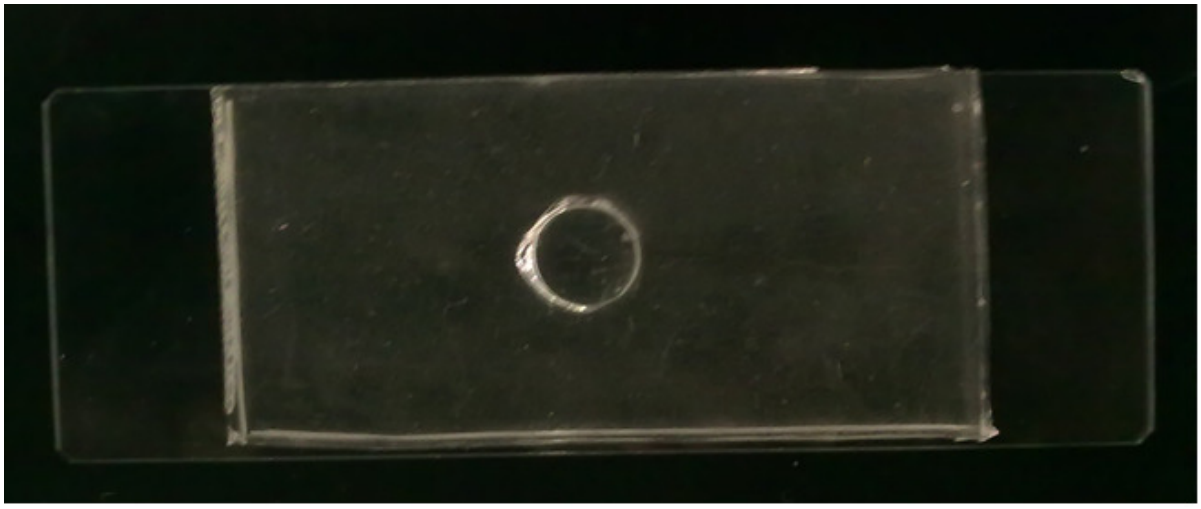

Figure 7 - Single Chamber Microfluidic Prototype

The simplistic design of the chip allowed for simple, quick manufacturing and testing without needing any additional equipment to control the fluid flow, valve actuation, insertion or extraction. The reagents are injected into the chamber using a hypodermic needle, and extracted in the same manner. PDMS is also an ideal substrate for this since it automatically self-seals should the needle gauge be small enough.

The designed volume of the chambers was a maximum of 50 µl. These small dimensions could not be achieved by the CSIR using the laser ablation technique and such a high volume could not be achieved using soft lithography etching on PDMS – discussed in *3.4 - µTAS Design Beginnings*.

3.3.2 Reaction Chamber

The single chamber design was intended to be used to allow the yield to be compared to that of an existing bench-top system. This was important because this allowed one to judge the overall efficiency of the developed substrate as well as gauge what sort of losses would be incurred due to the hydrophobic nature of PDMS and protein fouling.

The base of the testing chips was sealed both with glass and PDMS. This allowed for an overall comparison as to which would be the best base-platform to be used in conjunction with the thermal controller. Intuitively, the glass was the best choice before testing commenced simply due to the fact that it was a better thermal conductor which would respond better to thermal changes as well as its hydrophilic nature which would promote less overall protein fouling.

3.3.3 Glass vs PDMS

Glass has a number of advantages over PDMS when it comes to being a fluidic substrate as well as a thermal conductor and the pros and cons of each are shown below:

Table 3 - PDMS vs Glass

PDMS	Glass
+ Biocompatible	+ Biocompatible
+ Inexpensive	+ Inexpensive
+ Easy to mould	+ Dimensions less flexible (microscope slides)
+ Robust	- Fragile
- Hydrophobic (high levels of protein fouling)	+ Hydrophilic (lower levels of protein fouling)
- Very poor thermal conductivity (k < 0.2 W/mK)	+ Higher thermal conductivity (k = 1-1.2 W/mK)
- Thermally slow	+ Quicker thermal response than PDMS

The fact that the PDMS has a slower thermal response than glass is both an advantage and a disadvantage. A slow thermal response means that the system will take longer to reach the desired temperature at the same heat conduction levels as the glass and any adjustments to the temperature will also responds slower than the glass. However, once the PDMS stabilizes at the desired temperature, the deviation from the temperature will be slower. This was one of the design challenges which would need to be taken into account in the design of the thermal controller.

3.4 µTAS Design Beginnings

An advancement on the simple, single reaction chamber design was a simple µTAS chip design which included 3 distinct stages rather than a singular reaction chamber. These chips were manufactured by the CSIR based on functional designs which were developed as part of the research. The manufacturing of the chips and the introduction of the Tesla mixers was performed by the CSIR. The more advanced microfluidic analysis chip consisted of:

a) Reaction Chamber
b) Long-path mixing channels
c) Detection / Elution / Extraction Chamber

The design template of the chip can be seen below (Fig. 7):

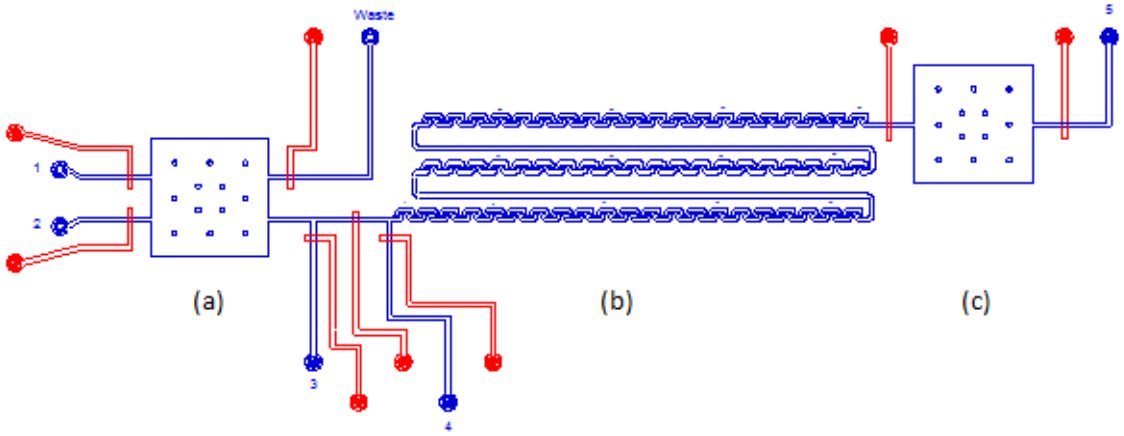

Figure 8 - µTAS Prototype Schematic

Image courtesy of the CSIR – Mechatronics and Micro Manufacturing Group

The image above shows both red and blue channels. The red channels are to indicate pneumatic channels for valve actuation and the blue channels are indicative of fluidic channels. These types of chips require a pneumatic layer in the design in order to close and open valves which allow for control of the fluid. The valves restrict the movement of fluid in different zones allowing for fluid to be kept in a single zone to fill or allow for controlled flow through the channels.

The construction of the pneumatic-fluid layer is shown in the diagram below with the temperature sensor layer omitted in this illustration (Fig. 8).

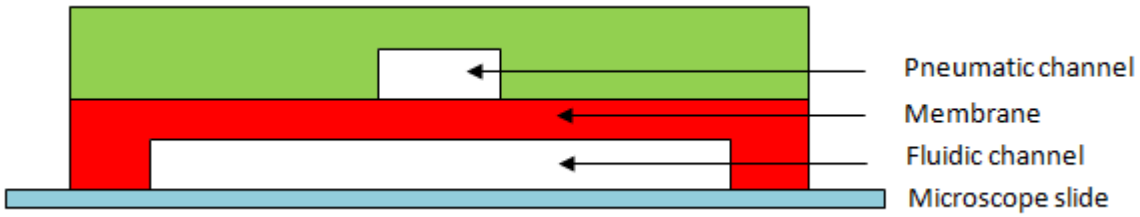

Figure 9 - Microfluidic Pneumatic Actuation

The construction of the pneumatic channels is simple both by design and functionality. The key to the application of the pneumatic channels is in the thin membrane which separates the respective pneumatic and fluidic channels. The membrane width between these layers is typically around 40µm. The PDMS membrane being so exceptionally thin allows for flexing between the channels.

3.4.1 Fabrication of the Device

The fabrication of the prototype devices is accomplished in what is known as a "soft lithography" photolithography process (Fig. 9). Basically, what this entails is casting a photoresist dye (SU-8) onto a 4-inch silicon wafer using a precision print schematic of the circuit. The dye then protects the portions of the silicon surface which have been exposed whilst all the unexposed areas are etched away in a very controlled manner by means of a UV-light source [29].

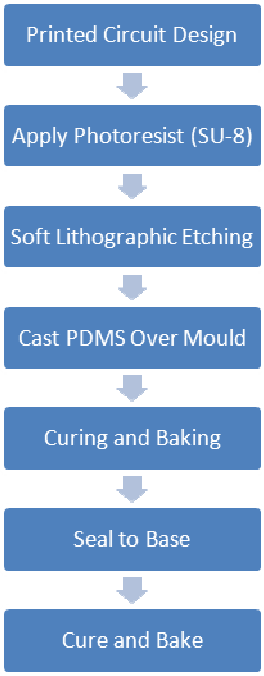

Figure 10 - Substrate Development Process

This process is also known as *negative photolithography* since whatever is etched away, the negative impression will appear on the casting material (i.e. a circular hole will be cast as a rounded, raised structure).

Each separate layer for fluid and pneumatic control layers need to be cast independently on the silicon wafers (since only 1 layer can be cast at a time) making the need for precision alignment absolutely critical for a functional design. The layers below show a 3 layer cast system which the prototype chips were developed on.

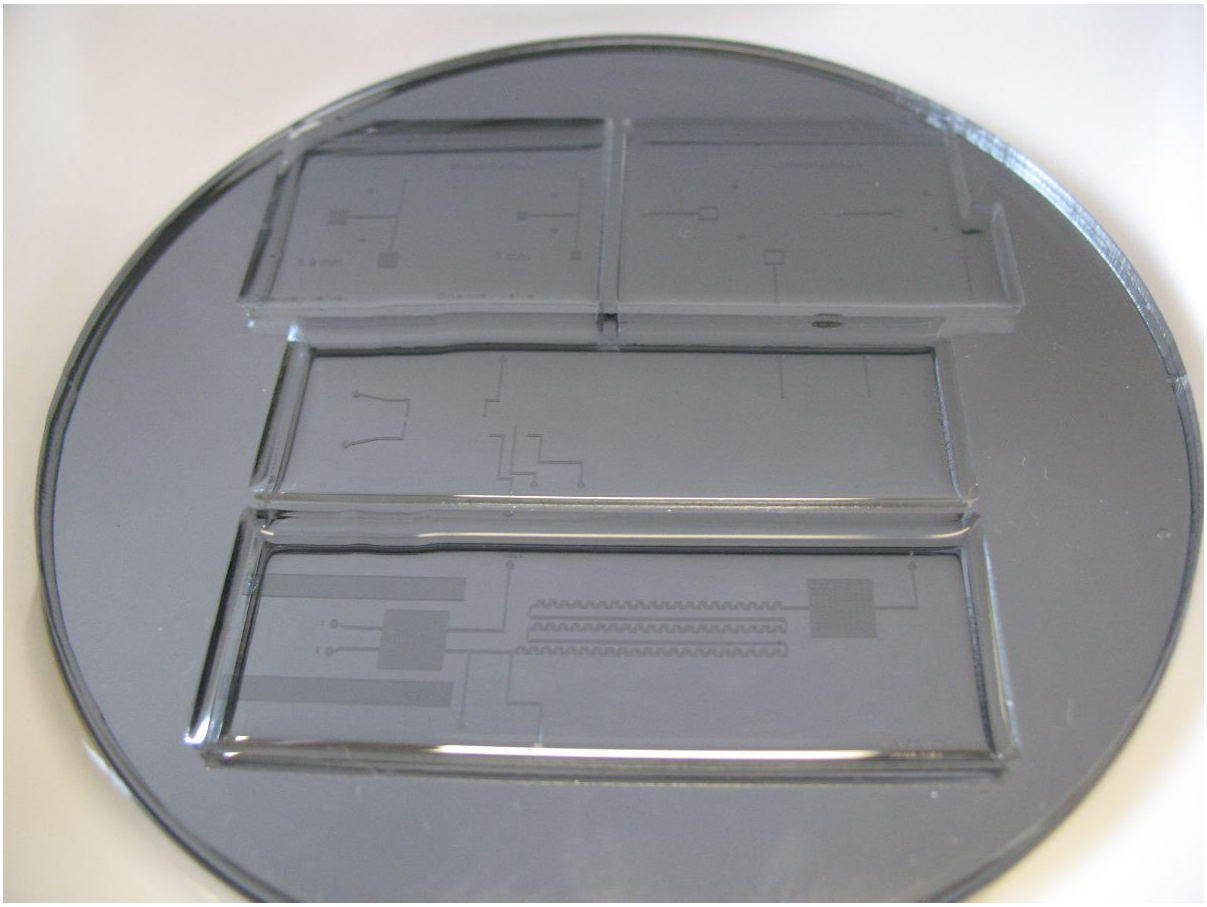

Figure 11 - 3 Layer Substrate Casting

Image courtesy of the CSIR – Mechatronics and Micro Manufacturing Group

The three distinct layers used for casting were:

1. Fluid Layer
2. Pneumatic Layer
3. Temperature Sensor Layer

The fluid channels are etched at 200µm width and 70µm depth allowing for a maximum volume of just under 5µl for the entire chip.

Two cassette implementations have been created using the above schematic (Fig. 10) with the main differences being how the devices have been sealed at the base. The bases which have been selected are microscope slides (glass) and PDMS cast bases. These 2 distinct base types will be used to show the effects of protein fouling by exposing the hydrophilic nature of glass and the hydrophobic nature of PDMS. Significantly different levels of protein loss due to the surface absorption of enzymes are expected to be seen between these substrates with glass fouling the proteins significantly less.

3.4.2 Design Constraints

In designing chambers and structures, which range well below the millimetre range, structural load bearing, strain and maximum tensile stress of materials is often overlooked. These phenomena, however, are still very much part of the design process and have significant bearing on structures even in the micro-meter range. As you can see from the developed prototype (Fig. 7) in both (a) and (c) supportive structures are required within the amplification and detection chambers (Fig. 11) to prevent the membrane from collapsing (shown below).

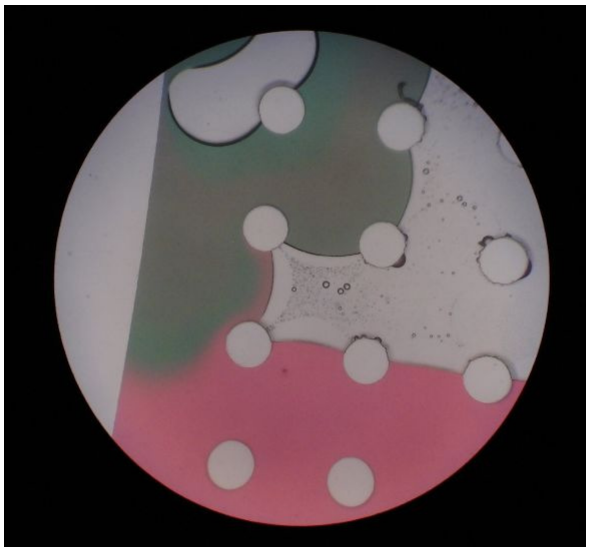

Figure 12 - Reaction Chamber Support Structures

Image courtesy of the CSIR – Mechatronics and Micro Manufacturing Group

The number of struts has been varied on some of the developed prototypes in an experimental manner in an attempt to find the minimum number of supporting structures needed. Collapsed chambers are already present on all of the prototype samples indicating that even more structural support is required.

A general "rule-of-thumb" employed in the development of microfluidic chips is a common 1:10 rule stating that the chamber/channel maximum depths and widths need to be designed in, at most, a 1:10 ratio to avoid structural collapse. This means that for a channel 10µm deep the width should be no more than 100µm.

3.4.3 Temperature Sensors

One of the most intricate design constraints was the selection and placement of thermal transducers in order to determine and control the temperature of the reaction chamber. At these dimensions minimal surface area is available for the placement of temperature sensors and any significantly large sensors would alter either the functioning or the design of the chips. For this reason, small (roughly 1mm) slivers were etched into the chip (on the temperate sensor layer) to allow for the insertion of thermocouple wires close to the reaction chamber. This would allow the transducers to be placed against the edges of the reaction chamber between the fluidic layer and the glass.

3.4.4 Pneumatic Valves (Sieve Valves)

Successful fluid control in microfluidic devices is often achieved using simple pneumatics. With this prototype (and many other devices) simple valves known as "sieve valves" are used for initial implementations of these systems.

As mentioned earlier, the chip consists of 3 levels – the temperature sensor layer, the fluidic layer and the pneumatic layer with an exceptionally thin membrane separating each of these. Valves are created via the pneumatic layer and are placed either above or below the fluidic layer depending on the chosen implementation. The initial prototypes designed have the control layer *above* the flow/fluidic layer in order to allow the flow layers contents to be exposed to a glass base and not limited to a purely PDMS channel design. The pneumatic actuation of the control layer is shown below with the temperature sensor layer omitted in the schematic.

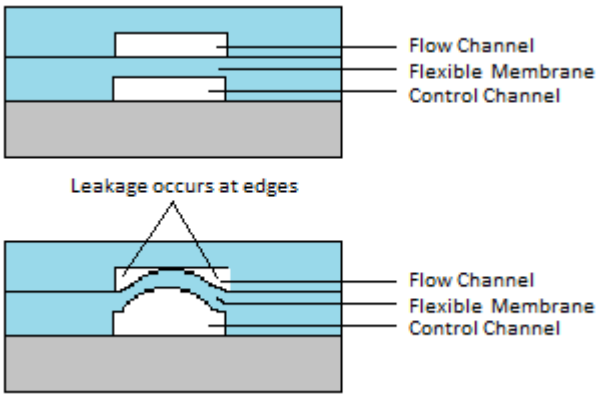

Figure 13 - Push Up/Down Valves

The pneumatic valves are actuated when compressed air is forced into the pneumatic chamber – known as the control channel (see Fig. 12 above). Since the membrane separating the control channel is made of flexible PDMS (spin coated to around 40µm) it does not take much pressure to cause the membrane to be flexed downwards (or upwards depending on the orientation of the channels) into the flow channel effectively sealing it off.

Sieve values, though useful in prototypes, are not ideal for functional device applications due to the geometry of the channel construction for which they are used. Square channels do not allow for the complete depression of the membrane and small gaps are left open at the edges which cause fluidic leakage in the system. This is not a major issue in the proof of principle stages as compared to a strict, well controlled functional chip. Similar implementations using valves which make use of circular channels will need to be investigated for a more effective design.

3.4.5 Effects of Laminar Flow

Encyclopaedia Britannica defines laminar flow: "*Laminar flow, sometimes called streamline flow, the velocity, pressure, and other flow properties at each point in the fluid remain constant. Laminar flow over a horizontal surface may be thought of as consisting of thin layers, or laminae, all parallel to each other. The fluid in contact with the horizontal surface is stationary, but all the other layers slide over each other.*"

In microfluidics laminar flow can be seen in its purest form since turbulence at these scales is non-existent. This means that 2 fluids of the same viscosity, being passed through a channel at the same velocity will only mix through diffusion (i.e. at the fluid interfaces) which is incredibly small and the mixing result insignificant.

Below (Fig. 13) is an image of passing 2 liquids through one of the prototype chips with the pneumatic valve (above the fluid) left open. At the fluid boundary (just before the fluids enter the channel) minimal diffusion between the 2 liquids is barely discernable.

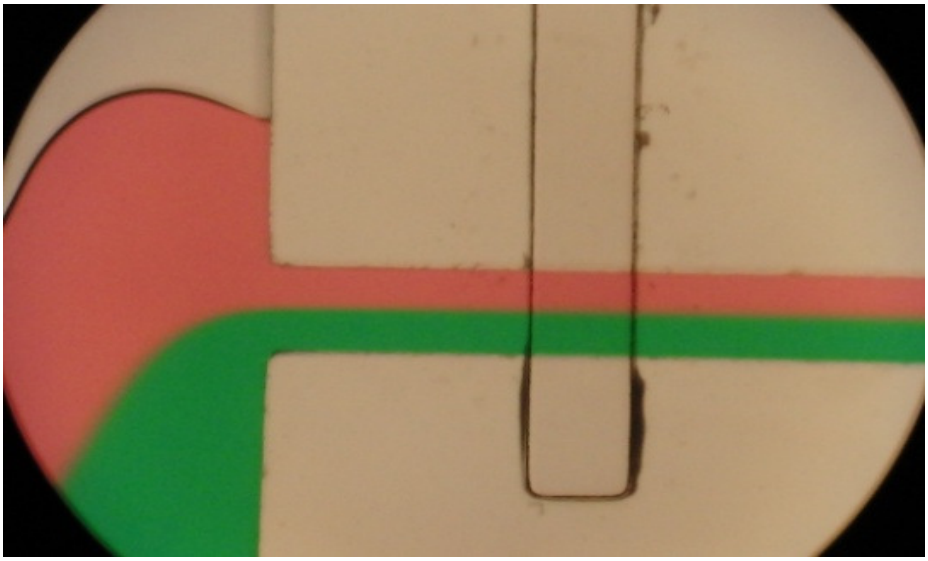

Figure 14 - Laminar Flow Demonstration

Image courtesy of the CSIR – Mechatronics and Micro Manufacturing Group

The above image illustrates the effects of laminar flow of 2 fluids (in this case food colouring) being passed through the channel with minimal diffusion at the interface.

3.4.6 Mixing Fluids

Laminar flow in microfluidic devices is advantageous when attempting to transport separate fluids which are not intended to mix, since they can simply be injected into a channel together and separated into their individual components at the end. The problem is, however, when the 2 fluids introduced into the channel are intended to mix.

The application for mixing in these prototypes was to mix the amplified vRNA (viral-RNA) product with capture probes which are bound to fluorescent molecules. In order to reduce the mixing distance required to mix two fluids, structures known as Tesla Mixers (see below) were introduced into the system in order to promote the mixing of the fluids by disturbing the interface / boundary between them [30].

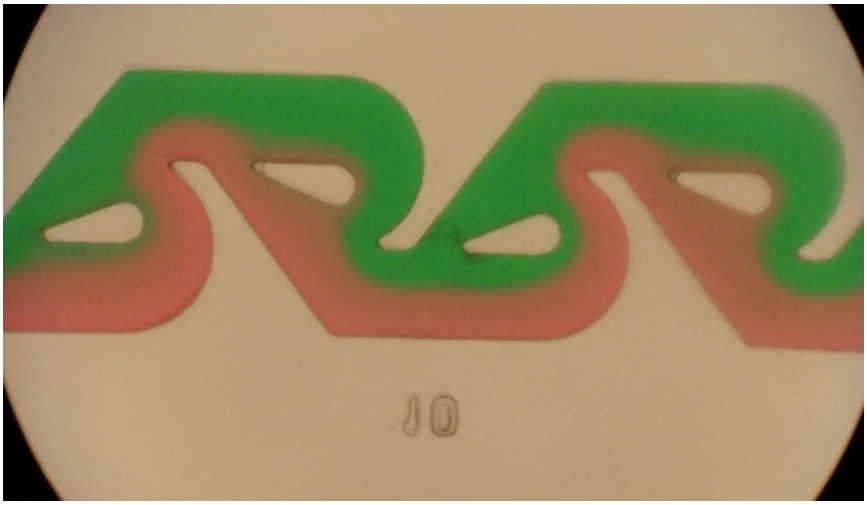

Figure 15 - Tesla Mixer Implementation

Image courtesy of the CSIR – Mechatronics and Micro Manufacturing Group

These mixers (Fig. 14, 15) disrupt the fluid boundaries between the individual liquids and intend to create some extent of turbulence by altering the fluid velocity around the tesla mixers in attempt to disturb the laminar conditions and promote mixing. In the above a slightly broader mixing area between the fluids can be seen.

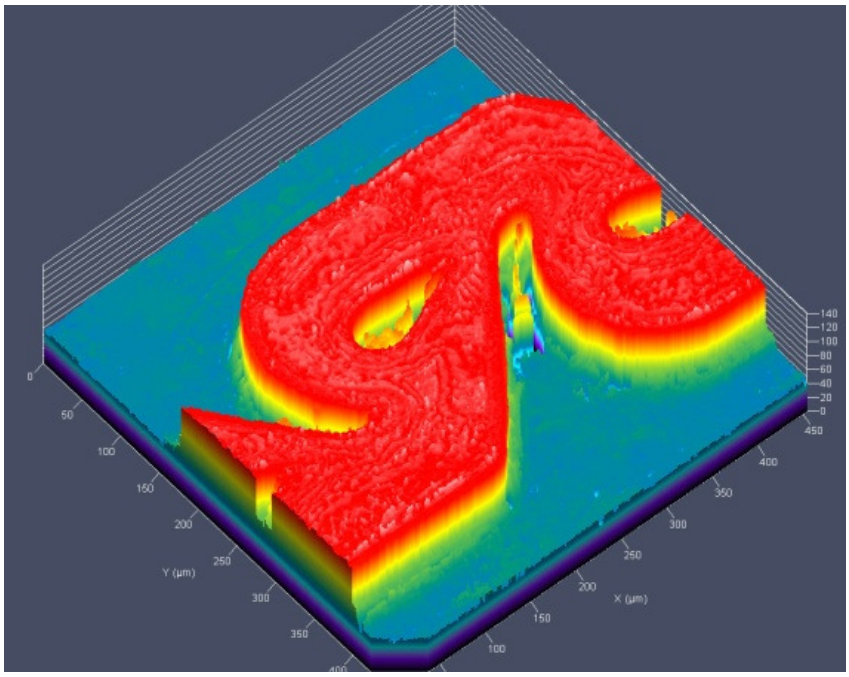

Figure 16 - Confocal Laser Scan of Tesla Mixer

Image courtesy of the CSIR – Mechatronics and Micro Manufacturing Group

The long mixing channel path will expose the product to the hydrophobic nature of the PDMS, however, protein fouling at the mixing stage is not an issue. The reagents used in the amplification cycle should all have been used up at this point and any remnants remaining will play no further role in the process and will not be considered a 'loss' in the overall effectiveness.

3.4.7 Non-Uniform Chamber Fill

One of the other issues which has become apparent in the initial prototype design is the shape of both the amplification and detection chambers in Fig. 7 (a) and (c). Fluid actuation in the microliter range on the micro-meter scale not only presents the true nature of laminar flow, but also exposes the preference to flow linearity and surface tension of the fluids as can be seen below:

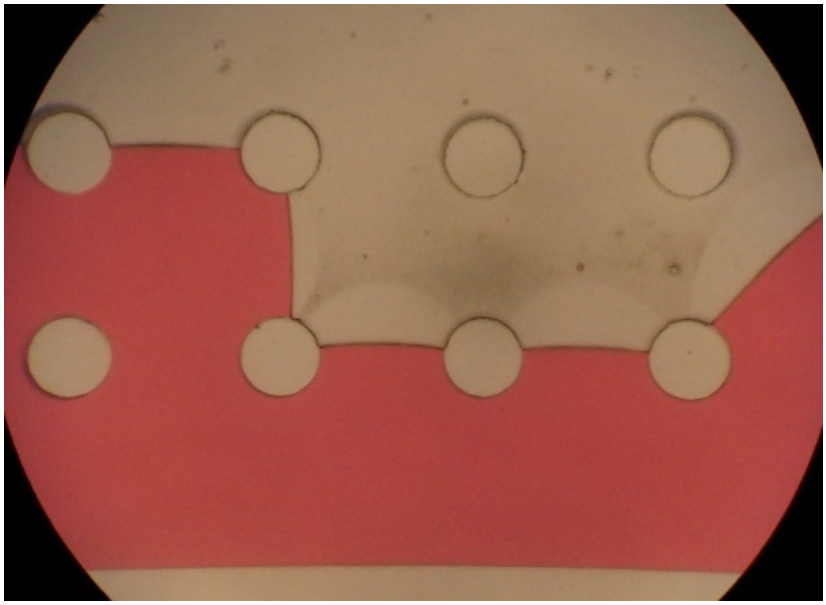

Figure 17 - Non-Uniform Chamber Fill

Image courtesy of the CSIR – Mechatronics and Micro Manufacturing Group

From the image above (Fig. 16) it is shown that the fluid forms straight lines between the supportive structures of the chambers and tends to fill the chamber in a non-uniform fashion. This becomes an issue when attempting to fill the chamber to capacity (Fig. 17 below).

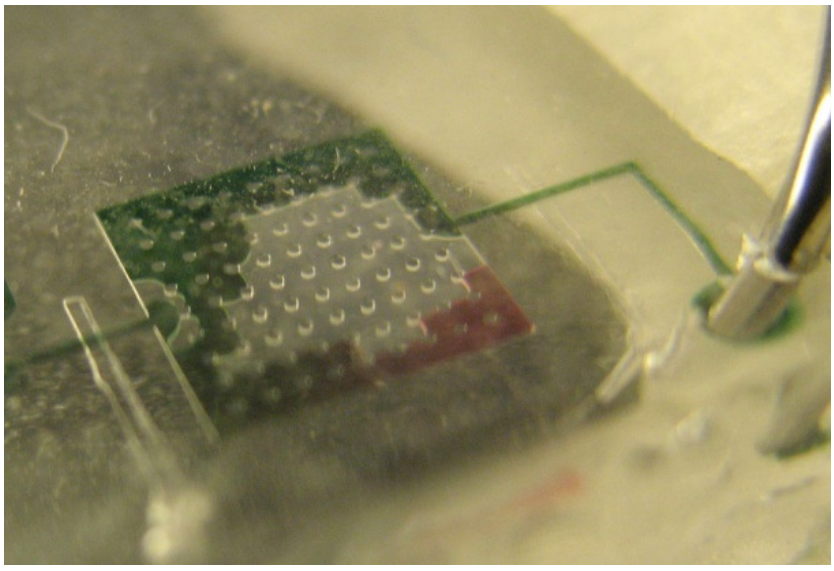

Figure 18 - Maximum Chamber Capacity

Image courtesy of the CSIR – Mechatronics and Micro Manufacturing Group

When attempting to fill the chamber, due to surface tension, the fluids tends to bind onto the supportive structures and does not present a uniform fill of the chamber. This introduces a slight problem into the design since areas of the chamber are left unoccupied by fluid. Another issue which would need to be incorporated into future designs is an escape valve for air in the chamber. The chamber gets filled compressing the air to the point where no more fluid can enter the chamber without first extracting air.

3.4.8 Detection Chamber/Channel

One of the reasons for the multi-loop mixing channel was to allow for the spotting of the channel with probes to capture the target amplicon (capture probes). Capture probes, are effectively immobilized oligonucleotide probes spotted onto the surface of the chamber (or channel) which have been designed to bind to the desired amplified target. The design of this is the same principle used in micro-array technology in order to capture the nucleic products of interest.

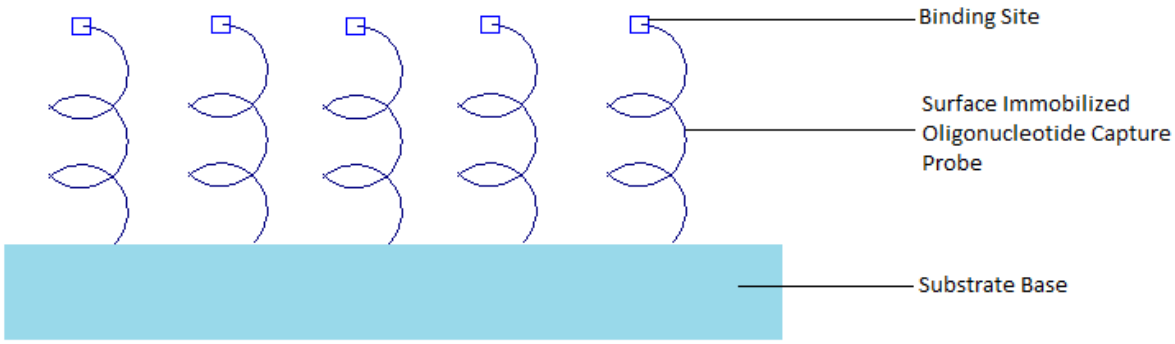

Figure 19 - Immobilized Surface Capture Probes

Spotting a known number of capture probes uniformly across each loop of the mixing channel (Fig. 18), having multiple loops allows for an exceptionally simple semi-quantitative fluorescent evaluation of the amplified product. Alternatively, should the channels not be spotted with capture probes, the detection chamber in Fig. 7 (c) could be used for the evaluation of the yield.

The spotting of the surface with capture probes is not a simple task, however, can be successfully implemented with great accuracy [31-35]. The technology to do so was also not available at the CSIR during the development stages.

The Tesla channels function would then be to mix in a fluorescent binding agent specific to the target amplicon in the mixing stages and transport the fluid to the detection chamber. This would then be used for fluorescent intensity semi-quantification of the product (i.e. the viral load present).

3.4.9 Evaluation of µTAS Chip

Initial prototypes for functional testing have been developed. These microfluidic prototypes have been cast on both glass and silicon base substrates for evaluation into the most efficient material to be used for the controlled amplification and fluorescent based detection of HIV-1 viral-RNA.

From the initial developed prototypes, a number of different issues which will require revision of some of the elements of the design are immediately apparent:

- Structural collapse is apparently on all of the developed prototypes which prevented the chips from being used as a functional evaluation platform for the isothermal amplification system.
- Amplification and detection chambers do not fill uniformly – changing the chamber shape and the placement of the supportive structures to change the fill pattern need to be investigated.
- The pressure in the chambers needs to be noted an escape valve for the air present needs to be investigated.
- Channel depths may need to be reduced to around 45µm in order for the sieve valves to seal correctly. This, however, has an effect on the overall volume capacity and the channels would need to be lengthened.
- Sieve valves are far from ideal but can be used for initial testing.

- Protein fouling will definitely be present on the PDMS substrate in the reaction chamber.

The temperature controller intended to interface with the single chamber substrates and µTAS designs is described in the following chapter giving a breakdown of the selected hardware and presenting an in depth evaluation of the developed solution.

4. TEMPERATURE CONTROLLER AND TRANSDUCER

Any POC implementation requires some hardware and sensors in order to measure and manipulate a desired constraint such as pneumatic pressure, fluorescent levels or temperature. This application required the development of a controller which was capable of sensing low voltage values from thermal transducers with high accuracy. In keeping with the main indirect objective of contributing towards the development of low cost POC technologies, readily available components were chosen for the implementation averting the need for specialized equipment.

The successful implementation of a thermal control system required the development of a PCB which exhibits a substantially high signal to noise ratio in order to be used with low voltage temperature sensors. The initial testing was conducted on the standard PICDEM2+ development kit, connected via twisted pair wires to the thermal sensors. This configuration exhibited noise levels comparable to the signal levels being measured. For this reason, a custom PCB was developed with the intention to minimize the noise levels present in the circuit as much as possible.

4.1 Selected Hardware

The hardware selected for the implementation of the thermal controller is described below:

a) PIC18F452 Microprocessor
b) Class 1, Single Core (0.2mm), Twisted, K type thermocouple wire
c) Analogue Devices 595C Thermocouple Amplifier

A brief description of each of the major design elements is given below.

4.1.1 PIC18F452 Microprocessor

The PIC18F452 Microprocessor was chosen for a number of different reasons which made it appealing as a development platform as will be discussed in the design. When working with temperature sensors (especially electronic) the output often takes the form of a low, analogue voltage. The device sensing the output voltages requires a sufficient resolution on the A/D converter to be able to accurately sample this voltage.

- The PIC 18F452 presents 8 available A/D converters at a 10bit resolution with the option of supplying both positive and negative reference voltages. Negative reference voltages are important should the sensors be required to measure temperatures below 0°C without the introduction of an offset. The introduction of a positive voltage signal allows the resolution of the A/D ports to be increased to in format: $resolution = \frac{V_{ref+}}{2^{10}} = \frac{V_{ref+}}{1024}$
- The standard operating frequency of the PIC18F452 is 4MHz with the option to enable clock multipliers to up the frequency to 16MHz which ensures more than sufficient operational capacity to do a number of complex calculations and sampling in the implementation of a thermal control algorithm.
- Two PWM control ports are present on the 18F452 with a 10bit resolution which allow for a number of possible variations in the duty cycle control signal.
- The PIC18F452 supports serial communications with the addressable Universal Synchronous Asynchronous Receiver Transmitter (USART) should any performance data need to be logged by a peripheral PC

The abovementioned criteria are drawn together in a design discussion in section *5.1 System Overview* and subsequent sections.

4.1.2 Thermocouple Transducer

The chosen thermocouple sensor was decided on as an IEC Class 1, K-type (chromel-alumel), single core (0.2mm), twisted thermocouple wire.

Table 4 - Thermocouple Specifications

Thermocouple Type	K
Wire Composites	Chromel-Alumel
Number of Cores	1
Core Diameter	0.2mm
Shielding	Twisted PTFE
IEC Tolerance Rating	Class 1
Tolerance	+/- 1.5°C below 350°C otherwise 0.4% of the current reading
Temperature Range	-40°C to 1000°C

This specific thermocouple wire was chosen for the following reasons:

- Single core of 0.2mm allowed for minimally invasive insertion of the joined tips into the microfluidic devices and channels.
- Twisted conductors aided (to some extent) the minimization of induced noise into the system.
- Class 1 tolerance allowed for the most accurate, obtainable readings present from thermocouple wires.

4.1.3 Thermocouple Amplifier

The need for a thermocouple amplifier arose from the fact that single, K type thermocouple transducers produce approximately 41µV/°C [36]. This is an extremely low voltage to measure, especially when working with a voltage range from 0°C to 50°C, with the maximum voltage being (approximately) 2.05mV at 50°C.

Taking the standard, 10 bit resolution of the PIC18F452 (with a default reference of 5V) a maximum resolution of 4.88mV is available. Stepping the quantization level down by making use of, say, 0.5V reference a resolution of 0.49mV is obtainable; which although sufficient to measure the values (without the presence of noise) only allows a quantization level of 4 (2 bits) at the 50°C signal making it impossible to obtain a 1°C sensitivity.

It was decided that the signal obtained from the thermocouple transducers would need to be amplified. For this purpose, the Analogue Devices AD595C thermocouple amplifier was chosen. This thermocouple amplifier offered a number of features:

- Pre-trimmed for K-type thermocouples
- Laser Wafer Trimmed to 1°C accuracy
- Internal Cold-Junction Compensation
- High Impedance Differential Input
- Linear, low impedance output voltage of 10mV/°C

The output voltage of 10mV/°C allowed for not only much higher voltages to be sampled by the microprocessor, but the fact that the voltage developed is linear allowed for a straight forward conversion from the sampled voltage to the measured temperature within 1°C accuracy. The output from thermocouples are not completely linear and including a device which caters for this and produces a linear output allows for significant simplifications in the low level design stages.

4.2 Development Criteria

The development criteria of the PCB for the high signal to noise ratio board had two major constraints imposed on it:

a) The output from the thermocouple and amplifier must be of sufficient voltage to be sampled by a 10 bit A/D Converter, with a sub 1°C achievable resolution.
b) The noise present on the signal line and power bus should not jeopardize the 1°C sensitivity of the system.

4.3 Implemented Solution

The noise present and signal integrity in any circuit is an important factor which is often taken for granted in circuit board designs and layouts. One of the key elements in ensuring the signal integrity and the reduction of noise at high frequencies is the inductance of the signal path on the digital plane of the board. This is not only important for the signal transmission lines (especially low voltage signals) but include that of the DC bus and power rails throughout the circuit.

In a closed loop the inductance is dependent on the loop shape, dimensions and geometry of the conductor itself. This introduces a number of different design principles in the routing of a PCB alongside the placement of the various components in an attempt to minimize the conduction path of the wires, or alternately change the geometry of the layout so as to minimize the closed-loop area created by the conductors.

The circuit diagram for the implemented solution can be found in *Appendix A – Supplementary Diagram, Diagram ii – Custom Developed PCB*.

The developed PCB (Fig. 19; below) was designed with noise minimization in mind and included thermocouple connectors and amplifiers for three thermocouple transducers. The microprocessor power, ICD-Interface, external clock and RS-232 interface system was implemented based on the recommended design from the Microchip® PIC guide [37].

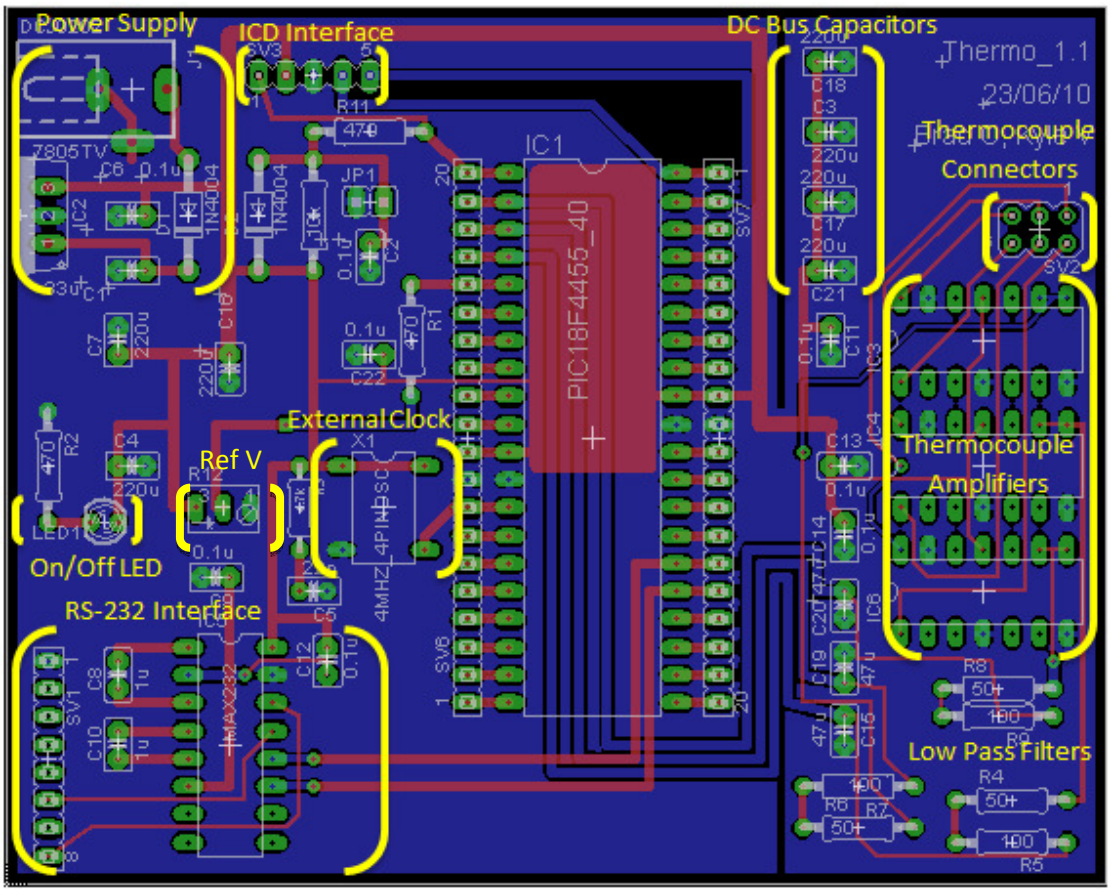

Figure 20 - Low Noise PCB Development

The above board (Fig. 19) was separated into two (bridged) ground planes. The left-hand plane for the high-speed digital electronics and the right-hand plane with the sensitive, slower analogue components. The justification for the separation of the power planes it outlined in *4.8 Separating Ground Planes*.

4.3.1 PCB Breakdown

A breakdown of the miscellaneous hardware used on the different sections of the PCB is given below. The relevant datasheets for the hardware can be found in the appendix.

Table 5 - PCB Components

PCB Section	*Hardware Breakdown*
Power Supply	LM7805, 5V 1A regulator
External Clock	EPSON SG-8002DC Programmable High Frequency Crystal Oscillator (4MHz)
RS-232 Interface	MAXIM Max220CPE Multichannel Driver/Receiver (only single channel used)
Board Power Indicator (On/Off LED)	5mm LED, Green
ICD Interface	Molex Pin-Header
Temperature Measurement Sensors	3x Analogue Devices® AD594C Thermocouple Amplifiers
Low Pass Filters	RC Filters with 22.5Hz cut-off
Reference Voltage (Ref V)	10kΩ Potentiometer to allow for adjustable reference voltage to the ADC Reference pin
DC Bus Capacitors	220µF Capacitor array placed between the DC Bus and ground planes

Power Supply

The selected regular (LM7805) provided a stable 5V source for the PIC18F452 Microprocessor with the capacity to supply 1A. The maximum draw of the implemented circuit is only 200mA, most of which is drawn by the power indicator LED. The 1A regulator, however, does allow for potential extension of the PCB to include more, less specialised functionality along with the temperature sensors.

RS-232 Interface

The MAX232 IC provided a serial interface to a PC to allow for communications and diagnostics. In this implementation the communication was in a single direction (from device to PC) sending all of the temperatures from the sensors to be logged by the PC.

Board Power Indicator

The LED on the board was connected directly to the 5V regulated supply to indicate that the board was powered.

ICD Interface

The ICD interface on the board was implemented using pin headers and RJ-12 cable. This allowed the processor to be programmed through a standard PIC® ICD/ICD2 without the removal of the chip from the board. This makes updating or changing code on the board a simple matter of connecting a cable.

Temperature Measurement Sensors

The thermocouple amplifiers and thermocouple connecters were placed on the analogue ground plane of the PCB. Three thermal transducers were chosen so that temperature measurements could be made (virtually simultaneously) at different points on the microfluidic cassettes.

Low Pass Filters

Low pass filters were implemented on the thermocouple signal lines using simple RC components in order to cut out any frequencies above 20Hz. No critical signals would be cut out by these filters since the response time of the thermal plant would be well below 10Hz.

Reference Voltage

The potentiometer was connected to the positive voltage reference of the A/D converter. This allowed the voltage quantization levels to be decreased by decreasing the reference voltage of the chip.

DC Bus Capacitors

An array of 220µF capacitors were placed on the analogue plane connected between the DC bus and the ground plane. These capacitors are used to attempt to keep the voltage from the DC bus on the analogue plane as stable and ripple free as possible. Any noise induced on the analogue plane has the potential to induce erroneous readings on the low voltage outputs of the thermocouple amplifiers.

The principles and techniques used for noise minimization in the development of the above mentioned PCB are discussed next.

4.4 DC Bus Noise Minimization

The inductance of a circuit board is, traditionally, the most difficult to quantify since it is a property of the closed loop current path throughout the board whereas capacitance and resistance of the board are not [38].

The inductance present in a circuit is calculated with the ratio of magnetic flux (Ψ) that passes through a closed path and the amplitude of the current (I) which causes the flux:

$$L = \frac{\Psi}{I}\,(H) \tag{3}$$

Noise on the power bus of a PCB due to high frequency switching and sudden changes of the current drawn are common problems. Not only does the noise compromise the signal integrity but is a potential source for radiating electromagnetic interference (EMI) [39].

The most common (and most flexible) method for noise reduction on the power bus is the use of discrete capacitors connected directly to the power bus lines. An alternative method used in the reduction of noise is the design of embedded capacitance into the PCB layout [40-42]. It has also been shown that PCB's with embedded capacitance built into the board have significantly damped resonance peaks in comparison with boards making use of the discrete component [43].

4.5 Capacitive Decoupling

One of the most commonly used and well known methods of decoupling busses, power rails and signal lines is that of capacitive decoupling and a number of different strategies exist.

4.5.1 Noise Reduction using Discrete Component Decoupling

Discrete capacitors used for decoupling take up large amounts of space on the surface of PCB's and their effectiveness is limited to (around) a few megahertz due to their own intrinsic inductance [44]. When using discrete capacitors (normally for low-frequency filtering) a number of different aspects need to be considered such as the value of the decoupling capacitors and their placement on the board.

4.5.2 Choosing the Decoupling Capacitor

The capacitor value chosen should reflect the current needs of the active device and be able to supply sufficient charge. Not only should the necessary capacitance be chosen, but it should also be ensured that the connection inductance present still allows the capacitor to respond quickly in the current demands of the active device [45]. The type of capacitor is also crucial to application of the PCB with some requiring much higher quality capacitors than what can generally be provided using standard electrolytic capacitors.

4.5.3 Guidelines for Placing Decoupling Capacitors

The placement of decoupling capacitors can be even more crucial than the value of the capacitors themselves depending on the type of board (single layer, 2 layer, multi-layer with power planes etc.). A number of useful techniques specifically focussing on capacitor placement on a standard 2 layer board were implemented [46]:

- At least one decoupling capacitor for each active device was provided and located as close to the device as possible.
- At least one bulk (> 1µF) capacitor was provided for each distributed voltage on the board.
- Local decouple capacitors were connected between the active devices ground and power pins.
- The loop area formed by the decoupling connections were minimized.
- Bulk decoupling on the board was provided near the point that the voltage is generated and the point where the voltage comes on to a separate plane of the board. .

Two decoupling capacitors with the same value are better than one with twice the value. Two capacitors have a lower overall inductance and provide better high frequency bus filtering [46]. However, on boards with closely spaced power planes (normally multi-layer) which take advantage of the embedded capacitance that this structure provides, it has been shown that the placement of decoupling capacitors is irrelevant and need not be located as close as possible to the active devices [46]. This board, however, does not take advantage of this and as such the capacitors were placed as close to the active devices as possible.

4.5.4 Determining the Decoupling Capacitor Value

The "Capacitance Ratio Approach" to determining the decoupling capacitance required on the board allows one to circumvent calculating the transient board currents directly by recognizing that high speed semi-conductor (CMOS) devices draw currents based on the capacitances of the board.

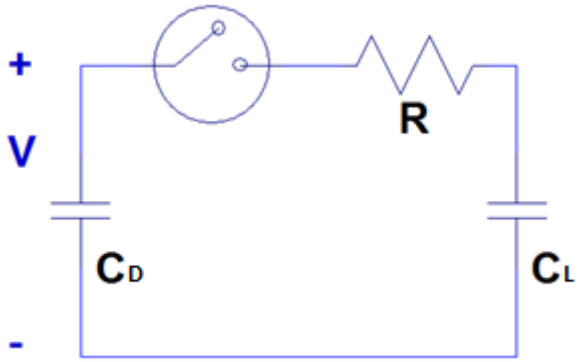

Figure 21- CMOS Model

The circuit above (Fig. 20) depicts a resistance R which includes the combined resistance and impedance of the component and bus as well as two capacitors, C_L the CMOS load capacitance and C_D the decoupling capacitor. Capacitor C_L draws current from the source once it is charged and C_D attempts to keep a constant voltage over the power bus. When the switch closes, C_L charges and this causes a slight dip in the power rail voltage. A higher ratio of C_D to C_L results in a smaller voltage decrease across the power bus.

The initial energy stored in the system is calculated from:

$$E_{initial} = \frac{1}{2} \times C_D \times V_i^2 \qquad (4)$$

Where V_i is the inital voltage across C_D. The energy dissipated in R in order to fully charge C_L is:

$$E_{dissipated} = \frac{1}{2} \times C_L \times V_f^2 \qquad (5)$$

Where V_f is the final voltage between C_D and C_L. Subtracting (5) from (4) and equating this to the total energy stored in the final state:

$$\frac{1}{2} \times C_D \times V_i^2 - \frac{1}{2} \times C_L \times V_f^2 = \frac{1}{2} \times (C_L + C_D) V_f^2 \qquad (6)$$

Solving for C_D in (6) yields:

$$C_D = \frac{2C_L}{\left(\frac{V_i}{V_f}\right)^2 - 1} \approx C_L \times \frac{V_i}{\Delta V} \qquad \text{for } \Delta V \ll V_i \qquad (7)$$

Where ΔV is the change in voltage ($V_i - V_f$). This equation suggests that the decoupling capacitance value should be set to the device capacitance times voltage power bus divided by the maximum allowable noise on the bus [47].

Example:

C_L is typically 400pF for the bus capacitive loading of the PIC18F452 and specifying a maximum allowable ripple of 1mV and a 5V supply:

$$C_D \approx C_L \times \frac{V_i}{\Delta V} = (400pF) \times \frac{5V}{1mV} = 2\mu F \qquad (8)$$

4.5.5 Embedded Capacitance Decoupling

The inherent capacitance present between the power and ground planes on PCB's also provides for decoupling, however, the capacitance is generally considered to be too small to be considered beneficial. The implemented board contained a single power island located above the ground plane just underneath the microprocessor. It has been shown that capacitance values of up to 10nF can be achieved using this methodology which eliminates the need for the discrete counterparts which generally have a poorer performance over a wide frequency range whereas the embedded capacitance in boards has been shown to be effective up to frequencies of 5GHz [39]. These implementations, however, generally require an entire layer dedicated to the power plane in order to achieve any form of reasonable capacitive decoupling. Even so, capacitance values of greater than 1µF are still needed on boards with embedded capacitance structures to reduce low-frequency noise.

4.6 DC-Bus Impedance and Noise Relationship

The power bus noise voltage at one point in the PCB can be calculated using the formula:

$$V_{noise} = I_{device} \times Z \qquad (9)$$

Where Z is the impedance between the power bus and the component [43]. This above equation shows that the key to the reduction of noise on the power bus lines is the reduction of the total transfer impedance between the components at their respective frequencies.

4.7 Reducing Noise Using Power Islands

Digital devices draw spiking currents from the supply when switching at high speeds. These current spikes result in voltage spikes on the power bus. In theory, gaps between the analogue and digital supplies on the board can help prevent spikes on the supply bus from spreading from the one section to the other. This helps minimize the noise created by the digital components affecting the operation of the analogue components.

One of the common methods of preventing the noise created on one supply to spread is to isolate the supply voltages on the different sections of the board – known as isolated power islands. With the absence of any direct connection between the two supplies (bridged islands) the only mechanism for noise to spread to a subsequent source is the electric field coupling across the gap [48].

Isolated power islands are not an easy, effective method for reducing the noise present on the power bus. This technique can be used for a low cost means of eliminating some of the noise on the power bus, however, only if extremely well designed. Even with an exceptionally good design, it has been shown that isolated power islands are completely ineffective at certain frequencies [48]. The more popular, more effective method of reducing the overall noise present in a PCB is the separation of the ground plane via gaps (bridged islands) rather than the power planes – especially on two layer boards.

4.8 Separating Ground Planes

Any signal from a component on a PCB creates a return current which flows through the ground plane. This current chooses the path of least resistance at low frequencies and the path of least inductance at higher frequencies. These currents attempt to create a return path directly under the signal track.

An important routing technique in the PCB design when looking for a low noise system is separating the ground planes into separate analogue and digital plane sections. The two grounds are essentially connected together at some bridging point, however, separating the analogue and digital current returns paths through the ground plane aids in eliminating noise with return currents not being 'mixed'.

The simplest method of separating ground planes is to create a 'gap' in the PCB routed ground plane which has a non-conductive isolation (i.e. no conductive plane) between the ground planes with a bridge in the middle that subsequently connects the two. This allows for effective placement of the high speed, digital components on the digital plane, and the slower input/output components on the analogue plane which allows the return currents of the two to be separated.

Return currents from a component attempt to run directly below the trace along the same path which they were conducted. Creating cuts in the ground planes causes the return currents to deviate from the conducted path in an attempt to return back to the component – often creating large loop areas. When creating a gap in the ground plane it is essential to eliminate large return-current loop areas. Routing tracks over the ground separation gap is a large source of radiated and absorbed energy since the loop area created by the return current effectively acts as a virtual antenna as illustrated by the figure below (Fig. 21) where the conducted currents on the power plane are shown in green and the return currents on the ground plane in red.

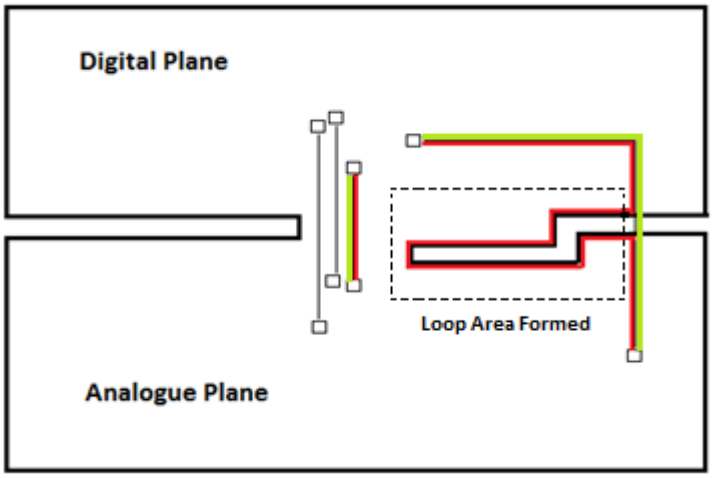

Figure 22 - Ground bridge loop currents

Another issue which arises when the outgoing and return currents are forced to diverge from each other is the increase in the path impedance, and as seen from (9) where the noise is directly proportional to the bus impedance present in the system. If connections between the two sections of the PCB need to be made then tracks should run over the connecting bridge between the ground planes which allows for a direct-path return current to fall directly under the trace without creating a looped current-return path.

Without a low impedance ground plane it is exceptionally difficult to minimize the parasitic effects of unwanted inductance and resistance – especially at high frequencies [49]. This does not mean that the ground plane cannot be cut to allow for tracks to be routed along this plane, however, adding tracks to the ground plane causes a more complex path for the return currents to follow and increases the chances that larger

return-current loop areas will be formed hence increasing the total ground plane impedance. Tracks in the ground plane were minimized in this implementation with the only major breach of this being the slow changing analogue lines connected to the A/D converters of the PIC for the temperature measurements.

The illustration below (Fig. 22) shows all connections to the power bus highlighted in yellow with the return current paths in red. Evaluating the return path currents, a minimal loop area is formed.

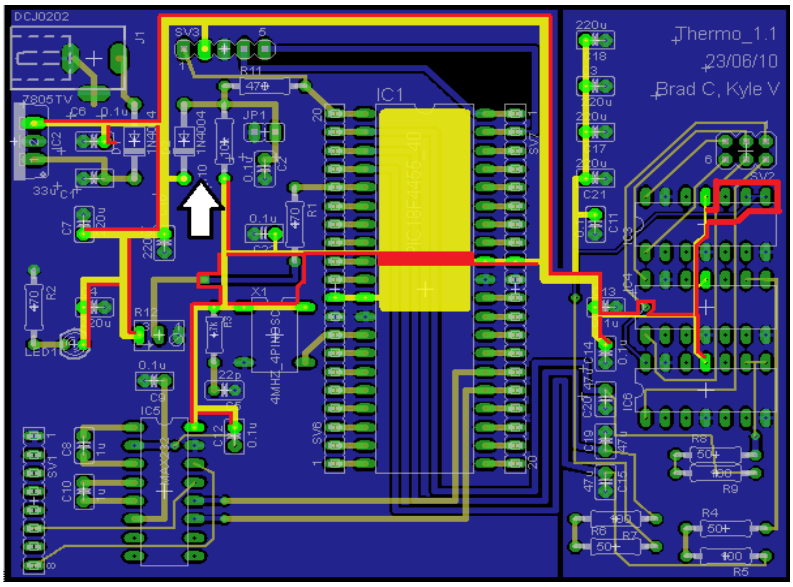

Figure 23 - PCB with power bus (bright yellow), ground plane (blue) and return current paths (red)

An error, however, has been made in the initial routing (indicated by the arrow above in Fig. 22). These two points should actually be connected together – since both connect to the power bus. Neglecting to connect these two points leads to a much longer return current path across the board rather than directly back to the source. This was included in this discussion so that the difference in the loop size could be shown as well as its effect on the overall inductance.

The illustration below (Fig. 23) shows the correction to this now having the two points connected together allowing for a much shorter return current path without having to traverse across the power plane and to the opposite side of the board. The shortening of this path significantly reduces the total inductance (shown in *4.11.1 – Measurement of the Path Inductance* to be a 44.6% reduction) as seen by the connection pins.

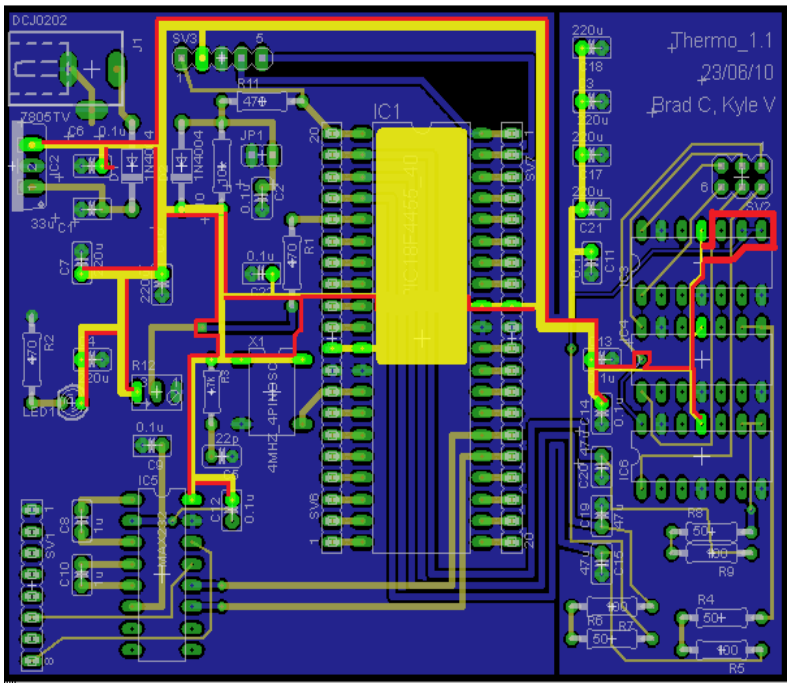

Figure 24 - Altered PCB with power bus (bright yellow), ground plane (blue) and return current paths (red)

4.9 Low-Pass Filter Implementation

The developed board was designed in such a way as to attempt to minimize as much noise as possible not only from the signal lines but noise generated from the power bus as well.

In order to reduce the noise picked up by the thermocouple wire acting as an antenna as well as the noise injected by the supply a basic RC low pass filter was implemented between the thermocouple amplifiers and the A/D port on the microprocessor (Fig. 24).

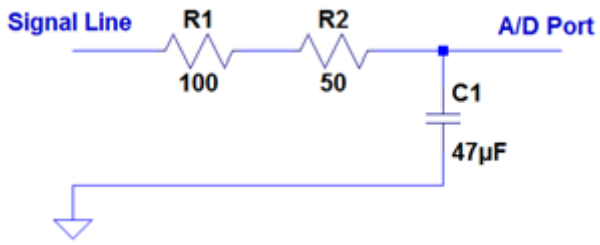

Figure 25 - RC Filter

The design of the RC filter was implemented using a cut-off frequency of 22Hz (-3dB) to eliminate any higher noise frequencies. The low pass filter can be implemented between the thermocouple amplifiers and the A/D ports on the microprocessor since the PDMS is a thermally 'slow' material and changes to the temperature will be in the region of < 1 Hz.

The frequency response and phase diagram for the implemented RC filter are shown *Appendix A: i. Bode Plot of RC Filter*. The implemented filter yields a 10dB signal attenuation at 50Hz which aids in eliminating residual noise from laboratory equipment, lighting, plugs and other such potential EMI noise emitting sources.

4.10 Noise Characterization of Developed PCB

In order to characterize the levels of noise present on the DC of the designed solution, the following methodology was employed to evaluate the overall bus design.

4.10.1 Methodology: Characterizing the DC Bus

One of the simplest methods for calculating the inherent inductance, capacitance and resistance as seen by the components connected to the power bus is described below:

1. Short the power supply
2. Remove all IC's
3. Connect a 50Ω terminated function generator to the +V and GND pins of a selected IC*
4. Set the frequency above 100kHz and to a square wave.
5. Set the amplitude to a known value.
6. Connect the oscilloscope probes to the function generator probes.
7. Evaluate the waveforms as described below.

* The probe connections for oscilloscope should be connected as close to the board as physically possible. A slight displacement on this can significantly increase the inductance results. An example of this can be seen in Fig. 28.

4.10.2 Equivalent Circuit Model

For the purposes of this evaluation we are looking to model the DC bus connected to each individual IC as a basic RLC series circuit connected to a current source. The circuit below (Fig. 25) depicts a current source with a 50Ω impedance connected to a bus which is being modelled as a RLC circuit. The voltages being measured throughout the evaluation is the potential between points *a* and *b* which is the point where the current source is connected to the power and ground pins of the IC respectively.

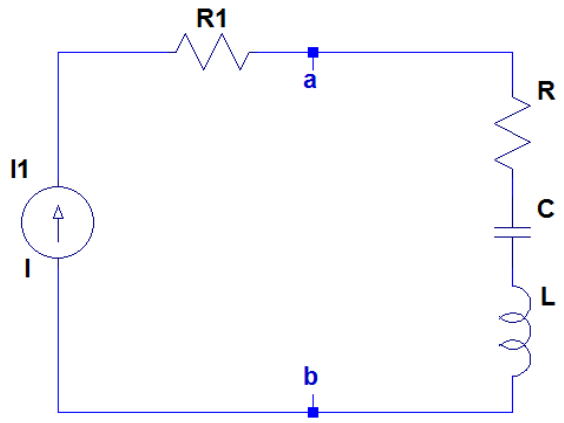

Figure 26 - Equivalent RLC Bus Model

The characteristics are to be calculated are:

i. The bus impedance (Z_{xy}); depicted above as *R*.
ii. The bus inductance (L_{xy}); depicted above as *L*.
iii. The bus capacitance (C_{xy}); depicted above as *C*.

Where Z*xy* denotes the impedance between the power bus and the selected IC.

4.10.3 Connecting the Function Generator to the IC Power

By connecting the function generator probes to the power pins of a selected IC (which must be repeated for all IC's to measure the path impedance, inductance and capacitance individually) on the power bus which has been shorted, the function generator acts as a current source instead of a voltage source. The voltage source now acts as a current source since it is connected to a short circuit and no voltage can be generated across the short. The current being supplied to the circuit is essentially:

$$I_{supplied} = \frac{V_{amplitude}}{50\Omega} \quad (10)$$

4.10.4 Essential Equations

From first principles the basic equations for calculating component capacitances and inductances can be obtained from:

$$i = C\frac{dv}{dt} \quad (11)$$

And

$$v = L\frac{di}{dt} \quad (12)$$

4.10.5 Calculating the path inductance

From the equivalent RCL model depicted (Fig. 25) an inductor in series with a switching current source is present. Inductors are known to oppose change in currents just as capacitors do to changing voltages. From this the path inductance can be easily calculated since the only factor which will be limiting the rise/fall time of the current is the function generator itself.

The following waveform is obtained as in Fig. 26 (below).

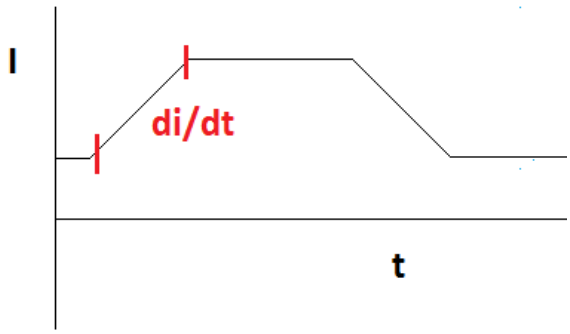

Figure 27 - Current Source Waveform

Using (12) the inductance can be calculated:

$$L_{xy} = \frac{v}{\left(\frac{di}{dt}\right)} \quad (13)$$

The only missing value from the above equation is the value of the voltage *v*. This voltage is NOT the amplitude of the waveform as set on the function generator but the peak voltage of the spike caused by the inductance in the system when the source 'current' switches from positive to negative, (V_{ab} from Fig. 25) as shown in Fig. 27 below.

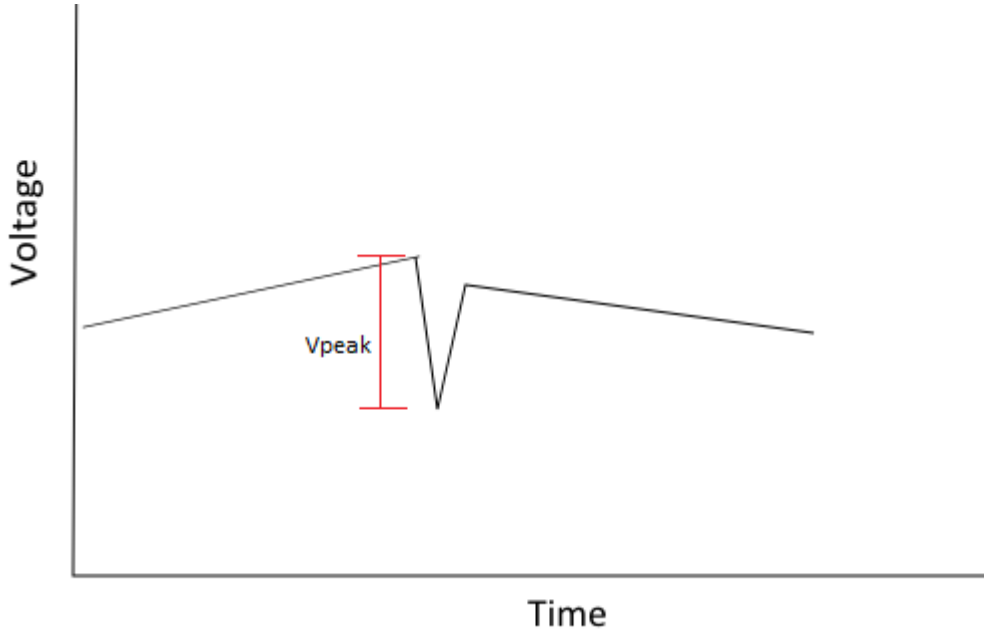

Figure 28 - Expected voltage waveform showing inductive spikes

The size of the voltage spike is representative of the inductance present in the system hence the higher the spike, the higher the inductance.

It must be noted that amplitude of this spike changes significantly based on the height of the actual probes connected above the PCB which makes it vital that the measurement is taken with the probes as close to the surface of the point of measurement as physically possibly to obtain accurate results.

The connection illustration has been included (Fig. 28) to represent how the probes were placed for the purposes of these measurements. The measurements are crucial on the placement of the *oscilloscope* probes being close to the surface and much less critical are the function generator connectors. Wire extensions were soldered onto the IC pins to allow for easier connection.

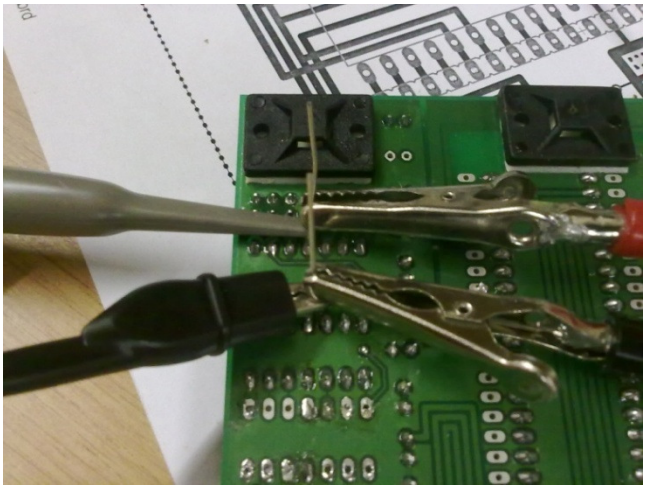

Figure 29 - Measurement connection taken as close the to the surface of the pins as possible

4.10.6 Calculating the path capacitance

Similarly for the capacitance in the equivalent circuit model the only factor limiting a rising and falling voltage in the circuit would be the present path capacitance between the selected IC and the power bus. This makes is easy to calculate the capacitance from a waveform depicted below (Fig. 29):

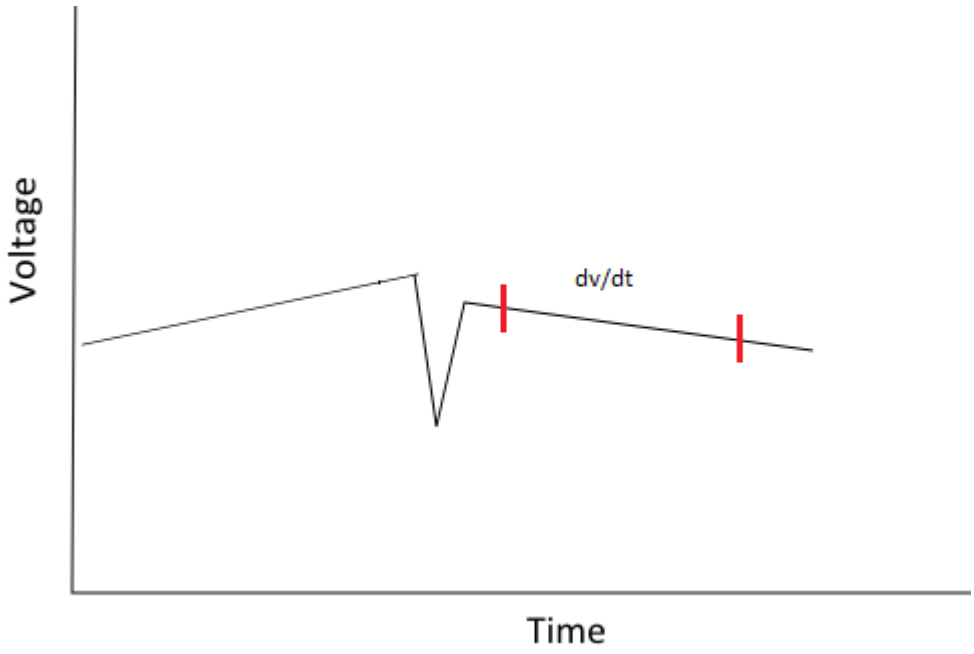

Figure 30 - Gradient of the voltage waveform

The gradient, although depicted linear in the figure above is actually an RC curve with and in order to solve for C to find the path capacitance which is represented by:

$$y(t) = A(e^{-t/RC}) \quad (14)$$

The gradient of the graph (Fig. 29) is not visible at high frequencies since, theoretically, an infinite capacitance is present in a short circuit. No matter the charge or current injected into the circuit under short, no change in voltage should be observed hence high capacitance values are expected to result.

4.10.7 Calculating the path impedance

Referring to the equivalent circuit model (Fig. 25) the only component left to be solved for is the path resistance between the component and the DC-Bus. This value is calculated from the voltage difference (or the level shift) between the two waveforms (Fig. 30; below):

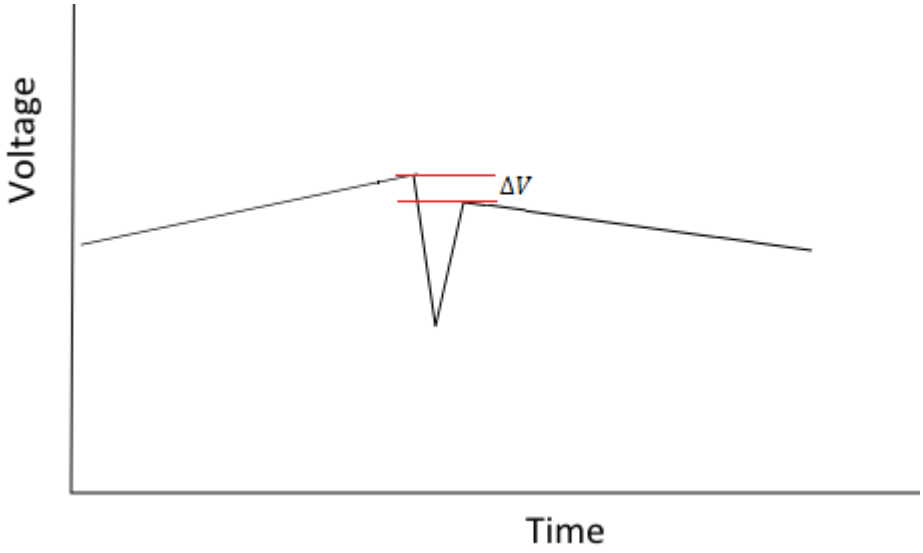

Figure 31 - Voltage level shift indicative of bus resistance

Measuring this voltage and applying it in (9) results in:

$$R_{xy} = \frac{\Delta V}{I_{supplied}} \qquad (15)$$

4.11 DC-BUS Characterization Results

The developed board makes use of a single bridged power island, bridged analogue and digital ground planes, and wide DC bus tracks to minimize the overall resistance as well as an embedded capacitance structure placed directly under the microprocessor.

Two points were used for the measurements on this board – the first being the power pins of the PIC processor on the digital plane and the second being the power pins of a thermocouple amplifier situated on the analogue plane on the opposite end of the board to the power source.

4.11.1 Measurement of the path Inductance

From the function generator the following waveforms are measured in order to determine $\frac{di}{dt}$ and Vpeak (Fig. 31):

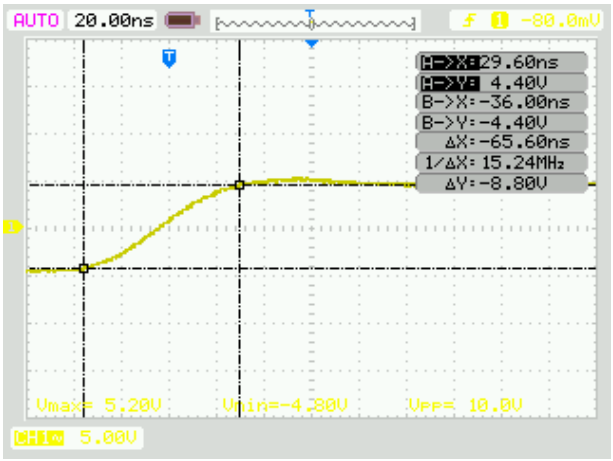

Figure 32 - Current waveform rise time and gradient

And the voltage peak caused by the inductance present in the board to be (Fig. 32):

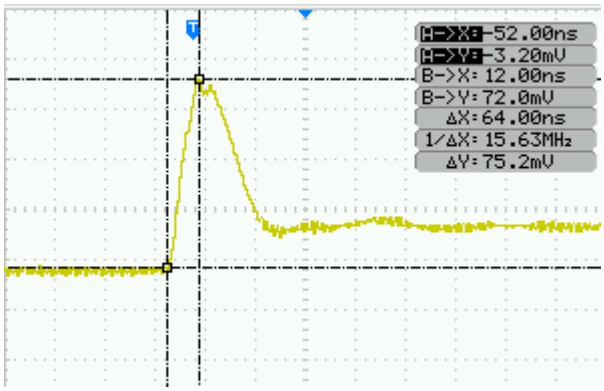

Figure 33 - Inductive voltage spike

From the above graphs (Fig. 31-32), calculating the gradient of Fig. 26 using (13) the path inductance for the thermocouple amplifier (located on the analogue plane to the far right of the board) to be:

$$L_{thermocouple\ amplifier} = 682pH$$

Similarly for the PIC processor, evaluating the inductance for the cases mentioned in *4.8 Separating Ground Planes* where an evaluation of different path lengths is presented, the first being the longer path through the power island, the second being the direct path to the source. A significant difference in the inductive peak voltage spikes is found:

$$V_{inductive\ (long\ path)} = 65.1mV$$

$$V_{inductive\ (direct\ path)} = 29.6mV$$

And yielding respecting inductive values of:

$$L_{(long\ path)} = 426pH$$

$$L_{(direct)} = 190pH$$

Which is a sizeable reduction (44.6%) in the overall path inductance.

The low inductive values also help in the minimization of the noise created under high switching conditions with the rise time of 10ns yielding a knee frequency of 50MHz and an overall inductive impedance of 0.21Ω at this frequency.

4.11.2 Measurement of the Impedance

The impedance of the bus is determined using the change in voltage levels (Fig. 33) before and after the spike using (15) and knowing the source current (from the 50Ω terminated generator with a 10Vp-p) to be 200mA.

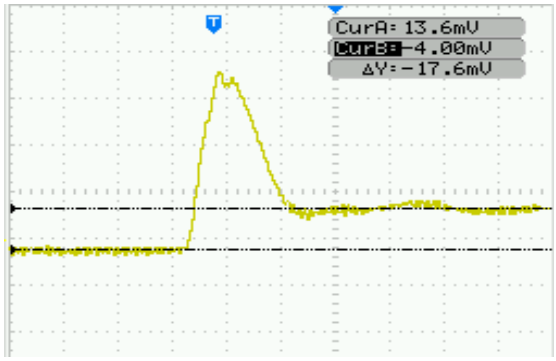

Figure 34 - Level shift in voltages

The path impedances are found to be:

$$Z_{thermocouple\ amplifier} = 0.12\Omega$$

$$Z_{PIC\ (direct\ path)} = 0.052\Omega$$

4.11.3 Measurement of the path Capacitance

The measurement of the path capacitance yielded no discernable gradient on the voltage waveform between the spikes at a frequency of 100kHz. In order to measure the gradient of this (since there is not technically an infinite capacitance) stepping the frequency down to a lower level (4kHz for example) allows for a clearer gradient to be found (Fig. 34).

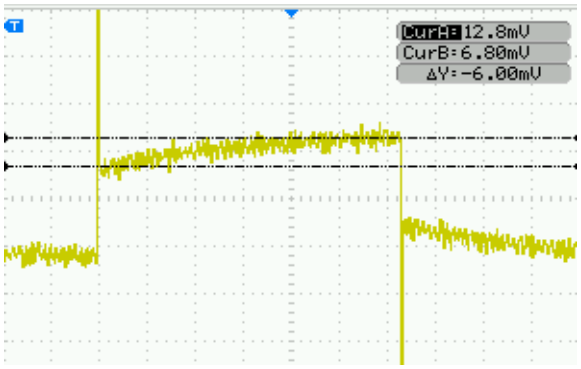

Figure 35 - Gradient of the voltage waveform (4kHz)

The curve of the above image may initially appear linear; however, is actually a typical RC charge curve. In this case, the resistance is the inherent resistance of the board which was calculated previously. Modelling the above graph as decreasing (as it would on the negative cycle) rather than increasing the known standard RC discharge would be:

$$y(t) = A(e^{-t/RC}) \quad (16)$$

Where *A* is the peak from which discharge occurs. Knowing 2 distinct points, say y_1 and y_2 and taking the ratio of the two solving for C:

$$\frac{y_1(t)}{y_2(t)} = \frac{Ae^{-t_1/RC}}{Ae^{-t_2/RC}} \quad (17)$$

$$ln\left(\frac{y_1(t)}{y_2(t)}\right) = ln\left(\frac{Ae^{-t_1/RC}}{Ae^{-t_2/RC}}\right) \quad (18)$$

Since the only unknown is C, solving yields:

$$C = \frac{(t_2 - t_1)}{R \times (\ln(y_1(t)) - \ln(y_2(t))} \quad (19)$$

Substituting the respective values for the amplitude with the time difference being 126µs in both cases and bus impedances of both the PIC and thermocouple amplifier, the capacitance is found to be:

$$C_{thermocouple\ amplifier} = 2.38mF$$

$$C_{PIC} = 3.83mF$$

This calculation cannot be thought of as a real capacitance; it is more of an indication of the stiffness of the system.

4.11.4 Evaluation

Comparing the stability of the signal between the Microchip PICDEM2 board and the custom developed temperature logging board, a significant reduction in overall signal oscillation is observed. The results were taken with both boards being supplied with the same 9V regulated supply so as to keep the noise injected by the power supply to the boards as consistent as possible.

The A/D converters on the PIC Microprocessors allow a predefined port as a reference voltage from which all of the other ports will be scaled to in a 10-bit quantization resolution. For the purposes of this application only one (positive) reference voltage was required since the temperature range to be measured would always be a positive temperature.

The signal voltage measured on the A/D ports should never exceed the reference voltage. Any voltage on the A/D ports greater than or equal to the reference voltage will be shown as “full-value” (i.e. 1023/1023) upon internal conversion by the processor. The isothermal amplification system requires a constant temperature of 41°C and so an assumption is made that the measured temperature can never exceed 60°C. This assumption is valid since the peltier heating element will actively pump heat away from the heated system in order to maintain a temperature of 41°C should the temperature ever exceed this.

Taking the assumption that the absolute maximum temperature to be measured may – under critical failure- reach 60°C the reference voltage for the A/D converters can be adjusted to 600mV and give a lower voltage quantization level of:

$$quantization\ resolution = \frac{reference\ voltage}{bit\ resolution} = \frac{0.600}{1024} = 586\mu V \quad (20)$$

For the measurements recorded below the development area available on the PICDEM2 board was used which required additional wires being soldered onto the board and running across multiple traces (over multiple layers) to reach the development area creating large current loop return paths.

4.11.5 PICDEM2 Plus

For the evaluation of the PICDEM2+ board low noise values are present which would (most likely) be considered negligible in other applications. The oscillation present on the signal line produces a pronounced 5mV (average) oscillation above and below a mean value with the highest oscillation recorded at 14mV (Fig. 35). Normally a 5mV oscillation on a signal may be deemed acceptable, however, in this application 10mV equates to 1°C and a 5mV oscillation introduces a 50% error to every reading in a system with a required 1°C tolerance.

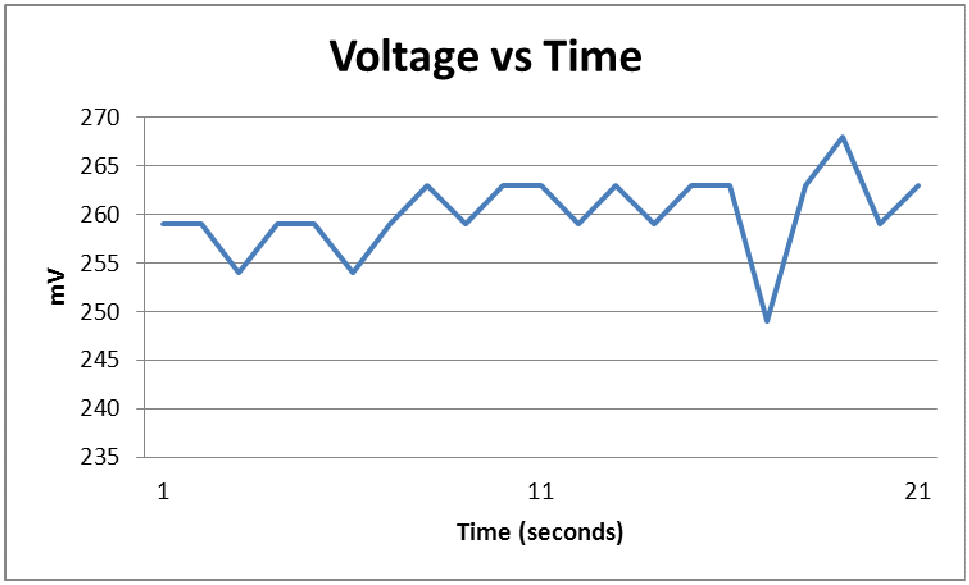

Figure 36 - PICDEM2 Plus - Recorded Voltages

One method of reducing the oscillations in the code of the microprocessor is to average the values and it is important to note that the above oscillation was present in spite of sampling and averaging 20 readings per value.

Calculating the signal to noise ratio (SNR) for the system having the signal being 10mV and the induced noise in the system being 14mV results in:

$$SNR = 20\log_{10}\left(\frac{A_{signal}}{A_{noise}}\right) \quad (21)$$

The evaluation above results in a signal to noise ratio (SNR) of -2.9 showing that the noise present in the system is of greater value than of the actual signal. The exceptionally poor SNR present with this configuration of the PICDEM2 board resulted in it being unusable as a reliable measurement device for this application.

4.11.6 Custom Developed Temperature Sensing Board

A significant reduction in signal oscillation can be seen on the custom developed board. The maximum recorded voltage oscillation being 3mV (translating to 0.3°C) in the recorded sample. The custom developed board exhibits a much lower overall oscillation on the signal line as well as higher signal stability (Fig. 36).

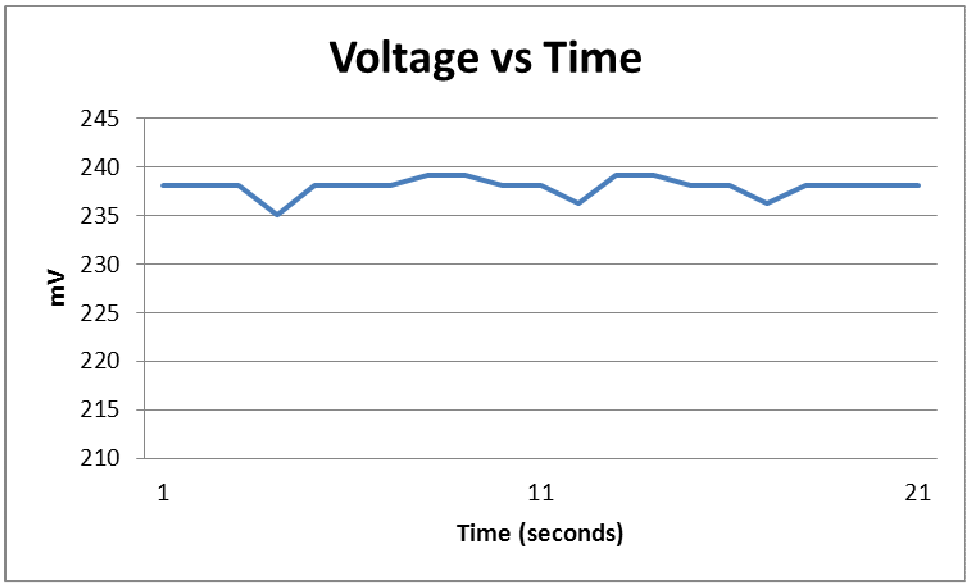

Figure 37 – Custom Developed PCB – Recorded Voltages

The SNR on the custom developed board improves to a value of 10.5 with the new maximum oscillation being recorded as 3mV. The improvement on the noise ratio between the maximum noise measured on the PICDEM2 board (14mV) and the custom developed board's maximum oscillation (3mV) shows a 78.5% reduction in the noise present.

4.11.7 Conclusion

Intuitively the components with the longest current path to and from the source are expected to have higher impedance values on the bus than those which are situated nearby – an assumption validated in the results. The thermocouple amplifier chip placed on the opposite end of the board to the supply exhibits twice the path impedance than the PIC processor does.

The PIC processor power line situated a few centimetres from the supply voltage has an large power island (with embedded capacitance) to draw required currents from whereas the thermocouple amplifiers have a much narrower bus from which the power is drawn at the opposite end of the board from the source and exhibit (approximately) 3 times more inductance along the path.

The overall bus impedance is quite low to the components and this can be attributed to the relatively small board size as well as the intentional design to create wide conductive tracks on the PC board in order to minimize the resistance.

High inherent capacitance values were measured (above 2mF) – as was expected since, in theory, a short circuit exhibits an infinite capacitance.

The inductances calculated for the respective paths on the board are relatively small values, the highest of which being 690pH. This shows that the board has a good design against susceptibility to EMI and external noise being picked up in large loop-current areas as well as protection against the generation of internal noise due to excessive looped paths.

The overall reduction in signal noise (78.5%) of the developed board as compared to that using the PICDEM2 Plus board shows that the implemented techniques were successful in minimizing the overall noise present in the system quite significantly.

Recommendations relating to this design would include a deeper investigation into the reduction of the path length of the bus across the board, possibly by relocating the ground plane bridge area towards the top of the board cutting out almost an entire half board width across which the power bus has to run in an attempt to lower both the bus resistance and inductance.

5. MINIATURIZED NUCLEIC ACID AMPLIFICATION SYSTEM

This chapter serves to introduce the interfacing and data flow present in the developed system, including a brief evaluation of some of the components and subsystems developed. The development of the temperature controller (from a hardware perspective) was presented in the previous chapter (*Chapter 4 – Temperature Controller and Transducers*). This chapters aims to present more of a data flow between the developed sub-systems from sensing to controlling the temperature and how each stage links to the next alongside any errors which may propagate through the system components.

5.1 System Overview

A brief system overview is presented below describing the overall function of the system as a whole (Fig. 37):

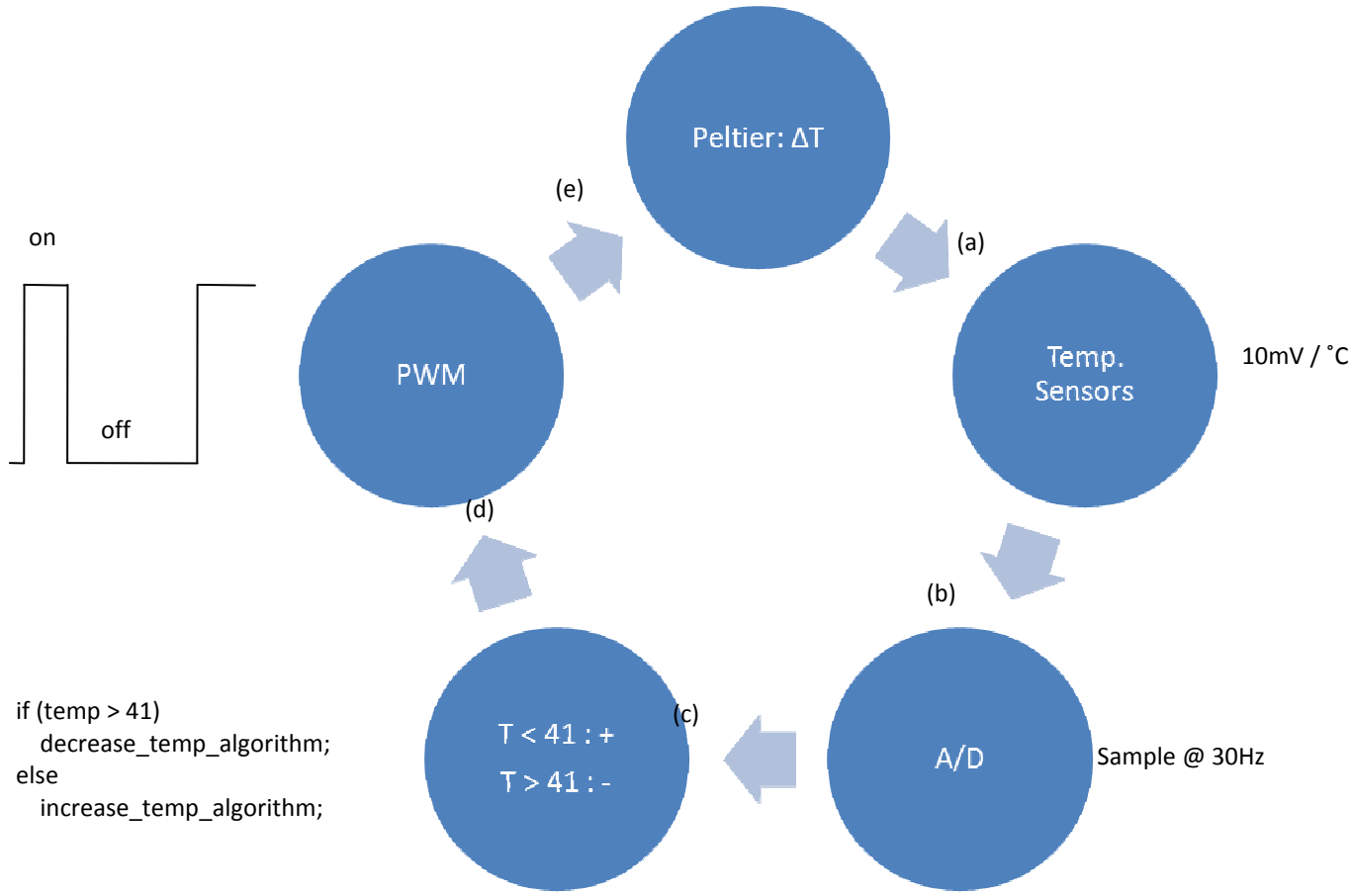

Figure 38 - System Flow Diagram

Stage:

a) The current temperature is measured by the thermocouple transducer and amplified by the respective thermocouple amplifier giving a linear progression of 10mV/°C
b) The temperature-representative voltage is sampled by the A/D ports on the microprocessor and converted back to a semantic temperature measurement which is passed to the control algorithm.
c) The control algorithm checks the temperature to see if the system needs to be heated or cooled and calculates the extent of the required heating / cooling.

d) The PWM controller converts the required heating or cooling value into a duty cycle ratio and – using the PWM ports on the microcontroller – applies this duty cycle to the conduction pins of the peltier.
e) The peltier device conducts in the applied duty cycle ratio (at the frequency set by the PWM controller) and a new temperature is then measured beginning the process again.

Each stage (a-e) is expanded below describing the data flow, function and possible introduction of measurement errors.

5.1.1 Temperature Sensors

The entire process starts in thermal equilibrium with the environment at room temperature at which point a voltage is generated across the thermocouple wire due to the Seebeck effect [3,50]. This voltage is conducted into the respective chromel-alumel inputs of the pre-trimmed K type thermocouple amplifier and amplified according to the internal configuration which yields an output of 10mV/°C.

Result errors in the system may be induced from the thermocouple wire, thermocouple amplifiers and the noise present on the DC bus. The thermocouple used is a class 1 K type thermocouple wire which has a tolerance of 1.5°C. The chosen thermocouple amplifier (AD594C) has a tolerance of 1°C and the noise induced on the DC bus is in the order of 0.2°C (after temperature conversion).

Table 6 - System Tolerances

Error Source	Maximum Error Value
Thermocouple Wire	+/- 1.5°C
Thermocouple Amplifier	+/- 1°C
Induced Noise	+/- 0.2°C
Maximum Possible Noise Induction	+/- 2.7°C

The possibility of having a temperature measurement which is only within a 2.7°C may be sufficient for many applications which do not require such a strict accuracy on the actual temperature measurements (which is the normal application of thermocouple wires), however, is insufficient in a system which requires a 1°C tolerance.

Fortunately 2.7°C is the maximum possible error value which will not be present on most readings. Careful calibration to track the (repeatable) performance of the thermocouple wires and amplifiers and sample averaging to eliminate induced noise in the system is able to minimize the total tolerance to within acceptable limits of 1°C which is shown later.

5.1.2 A/D Converters

The voltage generated by the thermocouple amplifiers is conducted along the A/D ports of the microprocessor and sampled at 30Hz. The 10bit resolution of the A/D ports making use of a 0.6V reference allows for a maximum quantization error of 586µV (approximately 0.06°C). A 0.6V reference was chosen since the steady state operating temperature of the system should be 41°C. For this reason, the maximum measurable temperature was selected to be 60°C (or 0.6V). Any temperature above this reference would saturate the A/D conversion; however, this was not an issue since the temperature of the probe controlling the heat flow would not be required to reach this point.

5.1.3 Control Algorithm

The control algorithm (discussed in detail in *Chapter 7 – Thermal Controller*) action is based upon the average measured temperatures by a selected temperature sensor or group of sensors. The control algorithm averages a number of samples in order to minimize any induced noise in the system. The algorithm determines in which direction the peltier is required to conduct – be it forward biased to heat the sample, or reverse

biased to cool the sample down again (or any combination thereof). The extent to which the heating or cooling is needed is determined by the PWM control.

5.1.4 PWM Control

The PWM control cannot be intrinsically separated from the control algorithm since it is the most crucial aspect of the controller. The extent to which the heat can be controlled, altered and held stable determines the success or failure of the entire system.

The PWM control determines the extent to which the peltier induces heat into the sample. It does not, however, determine the extent to which the peltier is biased. The peltier – to allow for normal conduction – must be correctly biased at all times. The PWM control, however, alters the time periods that the peltier conducts in order to manipulate the temperature by controlling the induced heat rate in a controlled manner.

5.1.5 Peltier Heating / Cooling

The peltier device conduction periods are determined by the duty cycle ratios as calculated by the PWM controller. The peltier can conduct in both forward and reverse directions (manipulated by an H-Bridge discussed in *Chapter 7.1 – Switching Circuit*). Having, essentially, the ability for both heating and cooling allows for higher levels of flexibility and temperature ramping in the controller.

5.1.6 RS-232 Interface

The RS-232 interface is not included in the functional diagram since it does not play a role in the functioning or data flow of the system. This interface allows for peripheral logging of the temperatures measured from all of the current temperature sensors, however, no processing to control the system is done from the transmitted RS-232 data. All processing is done on the chip with the temperatures measured from their respective sensors being sent off board for data and performance analysis.

5.2 System Calibration

As mentioned earlier the overall system tolerance of the combined hardware resulted in a possible error of 2.7°C in each recorded temperature measurement. The application of this research required a minimum of 1°C sensitivity in the temperature measurements in order for the isothermal amplification system to function optimally. In order to reduce (and eliminate) some of the uncertainty present throughout the hardware performance the system was calibrated using a Fluke 5520A Multifunction Calibrator.

5.2.1 Calibration Procedure

The developed PCB was connected to the Fluke 5520A calibrator and a number of different temperatures increments were applied and the results recorded. This was conducted on two separate occasions in order to determine the repeatability of the results. All three of the thermocouple sensors were tested individually with the system averaging 20 samples per reading. The results were captured over the RS-232 PC interface and the performance of the three sensors is shown below:

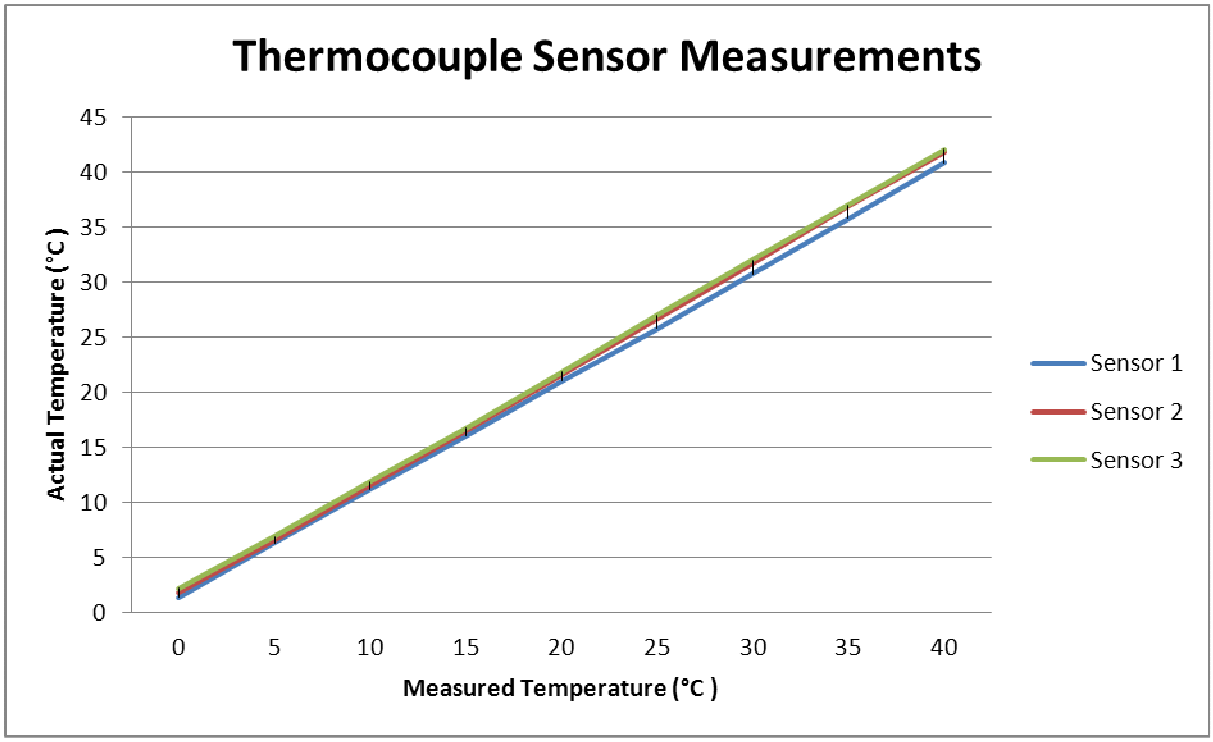

Figure 39 - Sensor Calibration Performance

From the above graph (Fig. 38) the output from the thermocouple amplifiers is shown to be linear with very little deviation between the results of any sensor. A slight offset of just over 1°C was apparent on all of the thermocouple amplifier outputs which were verified over a number of different measurements.

5.2.2 Calibration Results

The results from the calibration of a single thermal sensor are presented below in tabular form displaying the raw data measured from the RS232 interface along with a comparison of the calibration setting and the deviation.

Table 7 - Thermal Calibration (1st Calibration)

Calibration Temperature (°C)	Sensor 1 – 1st Calibration	Difference (°C)	% error
0	1.31	1.31	inf
5	6.56	1.56	31.20
10	11.61	1.61	16.10
15	16.42	1.42	9.47
20	21.58	1.58	7.90
25	26.48	1.48	5.92
30	31.67	1.67	5.57
35	36.71	1.71	4.89
40	41.81	1.81	4.53
45	46.28	1.28	2.84

In order to ensure repeatability a second calibration of the controlling thermal sensor was performed on a different day. The recorded results are tabulated below.

Table 8 - Thermal Calibration (2nd Calibration)

Calibration Temperature (°C)	Sensor 1 – 2nd Calibration	Difference (°C)	% error
0	1.26	1.26	inf
5	6.41	1.41	28.20
10	11.26	1.26	12.60
15	16.22	1.22	8.13
20	21.27	1.27	6.35
25	26.27	1.27	5.08
30	31.37	1.37	4.57
35	36.57	1.57	4.49
40	41.54	1.54	3.85
45	46.45	1.45	3.22

A comparison between the calibration data is shown below with the recorded temperature differences being highlighted.

Table 9 - Calibration Comparison

Calibration Temperature (°C)	Calibration 1	Calibration 2	Recorded Difference (°C)
0	1.31	1.26	0.05
5	6.56	6.41	0.15
10	11.61	11.36	0.25
15	16.42	16.22	0.2
20	21.48	21.27	0.21
25	26.48	26.27	0.21
30	31.67	31.47	0.2
35	36.71	36.57	0.14
40	41.81	41.54	0.27
45	46.28	46.45	-0.17

5.2.3 Thermal Drift Errors

The thermocouple amplifiers (AD594C) were used specifically since these chips have internal cold junction compensation (CJC). The CJC of the chips makes use of the current temperature of the chip as the reference for this calculation. The data sheet specifies that no more than a 0.6°C drift will occur above and below 25°C in the temperature range of 0°C to 50°C (Fig. 39).

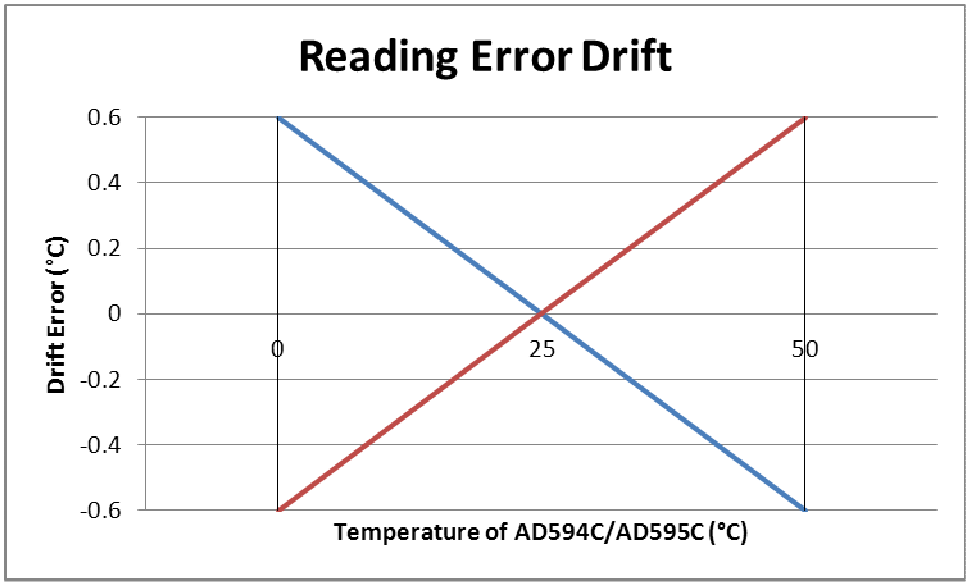

Figure 40 – Adapted from Analogue Devices Datasheet (AD595C)

Any drift of the measured temperatures dependant on the current climate in which the device is operating would significantly affect the reliability and accuracy of the system. In order to verify that the drift did not play a significant role the thermocouple sensors were attached to different points within an incubator and the thermocouple amplifiers slowly heated up using a standard 25W light bulb over a period of time (Fig. 40). The centre thermocouple amplifier (see below) was used to measure the temperature of the chips by using the feature which allows the output to be the temperature of the chip rather than an attached sensor.

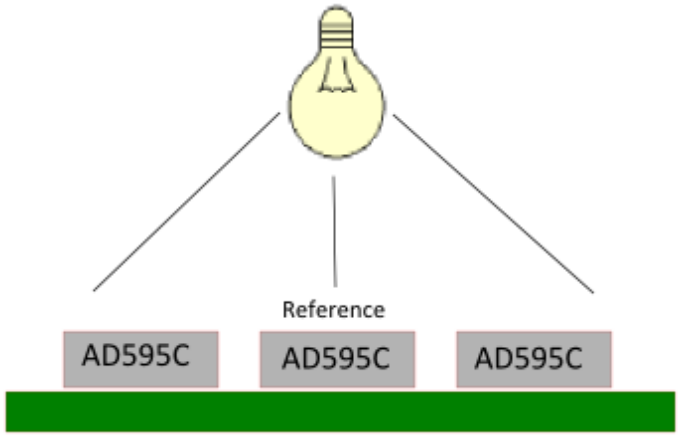

Figure 41 - Measurement Drift Experiment

The results of the experiment are given below:

Table 10 - Thermal Drift Verification

Sensor 1	Sensor 2 (Reference)	Sensor 3
24.27	25.27	**25.39**
24.45	27.09	**25.39**
24.57	27.21	**25.68**
24.45	27.68	**25.74**

24.34	28.09	**25.74**
24.16	29.03	**25.8**
24.1	29.5	**25.8**
24.16	30.02	**25.8**
24.1	30.5	**25.86**

From the above table very little drift was present with only minor deviations around the ambient temperature. The graph below demonstrates more intuitively the performance of the chips with a changing reference point.

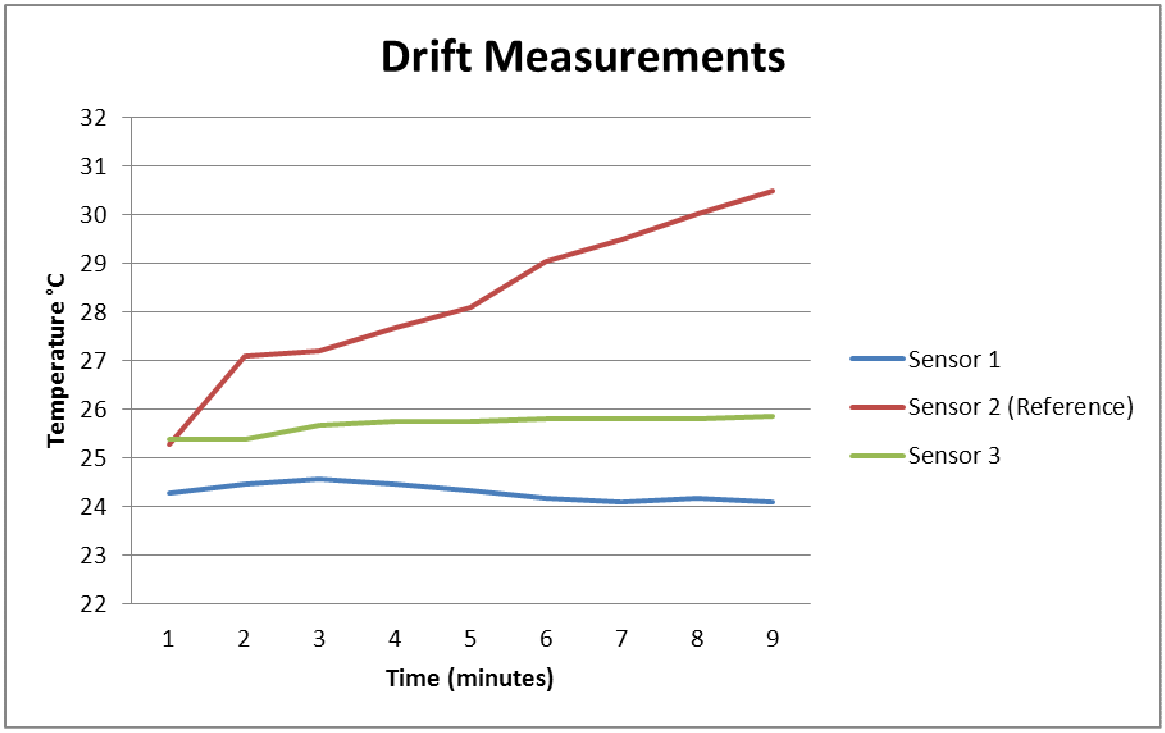

Figure 42 - Temperature Drift Evaluation

The drift experienced in the conditions of a changing reference point showed no significant changes against that of a stable reference temperature with the oscillations being of the same order experienced in normal operation (Fig. 41).

5.3 Performance Evaluation and Conclusion

An offset of just over 1°C was apparent in the recorded outputs of all three of the thermocouple amplifiers. The minimum offset value was both consistent and repeatable and recorded for each, individual amplifier to allow for compensation in the thermal control algorithm. With the elimination of the offset the thermocouple amplifiers performance is within a 1°C tolerance and the difference between readings on separate calibrations being within 0.3°C. The overall performance of the system meets the original criteria of being sensitive to within 1°C.

Measurement drift due to ambient heating shifting the reference temperature of the thermocouple amplifiers over a range of 5°C was not seen to affect the performance or accuracy of the devices. A 5°C shift was chosen since this was assumed the maximum operating temperature within a laboratory environment. The current process requires the manual preparation of the isothermal amplification assay which must be handled within a laboratory environment.

6. THERMAL CHARACTERIZATION OF PDMS

PolydimethylSiloxane (PDMS) is a commonly used polymer in biological microfluidic assays. The bio-compatibility, ease of fabrication, and comparatively low cost of the material make it an ideal platform for highly cost-effective prototyping of lab-on-a-chip technologies.

This material has been successfully applied in microfluidic Polymerase Chain Reaction (PCR) and similar systems by several research groups globally [15,51-55]. Most success has been obtained in continuous flow (CF) systems which, although successful, expose the hydrophobic nature of PDMS which leads to high surface absorption of critical process enzymes (protein fouling) which leads to the blockage of microfluidic channels limiting its applicability as a reliable technology.

6.1 PCR and Microfluidics

Conventional PCR systems (used for nucleic acid amplification) rely on 3 distinct temperature cycles for operation and the efficiency is highly dependent on rapid temperature changes. The thermal response of any material (not limited to PDMS) must be thoroughly understood before precise, controlled operations can be implemented in attempt to achieve and maintain a desired temperature.

Initial predictions were that the thermal insulation characteristics of PDMS dominate well beyond its thermal conductive capabilities, however, still make it a viable substrate for an isothermal amplification system. Isothermal amplification negates the need for continuous flow through distinct temperature zones or alternatively attempting to heat and cool a thermally slow conductor rapidly.

The traditional PCR process which is used to replicate (amplify) nucleic acid samples is a critical medical laboratory technique with applications ranging from viral load count (HIV/AIDS, TB, etc.) to forensic sciences and paternal/maternal testing [9]. These processes, however, are highly temperature sensitive and their efficiency is highly correlated with the ramping times required to change from the 3 distinct temperature cycles [55]. Miniaturizing such systems onto microfluidic substrates (such as PDMS) for point of care applications introduce huge advantages for clinical, often chronically ill, patients.

Since PDMS is known to be a poor thermal conductor, temperature cycling is incredibly slow and high rates of change almost unobtainable, leading most research groups to move towards continuous flow systems [15]. In CF systems (below) the fluid is continuously cycled between 3, separate temperature zones thus obtaining high temperature ramp times, but introducing crippling effects of protein fouling and channel blockage (Fig. 42).

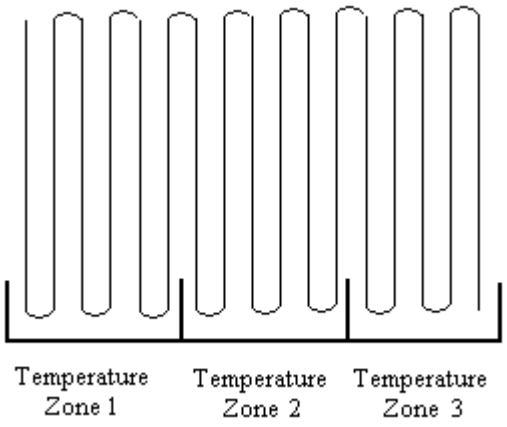

Figure 43 - Example of a continuous flow (CF) microfluidic PCR design

The proposed solution is to minimize the high surface area to volume ratio experienced in CF systems by

introducing an isothermal amplification technique eliminating the need for both temperature cycling and fluid actuation. In order to evaluate the effectiveness of PDMS as a thermally controllable material for an isothermal nucleic acid amplification system a number of thermal characteristics of the substrate need to be evaluated.

6.2 Background to Thermal Conduction and Conductivity

A brief background to the relevant theory and concepts of thermal conductivity and thermal conduction are introduced here with emphasis placed on the application of Fourier's Law of Thermal Conduction. This theory serves as the basis for the quantification of the thermal conductivity of both stainless steel and PDMS which was determined experimentally and validated against known conductivity values. The stainless steel was evaluated to act as the control substance to ensure the evaluation process produced viable results.

6.2.1 Thermal Conductivity of Materials

The thermal conductivity of a metal is a representation of its ability to conduct heat. The higher the value of the thermal conductivity, the lower the energy required to heat the material. The thermal conductivity of a metal over a very large temperature range can be calculated by:

$$k = k_0(1 + b\emptyset + c\emptyset^2) \quad (22)$$

Where k_0 is the thermal conductivity at the reference temperature, T_{ref}, and $\emptyset = T_x - T_{ref}$, where T_x is the current temperature. For a temperature range of only a few hundred degrees it is normally considered sufficient to simplify the equation to [56]:

$$k = k_0(1 + b\emptyset) \quad (23)$$

And for much smaller temperature differences (< 50°C), it can be assumed that the thermal conductivity is approximately the conductivity measured at the reference temperature.

6.2.2 Thermal Conduction

Fourier's law of thermal conduction states that a section of material exposed to a temperature gradient (Fig. 43) will experience a net flow of energy from the side of higher temperature potential to the lower side [57]. The net flow of energy can be determined from:

$$Q_y = -Ak\frac{dT}{dn} \quad (24)$$

Where Q_y is the energy conducted, *k* (W/mK) is the thermal conductivity of the material, *A* is the surface area through which the heat transfer is taking place. From the figure $^{dT}/_{dn}$ is the temperature gradient in the direction normal to the surface area. The negative sign is indicative of the 2nd law of thermodynamics specifying that a thermal energy transfer across a thermal gradient must be from a warmer to a colder region.

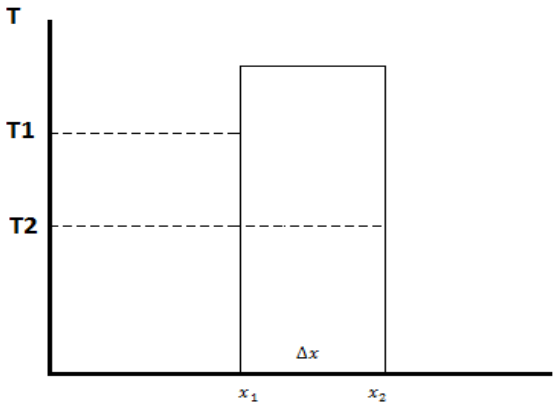

Figure 44 - Application of Fourier's Law

Any homogenous material with a fixed thermal conductivity (*k*), at steady state, will exhibit a linear temperature profile across it [56]. Fourier's equation can, therefore, be simplified to:

$$Q_y = -Ak\frac{\Delta T}{\Delta x} \quad (25)$$

The above equation is not only useful when attempting to characterize a material in terms of its thermal conductivity, *k*, but also being able to make accurate temperature predictions (at steady state) of different points in the material once the net heat flux is known. To calculate the temperature at any given point in the material only one reference temperature (say T_y) need be known:

$$T(x) = \frac{Q_y}{kA}\Delta x + T_y \quad (26)$$

From Fourier's law it is possible to calculate an equivalent thermal impedance which is useful in both electro-thermal models and simulations. The thermal impedance is defined as:

$$R_{th} = \frac{\Delta T}{Q_y} = \frac{\Delta x}{kA} \quad (27)$$

Where $\Delta T = T_{hot} - T_{cold}$

6.2.3 Heat Transfer Coefficient

Mathematically, a materials heat transfer coefficient, *h*, is defined as [58]:

$$h = \frac{dQ}{dt} \times \frac{1}{A\Delta T} \quad (28)$$

This equation is derived from Newton's law of cooling and is used to define a material's convective heat transfer coefficient, *h*. This law states that whenever a solid body is exposed to a moving fluid of a different temperature, energy is convected away from the heated body. It is important to note that the fundamental heat exchange between a solid-fluid boundary is through convection. If the temperature of the fluid, at some point *x* away from the solid is T_x, and the temperature of the solid is T_s, (28) can be written as:

$$Q = hA(T_s - T_x) \quad (29)$$

Where *Q* is the heat transfer per unit time. Equating the above heat rate to that in Fourier's law (25) results in:

$$hA(T_s - T_w) = -kA\frac{\Delta T}{\Delta x} \qquad (30)$$

6.2.4 Heat Power Calculation

In order to experimentally determine the thermal conductivity coefficient (*k*) of PDMS making use of Fourier's equations the heat power conducted must be known. Estimating the power conducted from peltier elements is not a simple task and is dependent on the specific manufacturer, operating conditions, internal losses, unwanted heat induction and supply setup. A more general method to calculate the heat conducted through the system was used by looking at the temperature difference across 2 dissimilar conductors connected to the hot face of the peltier element and applying the equations developed in Fourier's law of thermal conduction.

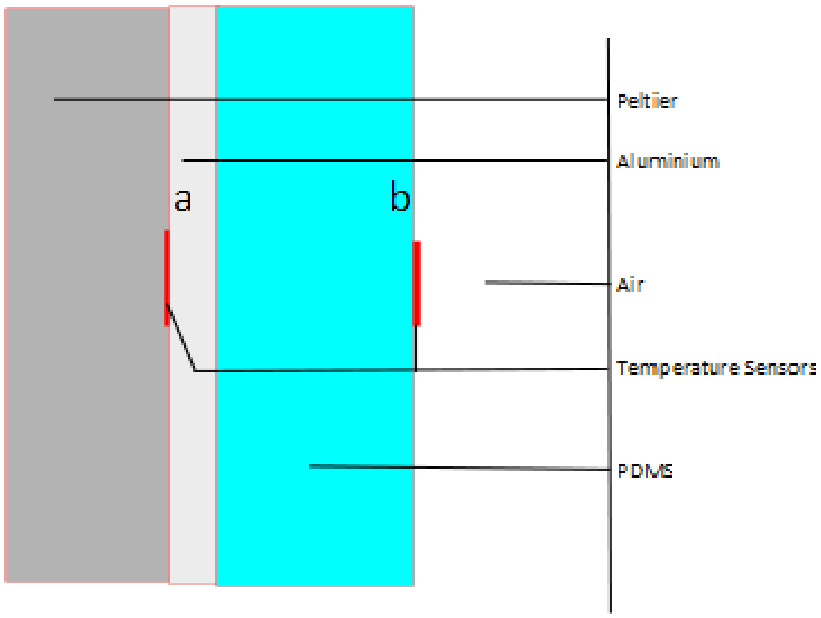

Figure 45 - Measuring the thermal conductivity

With the face of the first conductive material *'a'* kept at a constant, uniform temperature it is possible to calculate the heat conducted through the system (Fig. 44). The heat energy, *q*, flowing into the face at *a* is the same as the heat flowing out of the face of *b*.

The heat energy expression for the surface at *a* can be written as:

$$q = -k_a \times A \times \frac{T_1 - T_2}{x_a} \qquad (31)$$

Similarly, the heat flowing out of *b* can be expressed:

$$q = -k_b \times A \times \frac{T_2 - T_3}{x_b} \qquad (32)$$

Solving and substituting for T_2 the expression for the total power conducted through the system eventuates to:

$$q = \frac{T_1 - T_2}{\frac{x_a}{k_a \times A_a} + \frac{x_b}{k_b \times A_b}} \quad (33)$$

6.2.5 Biot Number

The Biot number is a dimensionless constant which characterizes the rate of heat transfer from the objects surface to the surroundings relative to the internal heat conduction. This number gives a good estimation of whether the spatial temperature distribution will vary significantly within the material [59].

This number is used as an indication as to whether or not lumped parameter analysis can be used to model the thermal response of a system or whether more exact methods will be needed at unsteady state. A general guideline for Biot numbers is that if $B < 0.1$ then lumped parameter analysis will provide at most a 5% error. If $B > 0.1$ then more precise modelling methods will need to be employed [60].

The Biot number is defined as:

$$B_i = \frac{hL_c}{k} \quad (34)$$

Where $L_c = \frac{V_{body}}{A_{surface}}$; *h* is the heat transfer co-efficient and *k* the thermal conductivity of the material.

Employing this method on any geometry that resembles a sphere, plate or cylinder allows one to assume to a uniform temperature distribution throughout the material and the resulting modeling error to be less than 5% if the Biot number is less than 0.1 [60].

6.3 Calculations and Methodology

In order for the accurate measurement and characterization of the sample PDMS material a K-type thermocouple probe was attached to the air exposed surface of the PDMS (shown below) which connected directly to the AD594C thermocouple amplifier. The AD594 allowed for a linear progression of 10mW/°C increase in voltage for the increasing temperatures. The output of the thermocouple amplifier was connected to the A/D converter of the PIC processor and sampled at 30Hz.

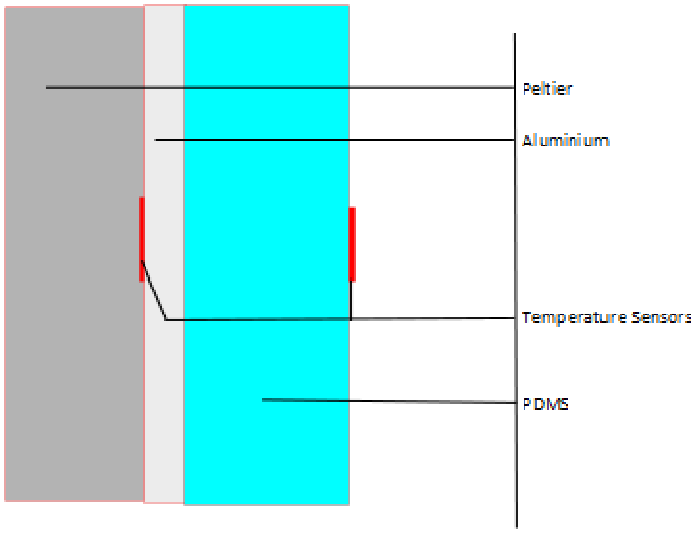

Figure 46 - Experimental Setup for Conductivity Verification

Similarly, a pre-calibrated Vattell Heat Flux Meter was inserted between the peltier and the aluminium plate in order to determine the heat conducted through the aluminium plate into a sample of PDMS (Fig. 45). Knowing the heat energy conducted simplified the verification of the PDMS thermal conductivity. The thermocouple leads from the heat flux sensor (thermopile) also allowed for the measurement of the temperature at the surface of the aluminium. A second thermocouple sensor was connected to the air-exposed surface of the PDMS.

The temperature of the hot-side of the peltier heat source was regulated to 41.5°C making use of a PI (Proportional + Integral) controller which is discussed in *Chapter 7 – Thermal Controller*. Keeping the hot side of the peltier at a regulated temperature it is possible to simply measure the temperature at the surface of the PDMS sample.

A thin layer of thermal paste was used at the material interfaces (peltier / heat flux meter, heat flux meter / aluminium and aluminium / PDMS) to ensure good conduction and prevent any temperature non-uniformities due to air pockets between interfaces. A thin layer of paste was also spread over the air-exposed surface of the PDMS in which the temperature sensor was placed.

The same experiment was conducted using a stainless steel plate (thermal conductivity of 16W/mK) in order to verify the experimentation values. The calculation of the thermal conductivity for a material must be done at steady state. If the internal material temperature is still varying incorrect calculations of the materials thermal conductivity will result.

6.3.1 Thermal Conductivity

The following measurements were taken for the stainless steel and PDMS samples respectively.

Table 11 - Stainless Steel Characteristics

Property	Measurement
Material	Stainless Steel
Heat Energy	$0.943W$
Aluminium plate Width	$0.001m$
Stainless Steel Plate Width	$0.002m$
Aluminium Conduction Area	$0.225 \times 10^{-3} m^2$
Stainless Steel Conduction Area	$0.225 \times 10^{-3} m^2$
Temperature at Aluminium Surface (T1)	41.5°C (314.66K)
Temperature at Stainless Steel Surface (T3)	40.9°C (314.06K)

Using the above results the thermal conductivity, *k*, of the Stainless Steel can be calculated using (33) as:

$$k_{ss} = \frac{x_{ss}}{A_{ss}\left(\frac{T_1 - T_3}{q} - \frac{x_{Al}}{k_{Al} \times A_{Al}}\right)} \quad (35)$$

$$k_{ss} = \frac{0.002}{0.225 \times 10^{-3}\left(\frac{41.5 - 40.9}{0.943} - \frac{0.001}{250 \times 0.225 \times 10^{-3}}\right)} \quad (36)$$

$$k_{ss} = 15.8 \mathrm{W/mK} \quad (37)$$

Obtaining a value of 15.8W/mK validates the experimental procedure since the value of the stainless steel is known to be 16W/mK. This shows that results correct within 5% of the actual values can be expected.

The recorded measurements for the PDMS are given below.

Table 12 - PDMS Characteristics

Property	Measurement
Material	PDMS
Heat Energy	$0.0754W$
Aluminium Plate Width	$0.001m$
PDMS Width	$0.001m$
Aluminium Conduction Area	$0.064 \times 10^{-3}\mathrm{m}^2$
PDMS Conduction Area	$0.064 \times 10^{-3}m^2$
Temperature at Aluminium Surface (T1)	41.5°C (314.66K)
Temperature at PDMS Surface (T3)	35.9°C (309.06K)
Ambient Temperature (Air)	23.0°C (296.16K)

And similarly calculating the thermal conductivity using (33) yields:

$$k_{PDMS} = \frac{x_{PDMS}}{A_{PDMS}\left(\frac{T_1 - T_3}{q} - \frac{x_{Al}}{k_{Al} \times A_{Al}}\right)} \tag{38}$$

$$k_{PDMS} = \frac{0.001}{0.064 \times 10^{-3}\left(\frac{41.5 - 35.9}{0.0754} - \frac{0.001}{250 \times 0.064 \times 10^{-3}}\right)} \tag{39}$$

$$k_{PDMS} = 0.211\mathrm{W/mK} \tag{40}$$

which is close within the thermal conductivity ranges of PDMS known to be between 0.17W/mK to 0.2W/mK. This allows us to assume that the curing process of the PDMS was performed correctly since the calculated thermal conductivity conforms to known values and these can be assumed in performing both validation and thermal simulations.

6.3.2 Thermal Impedance

The thermal impedance of the PDMS was calculated to be:

$$R_{\phi\,(PDMS)} = \frac{\Delta T}{P_{cond}} = \frac{d}{kA} = \frac{5.6}{0.0754} = 74.27\ ^{\circ}C/W \tag{41}$$

6.3.3 Heat Transfer Coefficient

Calculating the heat transfer coefficient for PDMS in air:

$$hA\left(T_{PDMS\ surface} - T_{ambient}\right) = -k_{PDMS}A\frac{\Delta T_{PDMS}}{\Delta x_{PDMS}} \tag{42}$$

$$h_{air} = 91.60\ W/m^2K \tag{43}$$

This value is not particularly descriptive in this application, however, allows us to calculate the Biot Number for the system.

6.3.4 Biot Number

The Biot number requires the calculation of the characteristic length of the material firstly. This is the ratio of the geometry volume to its surface area:

$$L_c = \frac{V_{body}}{A_{surface}} = \frac{(0.008)(0.008)(0.001)}{2(0.008)^2 + 4(0.008 \times 0.001)} = 0.4 \times 10^{-4} m \quad (44)$$

Using this in the equation for the Biot number as well as the previously calculated values for the heat transfer coefficient and thermal conductivity:

$$B_i = \frac{hL_c}{k} \quad (44)$$

$$B_i = \frac{hL_c}{k} = \frac{91.6 \times 0.4 \times 10^{-4}}{0.211} = 0.177 \ (dimenstonles) \quad (45)$$

6.4 Conclusion

The thermal conductivities determined experimentally for both stainless steel and the PDMS confirmed their respective documented thermal conductivities. The thermal conductivity of the stainless steel was measured in order to test the applicability and accuracy of the experimental procedure. The measured thermal conductivity of stainless steel (15.8 W/mK) compared well to the documented value of 16 W/mK.

The experimentally determined thermal conductivity of PDMS (0.21 W/mK) was close to the range of known values for its conductivity, which are typically considered to be between 0.17 W/mK and 0.2 W/mK [61-63].

The Biot number calculated for the system equated to 0.177 (>0.1) which confirms that a spatially non-uniform temperature distribution is apparent across the PDMS as expected. Lumped parameter analysis, therefore, does not apply in modelling techniques and more complex models would need to be employed in order to model the internal temperature profile of the PDMS material.

The high thermal impedance of PDMS for conventional PCR systems is a significant design factor which must be considered in the development of LOC devices. When applied to isothermal amplification systems a slow thermal response becomes manageable – once the temperature reaches the required value, it is more likely to stay stable rather than fluctuate regardless of the ambient conditions.

An isothermal system implemented in PDMS also minimizes the need for extended amounts of fluid actuation from point to point in the system significantly reducing the effects of protein fouling and channel blockage. This also negates the requirement for altering the temperature of the material making the high thermal impedance less of a performance hindrance.

The evaluation of PDMS as a substrate for a microfluidic isothermal amplification system indicates that, although higher conduction power will be required for the system to reach the desired temperature, the advantages of cost, manufacturability, and rapid development make PDMS an ideal candidate for (at least) prototype systems and especially those taking advantage of isothermal nucleic acid amplification systems

.

7. THERMAL CONTROLLER

Any system performing sensitive temperature manipulations on a biological assay require an accurate and stable control system. This not only applies to POC developments but even in strict laboratory devices. The thermal controller must be reliable, responsive and above all – accurate. In order to have an accurately controlled temperature – sensitive to within 1°C – a strict control algorithm is needed. A number of different control algorithms were evaluated namely:

1. Simple hysteresis heat regulation
2. Proportional Control (P)
3. Proportional + Integral Control (PI)

A comparison of the above three control algorithms is presented briefly and the chosen algorithm (PI) was implemented in the physical system used for the evaluation of the isothermal nucleic acid amplification system on the PDMS-glass hybrid substrate.

7.1 Switching Circuit

The design of the thermal control circuitry included the implementation of an H-Bridge configuration used to drive the peltier device. Not only does this allow strict control over the switching of the peltier for heating purposes, but also allows the peltier to be used in its 'cooling' state by simply reversing the polarity. This is advantageous since the design allowed any overshoot in temperature to be quickly cooled and also allows for the possible extension of the device to be used in a standard 3 cycle, temperature ramping, PCR manner.

7.1.1 H-Bridge Implementation

The implemented H-Bridge (Fig. 46; below) was constructed using four IRL2203 N-Channel MOSFETs and resistors R2 and R3 to supply the required gate current. The IRL2203 N-Channel MOSFETs were chosen for the low threshold voltage (1V) and the ability to conduct 3A. The Peltier device chosen (SuperCool 8W PE-031-10-13) has a maximum forward (and reverse) conduction voltage of 3.8V drawing 3.9A of current. Any supply voltage higher than a voltage (V+) of 3.8V would require either a high power resistor to dissipate the excess energy or otherwise dump the energy into the driving MOSFETs causing an excessive heat build-up.

The PIC18F452 is able to both source and sink 25mA (maximum current) on the I/O ports which is sufficient to drive a switching MOSFET pair in the H-Bridge implementation. Resistors R2 and R3 are simply to limit the current drawn to levels which allow both MOSFETS to switch whilst preventing current saturation. The control signals *A* and *B* are displayed on the diagram below indicating which MOSFET pair is driven with each signal.

This is an unconventional H-Bridge design and this implementation will only work if the driving signals V_A, V_B are bigger than the supply voltage of $+V$ (Fig.46).

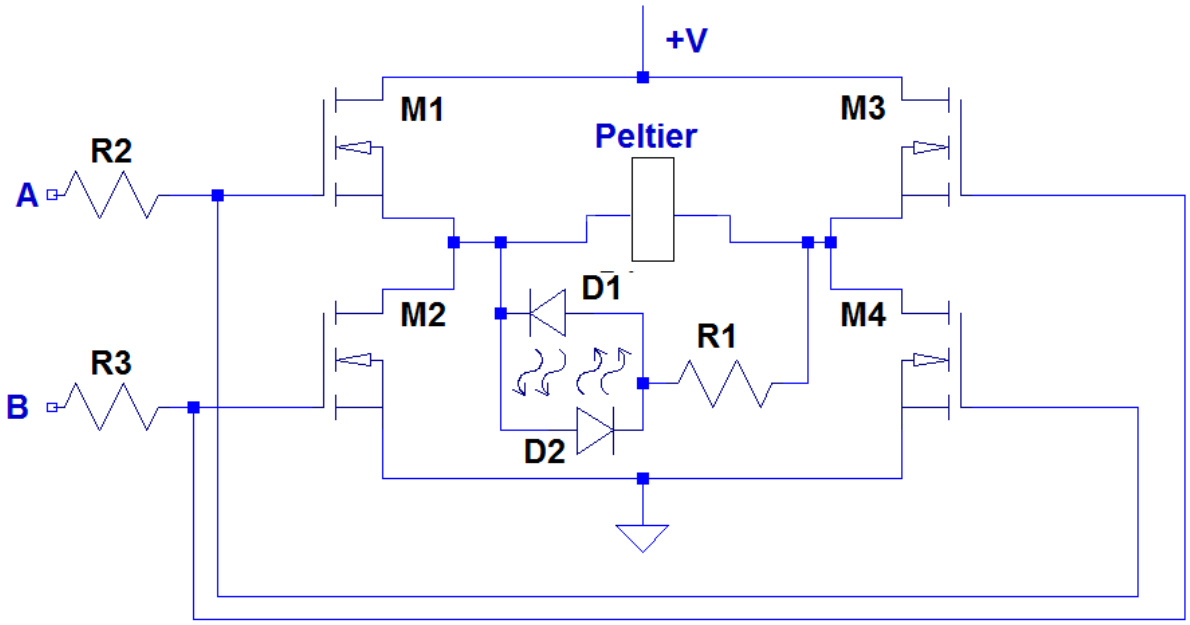

Figure 47 - H Bridge Implementation

The thermal system to be controlled is one with an exceptionally slow response time (relatively speaking) and hence high switching frequencies were not needed. Series resistors (R2, R3) of value 680Ω slow the rise time on the gates of the MOSFET's, however, this was considered negligible for implementation in this application.

The diodes included in the construction (D1, D2) are simply two LED's of dissimilar colour used to indicate the direction the peltier device is conducting. These LED's allow for a quick method of determining whether the peltier device is either 'heating' or 'cooling'. The determining factor to whether the peltier is in its heating or cooling mode is determined by driving the opposed MOSFET pairs in the H-Bridge. In the above schematic the gates for the MOSFETs are driven with either gate signal *A* or *B*. The gates of MOSFETs M1 and M4 were directly connected together, signal *A*, and similarly the gates of M3 and M2 were directly connected together and driven with signal *B*. The control signals *A* and *B* were obtained directly from the PWM ports (CCP2 and CCP1 respectively) on the PIC18F452 controller.

7.1.2 Functional Overview of H-Bridge

The functioning of the implemented H-Bridge is the same as any normal H-Bridge operation and a brief functional overview is described.

With V+ set to 3V and both control signals A and B being LOW the voltage seen at the gate of all the MOSFETs (due to the voltage divider between the pull-up and the series resistors) will be 0V which is below the gate threshold voltage of the MOSFETs which ensures no switching and hence no current drawn in the circuit. With a control signal, say A, being set HIGH (+5V) the gates of MOSFETs M1 and M4 are set high switching on the driving pair. With MOSFETs M1 and M4 now conducting the voltage V+ (3V) is seen across the peltier and LED parallel combination since M4 completes the conduction path to ground. In this instance – with signal A being HIGH and signal B being LOW diode D2 will conduct indicating forward conduction of the peltier device (i.e. heating in this orientation). Similarly the function of M2 and M3 can be described with control signal A being LOW and signal B being HIGH.

Care was taken in the configuring of control signals A and B – especially since this is done in code on the PIC processor. Each control signal was switched OFF before any other control signal can be set high to avoid a

direct short circuit. Having both signals A and B HIGH simultaneously results in a direct short circuit to ground from V+.

The overall effect of the resistors R2 and R3 connected to the gate of the MOSFETs slow the rise time of the signal to just under 4µs – which in this thermally slow system plays no significant role in the functioning of the system other than increasing the switching losses in the MOSFETs which was assumed negligible. The peltier device recommends a minimum switching frequency of 5kHz when making use of PWM control and the chosen PWM control signals operated at 13kHz which is well within the peltier conduction range and sufficiently fast enough to successfully control the thermal system.

7.2 Controller Design

The design of the 3 implemented algorithms is briefly discussed below. A small copper plate was used to provide a heat source (reservoir). The heat reservoir lowers the overall power requirements of the peltier device since the peltier requires a source of heat for the initial stages of operation (Fig. 47). Conducting heat away from a copper heat plate requires far less energy than attempting to conduct heat from the ambient environment (air). The peltier device – ideally – simply conducts heat from one face to the other. This requires some form of initial heat source.

Surprisingly, the fact that the peltier device is not 100% efficient is advantageous (to some extent) in this system. The peltier generates a small amount of heat during normal operation which is usually seen as unwanted and "lost" energy in standard electronics. Since the copper plate can only supply so much energy to the system before it has been depleted - without an external source injecting a net influx of heat energy – the heat generated by the peltier device, itself, serves as a heat source. The amount of heat generated by the peltier device was found to be not only sufficient to maintain the plant at the desired temperature, but also sufficiently small so as not to cause long term heating of either the microfluidics chip or the copper plate depending upon the implemented control algorithm.

The desired temperature at which the plant is to be controlled to (in the following discussions) is called the set point.

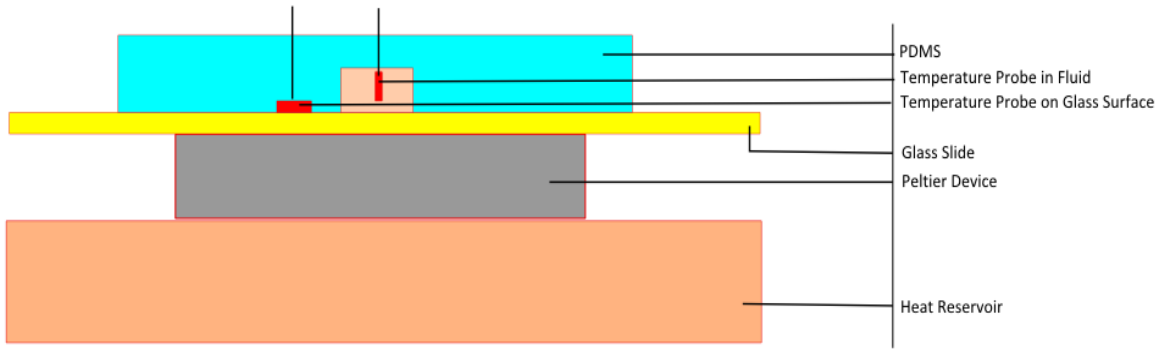

Figure 48 - Thermal Plant to be Controlled

7.2.1 Hysteresis Control Algorithm

The simplest of the control algorithms is that of a standard thermostat – remain on until the desired temperature has been reached, and then turn off. Intuitively an oscillating temperature-time profile is expected, the only question is the amplitude of the oscillations and the time required for the oscillations to minimize. The oscillations incurred are known as the hysteresis band, the frequency of which can be adjusted by adjusting the extent of over and undershoot. This frequency can be tuned up until a point which ultimately leads to system instability.

A slight alteration to this algorithm (since the capacity is available with the reverse biasing of the peltier device) is a heat-cool algorithm. Instead of simply turning the heating element off, the heating element is switched to a cooling element in an attempt to keep the temperature as close to the set point as possible. In a system with a high characteristic thermal time delay – since PDMS is being used whose temperature changes very slowly –high levels of oscillation around the set point with both overshoot and undershoot occurring in equal proportions is expected. The speed of the system (or the response time of the controller) is governed by how quickly the microprocessor can sample, calculate and translate the given data into a control signal. This control signal then governs the energy conducted into the system. The delay, however, is the time taken by the PDMS to respond to these control signals. A signal given to stop conducting heat into the system is not reflected immediately in the PDMS substrate since heat energy is still being conducted internally (system delay) which results in both overshoot and undershoot in the system.

A simple on/reverse on or hysteresis algorithm was implemented and evaluated. The basic structure of this algorithm takes the form of:

```
On off algorithm(current temperature, set point)
{
        if (current temperature < set point)
                turn heater on
        if (current temperature > set point)
                turn cooling on
}
```

7.2.2 Proportional Control Algorithm

Simple on off control, although easy to implement, lacks sufficient precision to allow for its use in a temperature sensitive environment. One of the most basic, understood linear algorithms is that of proportional control. Proportional control not only allows for the scaling of a signal proportionately to allow for stricter control but also offers ease of implementation on embedded platforms since it is not a processing intensive algorithm. The duty cycle of the PWM controller on the PIC18F452 has a span of 0-512, 0 being a duty cycle of 0% and 512 being 100% duty cycle. This allows control over the extent to which the heating device is switched on in order to limit the heat conducted through to the elements.

The bias (or offset) for the proportional controller was determined experimentally and was selected as the minimum duty cycle required to keep the surface of the glass at a constant temperature. This was required since the error near the set point would be close to 0 and a duty cycle too close to 0 results in a loss of thermal energy and the glass surface cooling. This is an issue of system delay and the system speed.

The initial value of the room temperature for the system was variably set and for testing purposes assumed to be 20°C which is close to the standard room temperature and assuming the components are roughly in thermal equilibrium with the environment. The set point was set as 41.0°C and the span of the controller is calculated as: *span = set point – initial temperature*.

The scaling factor in the controller was used to scale the required duty cycle making use of the error value. This was determined by: *error value = set point – current value*. This error value was then scaled to make use of the 0-512 range and proportionately scale the duty cycle accordingly. From the error value, it was also possible to determine whether or not the system should be heating or cooling the plant.

The algorithm for the proportional control was coded in variable form so that the span, scaling factor and bias were all dynamically calculated with the user only specifying the required set point to which the temperature should be controlled. A cooling threshold could be set manually to allow the controller to work (as a proportional controller) in the opposite direction to cool the system towards the set point.

The pseudo code for the proportional algorithm (heating only) is given below:

```
Proportional Controller (current temperature, set point)
{
        initial temperature = 20°C
        scale factor = span / (set point – initial temperature)
        bias = (set point / span) * offset

        error = current temperature – set point
        proportional factor  gain = error * scale factor
        duty cycle = proportional factor + bias
        Set PWM (duty cycle, frequency)
}
```

To alter the algorithm to allow for proportional *cooling* all that changes is first checking whether the current temperature is higher than the set point and setting: *error = current value – set point* and removing the bias. The bias is not needed in order to cool the plant since the current (overshoot temperature) is not the desired temperature which should remain constant, rather the temperature is to be reduced – including the bias increases the rate of cooling leading to higher levels of undershoot.

7.2.3 Proportional and Integral Control Algorithm

The proportional control algorithm, although functional, introduces a steady state error. The ramp time for the system to initially reach the set point in this thermally slow system with only proportional control required a time of just over 3 minutes. The proportional control algorithm, although functional, suffers from a steady state error which keeps the system slightly below the required set point. This justified the inclusion of an integral term in the controller to eliminate and error induced at steady state.

The integral portion of the algorithm takes a number of error values and averages these in order to determine how far the controller is away from the set point. The error value is scaled higher than the proportional controller to allow for quick injections of heat energy into the system in an attempt to stabilize the system operation to the set point in a timely manner. The closer the plant is to the desired set point, the smaller the error values, the lower the average error and the less pronounced the integral effect is on the system. Similarly the further away the plant is from the set point, the higher the overall average and the more pronounced the integral term is in the control algorithm.

Having a high value in the integral scaling allows for large injections of heat power into the device. Since the device responds very slowly to changes in temperature large heat injections do not cause excessively high levels of overshoot since the sampling rate is fast enough to allow for the aggregate error to significantly reduce during any periods of oscillation. The inclusion of the integral control algorithm with the proportional component is simple enough since only the integral factor needs to be added to the PWM duty cycle.

The basic operation of the integral controller is described below:

```
Integral Controller(current temperature, set point)
{
        error results[number of errors]
        current error = set point – current temperature
        error results[current] = current error

        for (count = 0; count < number of errors; count++)
        {
                accumulative error = accumulative + error results[count]
```

```
        }

        average error = accumulative error / number of errors
        integral factor gain  = average error * integral scaling

        return (integral factor)
}
```

And setting the duty cycle for the PWM results in:
PWM duty cycle = proportional factor gain + integral factor gain + bias

Generally, PID controllers are considered to be more responsive than PI controllers. However, derivative control is based on the rate at which the error values change. The proportional and integral actions are sufficient to combat any oscillations introduced into this system at steady state. The thermal nature of this plant presents very slow time changing temperature gradients making derivate control unnecessary during steady state operation since the rapid response of the proportional control term is sufficient to correct any deviations. Although a large gradient is present when the system is heating up from the initial environmental conditions, the ramp time to get to steady state is not a significant design issue (3 minutes) since the system is required to be pre-heated to its steady state value which is reached sufficiently quickly.

7.3 Implementation

The developed algorithms were implemented and evaluated based on their ability to hold the plant to a constant set point. The thermal sensor used as the controller was a thermocouple wire inserted directly into the fluid which was to be controlled and heated (Fig. 46). Temperature measurements were also made by an additional two sensors, one placed on the face of the peltier device between the peltier and the glass surface and the other placed on the surface of the glass face joined to the PDMS substrate.

The temperature sensor placed on the surface of the peltier device was taped to the surface using conductive tape supplied with the previously used Vattell Thermal Flux Sensor *(Chapter 6 – Thermal Characterization of PDMS*). Silicone gel was used between the surface of the tape and the glass substrate to ensure good thermal coupling between the two faces.

The third transducer was used to compare the measured temperature of the glass face to that of the fluid.

7.3.1 Simple Hysteresis

In the preliminary functioning of the simple hysteresis algorithm there was no immediate problem introduced into the controllability of the system. The peltier was simply turned ON (fully) when the temperature measured was below the set-point and turned ON-Reverse when the measured temperature was above the set point in order to cool it. This simple ON/OFF algorithm (or in this case ON/REVERSED) is well documented and known to give rise to a hysteresis band which can clearly be seen from the image below [64]. The set point for the evaluation of the controller was set to 50.00°C – an arbitrary value in order to test the controllability and stability of the system.

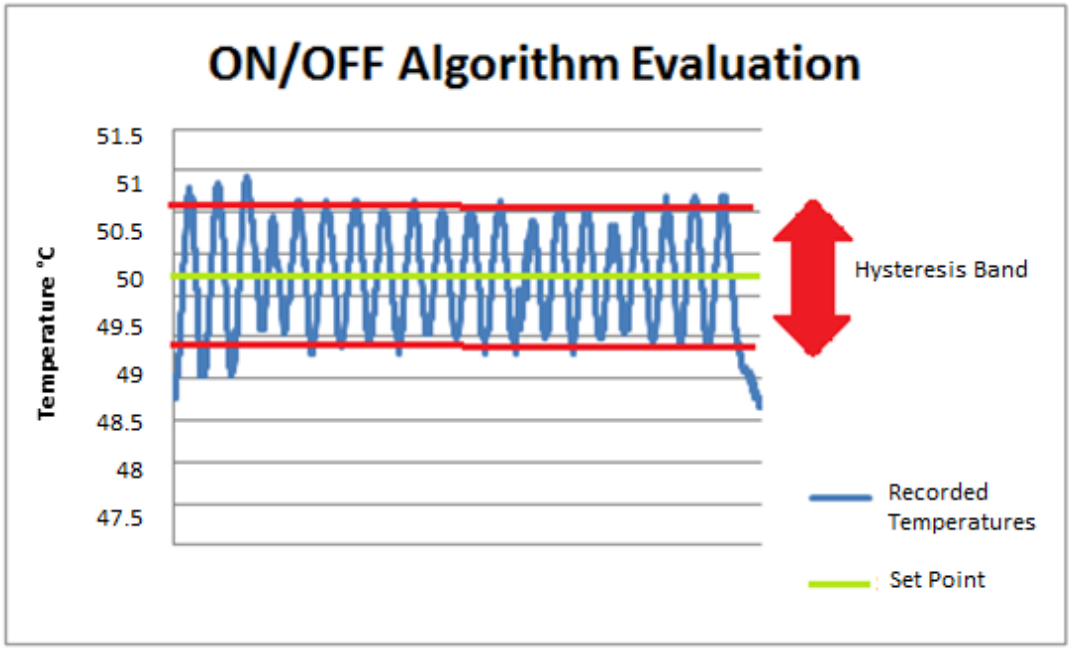

Figure 49 - ON/OFF Algorithm with a set point of 50°C

The above graph (Fig. 48) demonstrates the slow thermal response of PDMS and time delay present in the system. The temperatures were sampled at a rate of 30Hz and the controller immediately cooled the sample once the temperature rose above the set point. Even with this algorithm and sample time the system still manages to overshoot the set point by more than 0.5°C due to the nature of the slow thermal response.

However, a problem that arose in this configuration of heating and cooling constantly was that a substantial amount of heat was being stored in the heat reservoir every time the peltier had to cool the chip. In the cooling phase the heat is conducted away from the chip and into the copper plate. After a few minutes this significantly raises the temperature of the plate. This is due to the fact that the operational heat generated by the peltier switching from fully on to fully reversed is effectively being 'stored' in the heat reservoir and not being conducted into or away from the system. Although this provides a more readily available source for heating, it introduces a problem when cooling is required. Without an external source cooling the copper plate the net thermal exchange from the peltier device to the sink eventually raises the temperature of the heat reservoir to a point where the peltier can no longer conduct heat into it. The controller functions until the point where it can no longer cool the chip.

An alteration to this was an algorithm which was ON/OFF/COOL which attempted to minimize the heat being conducted into the heat sink in the cooling phase. This algorithm basically heated the chip to the correct temperature and then switched off (dead band) and only cooled if the temperature still managed to exceed the desired range due to the system delay. Since the thermal delay is so pronounced in this system overshoot was constant and although the cooling requirements were decreased, cooling was still required and again leads to an accumulation of stored heat in the heat reservoir.

The stored heat was not nearly as significant as in the simple hysteresis algorithm; however, another problem was introduced in the OFF phase of the ON/OFF/COOL algorithm. In the OFF phase the peltier device is effectively off. It is neither forward, nor reverse biased. It is simply off and it is seen as a material which can conduct heat by the copper plate. With an accumulation of heat in the reservoir, in the off phase, a temperature difference is created over the peltier device and heat is conducted towards the chip governed by Fourier's equation. In this state it was found that heat was still being conducted to the chip in the intended

'off' phase which – yet again – leads to the system attempting to cool the chip, which conducted more heat into the sink which prevented the ability to cool the system. Another design alternative would be to completely eliminate the cooling phase completely – allowing for only forward conduction of the heat into the chip and allow the temperature to drop without any external influence.

From the results obtained it was clear that a much more eloquent control algorithm would be needed to successfully control the amount of heat power which was conducted back into the heat sink in order to ensure that the temperature of the chip could remain stable and still cool the device – should it be required. The proportional and integral manage to negate the cumulative heat build-up in the copper reservoir by avoiding the need to cool the system and transfer heat into the reservoir on a regular basis.

7.3.2 Proportional Control

The preliminary results for the evaluation of the proportional controller gave good results displaying a sufficient ramp time and settling time. The proportional controller was manually tuned until acceptable performance levels were obtained. The set point for the thermal controller was set to 41°C for evaluation. For a system being controlled from room temperature the PDMS chamber began to approach the set point just after 2 minutes and stabilized just after 3 minutes. The graph below shows the response of the proportional controller controlling a system initially at 41°C.

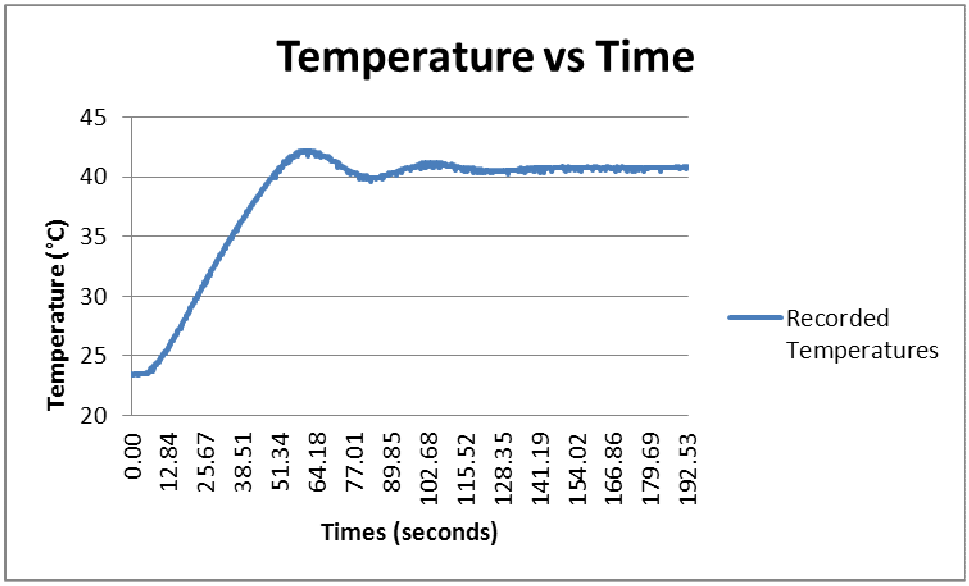

Figure 50 - Proportional Control Algorithm

From the above graph (Fig. 49) it becomes apparent that the controller requires 3 minutes to approach the required set point, however, an offset remains present just below the set point (40.77°C) which is common of proportional controllers. The offset can be adjusted by increasing the bias of the controller, however, with constant deviations the system is not guaranteed to return to the same value employing this method. Once at the set point the system remains stable unless any perturbations disturb the thermal state. No heating of the copper plate is present in this implementation since the heat is only ever conducted away from the heat reservoir after the initial overshoot. The cooling level is set to minimize the initial overshoot and only transfers heat away from the system during the initial, high overshoot portion. Otherwise conduction takes place purely from the reservoir to the PDMS.

7.3.3 Proportional and Integral Control

The proportional controller, although functional, could not successfully be implemented as a strict controller in a system which required a temperature sensitivity of 1°C. From the implementation of the proportional and

integral controller a stricter system response is achievable. The graph below shows the typical response of a PI controller which showed the system performance when heating the fluid to a 41°C set point. Manual tuning was again used to obtain the gain levels for the integral controller.

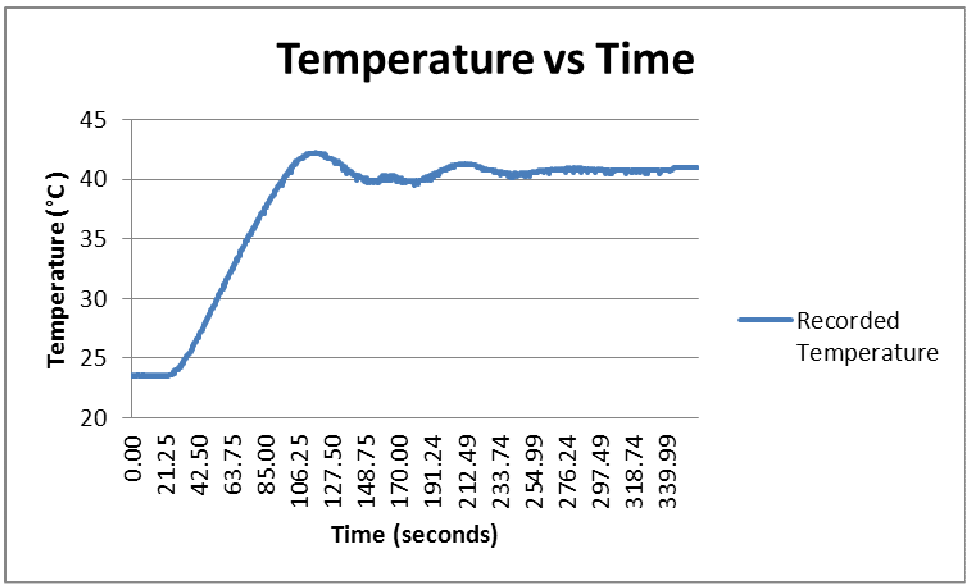

Figure 51 - Proportional and Integral Control Algorithm

The above graph (Fig. 50) shows a slightly longer response time of the system reaching the set point from room temperature in just under 6 minutes – as compared to 3 minutes in the proportional controller. The initial response time of the system is unchanged since the P term dominates the quick response. The introduced integral control term manages to eliminate the error with the system stabilizing at 40.99°C. The negative aspect of introducing the integral term in the controller is that the time taken to reach steady state has increased since the integral term responds slowly to perturbations.

7.4 Evaluation and Assumptions

The challenge introduced in successfully controlling the temperature of the fluid in the microfluidic cassette is in measuring the temperature of the fluid without having a sensor immersed within the fluid. A thermocouple transducer could not be introduced into the chamber and the reaction reagents. This was solved by verifying the assumption that there was a uniform temperature profile at the base of the glass directly above the face of the peltier device. A thermocouple sensor was placed inside the fluid in the chamber, and a second transducer was placed through the PDMS substrate against the face of the glass. The temperature readings of these two transducers were compared to verify that the temperature of the fluid at the base of the chamber was the same temperature as that of the face of the glass which was expected. This then allowed a control point which would be able to control the temperature of the fluid without having a sensor placed inside the chamber.

Having the temperature of the surface of the glass at the base of the chamber held constant at 41°C, Fourier's equation of heat conduction (24) ensure that the temperature inside the well cannot be higher than this – assuming the only heat source is that of the peltier device.

$$T_{(inside\ well)} = T_{surface\ of\ well} - \frac{Q_y}{kA}\Delta x \tag{46}$$

$$T_{(inside\ well)} = 41.0 - \frac{Q_y}{kA}\Delta x \tag{47}$$

The above equation shows us directly that the fluid inside the well can never reach a temperature higher than that of the surface. This constrains the upper bound of the temperature of the contents of the well, regardless of how thermally conductive the fluid is.

It was noted during the evaluation that there was a distinct temperature difference across the fluid inside the well. Experimentally the temperature difference across the fluid was measured to be around 1.5°C. PDMS is known to be a good thermal insulator and a poor thermal conductor. From this we can make the assumption that the temperature at the top surface of the chamber, due to thermal conduction through the PDMS, to be slightly lower than the 41.0°C experienced at the base of the chamber. This implies that the fluid at the top of the chamber will feel some – albeit small – cooling effect from the surface of the chamber until steady state and thermal equilibrium is reached.

The PDMS has a much larger thermal mass on the chip and the most likely result is the cooling of the fluid rather than the heating of the PDMS by the fluid although smaller interchanges will occur. This will most likely result in a small convective fluid flow within the chamber having the hotter fluid at the base rise causing the cooler fluid to fall to the base. A convective nucleic acid amplification system was not the intended development of the system nor should it be too consequential, although convective based PCR systems are well documented [12]. Since the temperature difference is relatively small (1.5°C) convective flow should be minimal in the early stages of the amplification and should not be present at all once the fluid inside the well has begun to reach thermal equilibrium.

7.5 Conclusion

The performance evaluation of the three presented control algorithms proved that the best suited algorithm for the thermal controller for this thermal plant was that of the proportional and integral controller. This algorithm yielded a sufficient response time, stability and operational performance being able to hold the fluid at the required set point without any excessive heating of the heat sink – or conversely attempting to draw too much heat from the reservoir. The high sampling rate (relatively speaking) for this thermal control system allowed fine adjustments to be made sufficiently quickly to keep the surface of the glass at the required temperature, and in so doing the fluid held within the chamber.

The working principle of the thermal control algorithm is based upon the temperature of the glass base of the PDMS substrate. Experimental results showed that the peltier device has a uniform temperature distribution across its surface except for the edges of the device which had a slightly lower temperature profile. A thermal transducer (being a K-type, Class 1 Thermocouple) was inserted through the PDMS layer via the use of a hypodermic needle and placed against the glass base. The glass based was thermally connected to the face of the peltier using a silicon paste to ensure no air gap was present between the conductive surface and the glass to aid in a uniform temperature distribution.

The glass was placed directly above the uniform temperature zone of the peltier device with the well being placed over the centre. This promotes a uniform thermal distribution of the glass directly above the peltier. This is not true, however, for the remainder of the glass since thermal conduction will occur laterally across the surface of the glass which will introduce a temperature gradient across it.

The area of interest on the surface of the glass is where the thermocouple sensor was placed. The contents of the fluidic chamber need to be kept at a constant temperature of 41°C within a 1°C tolerance. The enzymes in the isothermal amplification system are exceptionally sensitive to the functional temperature and become virtually inactive when the temperature strays more than 1°C from 41°C.

Ensuring the glass at the base of the chamber is kept at a constant temperature of 41°C ensures that the temperature of the fluid in the well will reach thermal equilibrium at some point. The fluid does not immediately reach thermal equilibrium with the glass surface since it does not have a, comparably,

insignificant thermal mass. The thermal conductivity of the contents of the chamber will determine how quickly thermal equilibrium is reached and it is assumed that the thermal conductivity is that of water. Water was used as an initial fluid in the well in order to test and verify the performance of the thermal controller setup and algorithm before any testing of the isothermal nucleic acid amplification assay. The fluid was found to reach thermal equilibrium after a period of 15 minutes.

The performance of the thermal controller demonstrates that the fluid can be kept within 1°C of the desired set point for long periods of time. The previous calibration of the measurement equipment (*5.3 Performance Evaluation and Conclusion*) showed the measurement equipment to be sensitive to within 0.3°C. This indicates that the system controller and equipment meet the requirement of the imposed 1°C sensitivity. The selected gains of both the proportional and integral algorithms were obtained using manual tuning and monitoring the system performance. These values may not have been the absolute optimal values (before the system reaches instability), however, were found to be sufficient for the purposes of this application.

8. THERMAL SIMULATIONS

Thermal simulations of the single chamber microfluidics chip were constructed using a COMSOL Multiphysics demo package. This finite element tool allows for a number of different thermal simulations to be constructed using both standard materials such as aluminium and user defined materials such as PDMS. COMSOL allows for the evaluation of thermal mapping of materials in three dimensions which was required for this system.

One of the complications introduced in this setup was that the thermal source (the peltier heater) was much smaller than the glass substrates to which it was attached. The standard thermal conduction equations described in Fourier's laws of thermal conduction catered only for two dimensions. The problem with having the heat source connected to a material which is structurally much wider, longer, of non-negligible width and with a low thermal conductivity means that thermal conduction is not going to be purely perpendicular to the source – as with two dimensional system - and significant lateral conduction is going to occur. It is due to this fact that a three dimensional, finite element model was required. A small peltier device needed to be chosen based on the size constraints imposed on the µTAS systems to correspond with the chamber dimensions.

The purpose of the thermal modeling is to validate the operational assumptions which were made as inputs to the thermal control system, namely:

1. The fluid within the chamber reaches the same temperature as the surface of the glass at the PDMS-glass interface, and
2. The placement of the thermal transducer is arbitrary as long as it is in contact with the abovementioned glass surface and that is it in contact in the vicinity directly above the peltier heating element.

8.1 Finite Difference Model Glass-PDMS

A finite difference model of the glass-PDMS chips was developed to replicate the construction and dimensions of the actual device. The dimensions of the PDMS and the chamber were replicated as closely as possible with the dimensions, thickness and length on each chip being slightly different due to the manufacturing process. The chamber cut-out of the PDMS was modeled to be filled with water rather than air to simulate the isothermal amplification reagents - which are assumed to have a similar thermal conductivity to water. The chamber position was modeled slightly off centre to more accurately simulate the normal working conditions since none of the chambers were situation in the exact middle of the chips.

An aluminium plate was modeled to be placed against the base of the glass as the heat source since modeling a peltier device thermally is problematic. The aluminium plate was modeled to the same dimensions as the peltier device. With the thermal conductivity of aluminium being high very little heat would not be conducted into the glass making it a good substitute heat source. The PDMS was simulated with a thermal conductivity of 0.17W/mK and with a specific heat of 1200 J/kgK [62].

8.2 Thermal Profile Simulations

Thermal profile simulations of the materials and their response to the heating element allow for a basic interpretation of the thermal gradients experienced by the device at steady state as well as being a good indicator of the validity of any thermal assumptions made. A number of different simulation profiles are shown below.

8.2.1 Thermal Profile – Top View

COMSOL Multiphysics allows for intuitive thermal profiles to be developed of three dimensional structures. These structures can be viewed from any angle and a colour chart is displayed alongside the image to allow for simple thermal profiling.

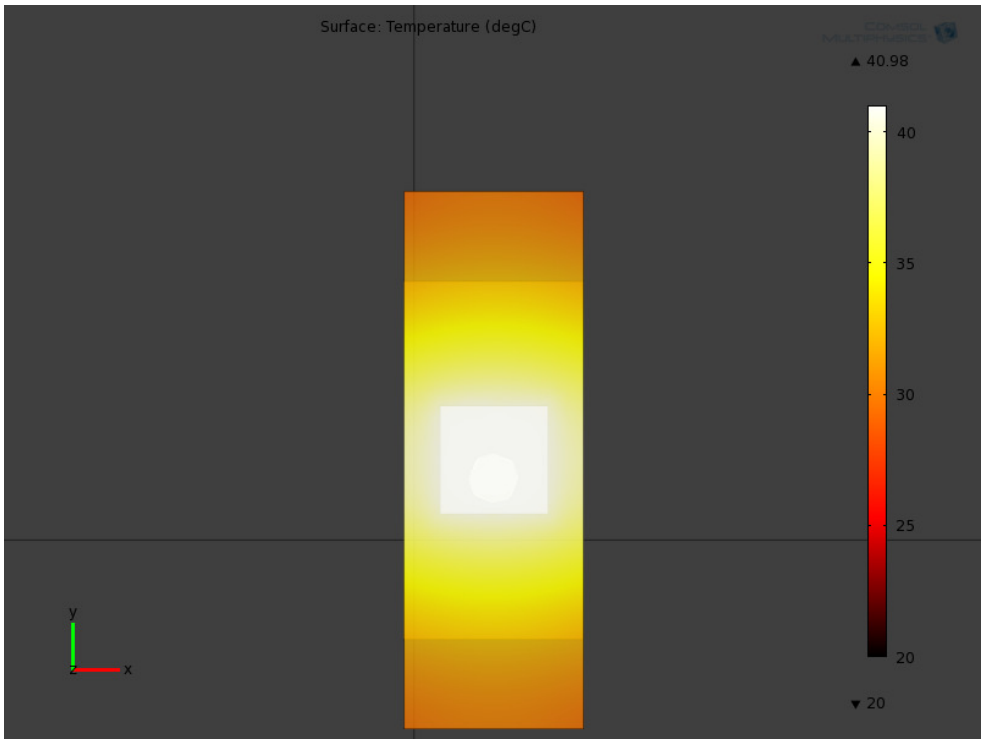

Figure 52 - Thermal Profile, Top View

The above image (Fig. 51) shows the thermal profile of the microfluidics chip as seen from the top. From this image it can be seen that the fluid (water) inside the well is close to the temperature of the heating element – which was expected. Significant levels of conduction across the face of the glass are apparent with the edges of the glass measuring just under 31°C. An enlarged image of the same section is shown below (Fig. 52) for clarity.

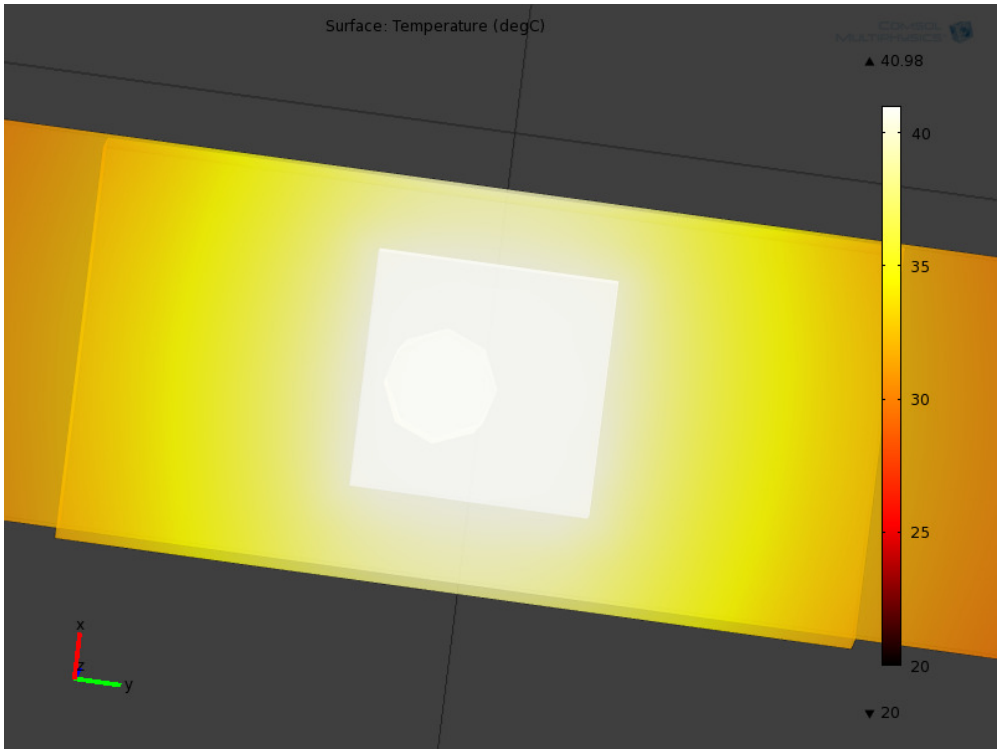

Figure 53 - Thermal Profile, Top View (increased)

The image above (Fig. 52) shows slightly more clearly the temperature difference developed across the PDMS as well as the temperature distribution within the well. A clearer lateral view of the contents of the well is shown below as well as giving an indication of the thermal profile of the glass directly above the heating element.

8.2.2 Thermal Profile – Lateral View

The lateral view of the fluidic cassette shows the temperature difference developed across the length of the glass and PDMS. The contents of the fluidic chamber can also be seen to be in thermal equilibrium with the surface of the glass face.

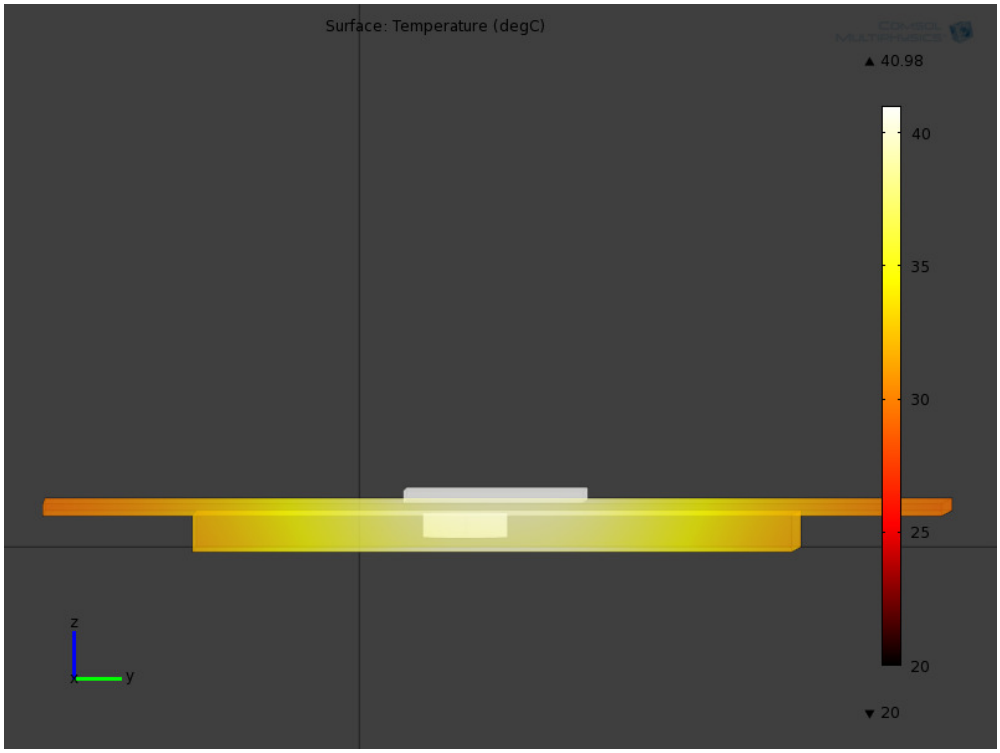

Figure 54 - Thermal Profile, Lateral View

The image above (Fig. 53) shows the chip flipped around the vertical axis.

8.3 Thermal Contours and Cross Sections

A slightly better indication of the thermal contents of the materials is a simple cross-sectional thermal profile (slice) through an area of interest. A slice is a tool used to display a thermal profile of a material in two dimensions which are not necessarily at the surface of the material. A slice cuts a cross-sectional profile through a material and displays the thermal profile at the level of the cut. This allows the thermal distribution within the material to be evaluated and not just that of the surface.

Contour lines known as isotherms allows for a thermal contour (or contour map) to be plotted showing the increasing levels of temperature similar to the way heights are represented on geographical maps. It is important to note that the units of the axes of the contour maps presented below are in **meters (m)** and the temperatures in **degrees Celsius.**

8.3.1 Thermal Cross Section – Glass Face

The cross section shown below (Fig. 54) is a thermal profile slice taken through the centre of the glass slide and parallel to its surface. This profile shows that the glass is indeed at the same temperature as the heating element alongside the laterally conducted heat power dissipating towards the edges.

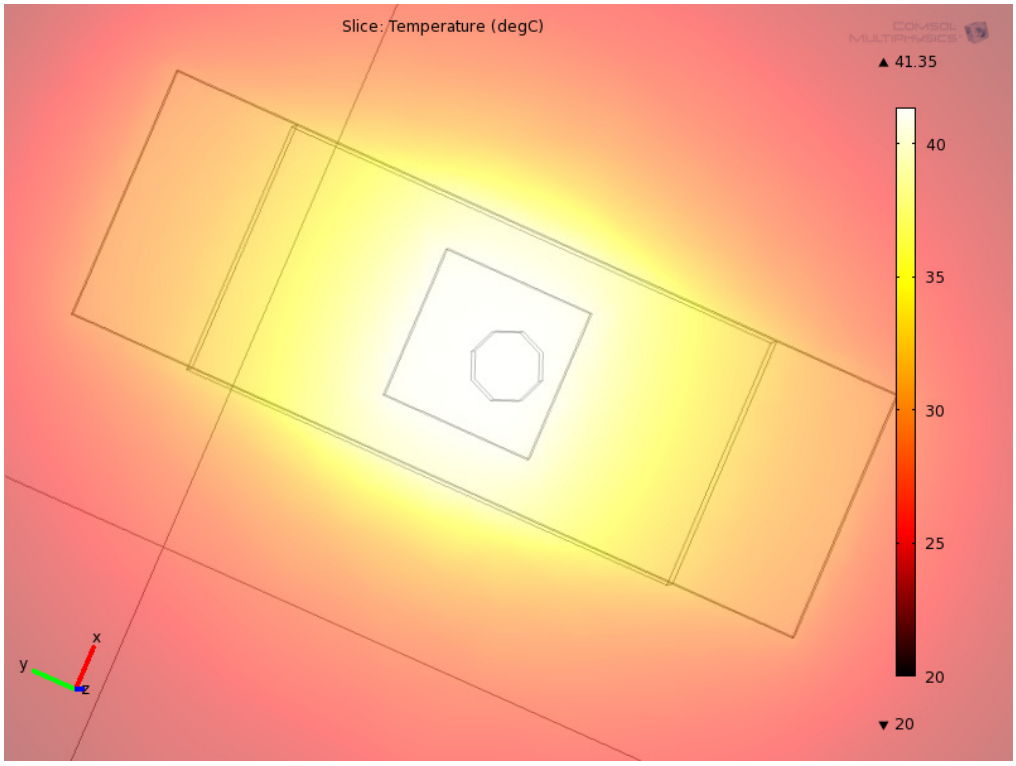

Figure 55 - Cross Sectional Thermal Gradient

8.3.2 Thermal Contour – Glass Face

The thermal contour presented below (Fig 55, 56) shows the temperature distribution across the face of the glass situated above the heating element.

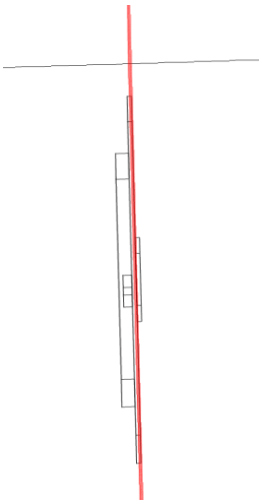

Figure 56 - Slice Angle

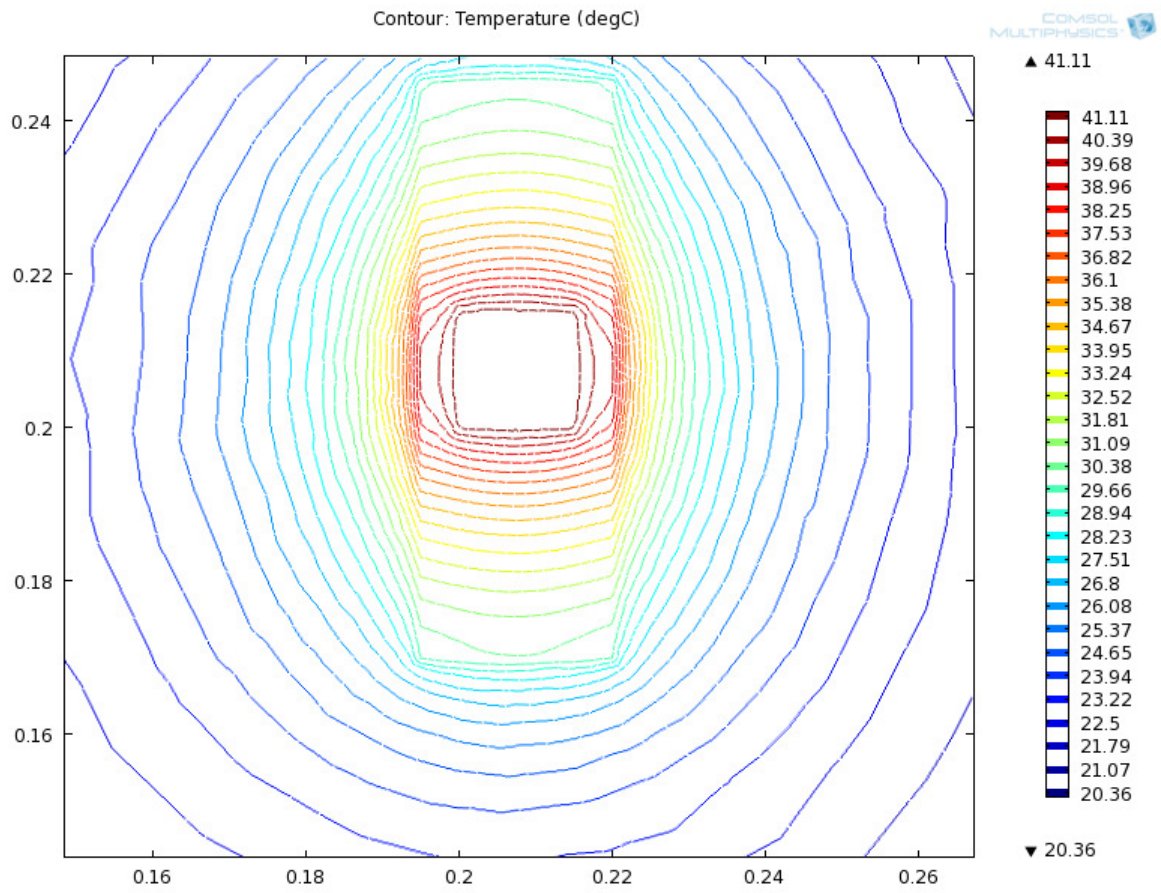

Figure 57 - Thermal Contour - Glass Face

The image above clearly shows the area of the glass above the peltier which at the same temperature as the heating element and the range (just under 15mm) of the surface which is in thermal equilibrium. The range of glass which remains at the same uniform temperature with the heating element is the area in which the heat sensor must be placed in order to accurately control the fluid within the chamber. Anywhere within this 15mm section will suffice.

8.3.3 Thermal Contour - Lateral Cross Section

The image below (Fig. 57) is a magnified thermal contour of the cross section focusing on the centre of the chip cut lengthwise across in order to give an understanding of the temperature differences present through the device.

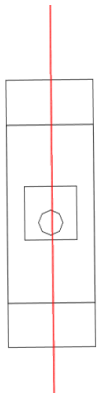

Figure 58 - Slice View. Cross Section

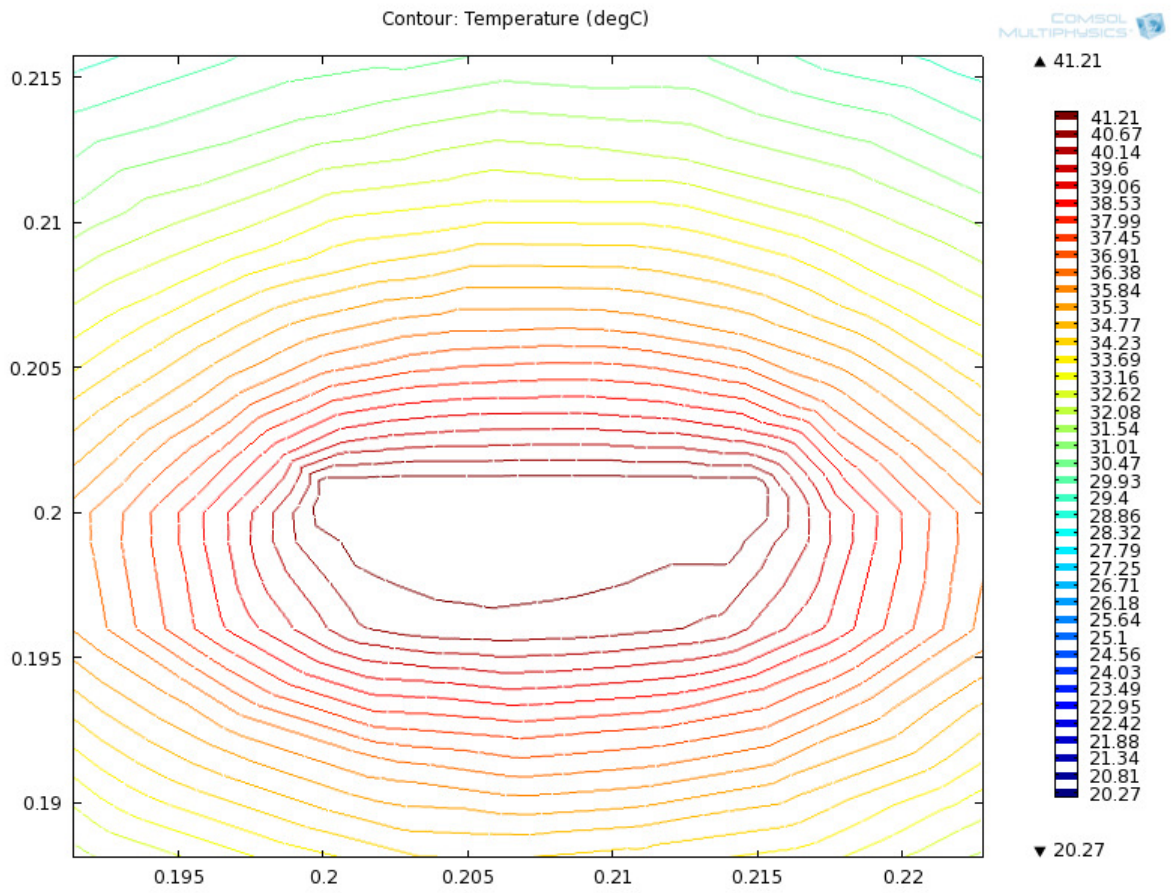

Figure 59 - Cross Sectional Thermal Contour

The thermal contour (Fig. 58) shows a 4mm section where the temperature measures 41.21°C. This contour extends (from the flat line being the hot surface of the aluminium) for 3mm into the device. This takes the thermal contour through the 1mm glass and into the fluidic chamber. This shows (as expected) that the fluid in the chamber directly above the glass surface is indeed in thermal equilibrium with the heating element.

8.3.4 Thermal Contour – The Reaction Chamber

Taking a thermal contour (Fig. 59; below) by raising the slice so that it is now centered within the PDMS in the middle of the chamber the innermost contour ring displayed in the liquid is found to measure 41.22°C at steady state. This simulation confirms the experimental data obtained showing that the fluid within the glass reaches the same temperature (or as close to as possible) with the glass surface. Hence controlling the temperature of the glass surface is successful in controlling the temperature of the fluid in the chamber to the same temperature.

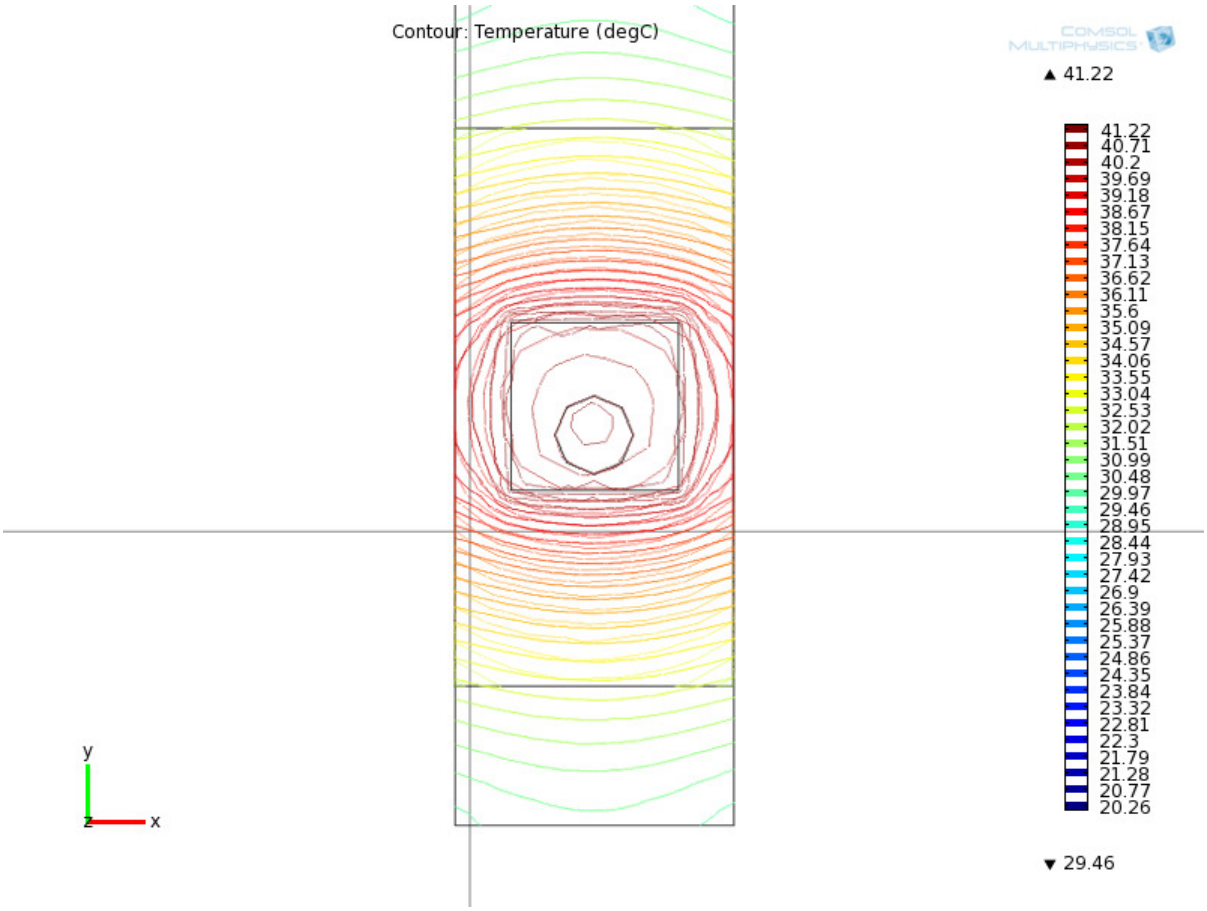

Figure 60 - Cross Sectional Gradient and Contour

8.4 Conclusion

The simulations presented in COMSOL accurately model the physical system and concur with the experimental data. These simulations provide an overall view of the thermal profile experienced by the developed microfluidic chips during run time. The simulated results also agree with the initial assumptions and operating principle of the thermal control system which was that the fluid inside the chamber reaches the same temperature as the glass face directly above the peltier heating element. It also showed that the placement of the thermal sensor within close vicinity to the glass is valid so long as it is within the 15mm range of glass which is in thermal equilibrium with the peltier device.

This simulation validates the assumptions that:

1. The temperature of the fluid within the chamber can be accurately controlled by controlling the temperature of the glass surface. This is due to the fact that the glass surface and fluid in the chamber are in thermal equilibrium and at the same temperature (at steady state).
2. The placement of the thermal transducer anywhere directly above the peltier heating element against the glass surface is valid since the portion of glass directly in contact with the heating element exhibits a uniform temperature profile, as is reflected on the surface of the peltier element.

9. RESULTS

The results of the system testing on samples supplied by the Department of Molecular Medicine and Haematology are discussed below as well as their implications on the overall performance of the developed solution. The developed solution includes:

- Single chamber PDMS-glass hybrid microfluidic cassettes
- Developed temperature measurement board with PC interface
- Temperature Control Algorithm

Initially to test the performance of the NucliSENS isothermal amplification assay a single test was run on a sample (viral RNA concentration 640,000 copies/ml) to verify that detectable products were generated as expected. This test succeeded in detecting amplified products. For the further testing and evaluation purposes each test was performed with three samples using FRET probe fluorescence detection. The three samples used were:

a. Negative Control (containing no HIV)
b. Sample to be evaluated on bench-top equivalent system
c. Sample to be evaluated on developed prototype system

The HIV positive samples (*b, c*) were the same sample which was divided to allow for viral load detection in the two different test platforms. The intention was to compare the yield between the two systems as a measurement of the performance of the developed prototype system.

9.1 Evaporation

One of the factors which were not considered until the final evaluations of the system was that of evaporation within the sealed chamber. This was shown to be a costly oversight in the initial testing which was performed with the Department of Molecular Medicine and Haematology on an actual high viral load HIV sample.

9.1.1 Initial Quantitative Evaluation

The sample and isothermal amplification reagents (40µl) filled approximately 20% of the chamber which has the capacity to hold between 80µl-100µl. The chips were initially designed to contain 50µl of fluid, however, the chips developed by the CSIR were made to larger dimensions and the maximum volume of the chips was increased. The larger dimensions had to be accommodated since the CSIR could not achieve smaller dimensions using the laser ablation techniques to create the chambers.

The high binding affinity of the droplet to the PDMS rather than spreading out over the glass meant that only a small portion of the chamber was filled. The isothermal amplification was allowed to run for 4 hours before sample evaluation. In this initial experiment, 75% of the 40µl in the chamber evaporated with less than 10µl remaining in the well despite the chamber being sealed. This sample size was insufficient for FRET analysis evaluation on the light-cycler and hence no result could be obtained.

The sample was diluted and a fluorescent evaluation of both the bench-top sample, negative control and diluted sample was performed using the light cycler. No fluorescence could be seen on the diluted sample – as was expected, however, a null result was also obtained on the positive sample which was evaluated in the bench-top system which was an unexpected result.

9.1.2 Factors Affecting Evaporative Rates

In order to minimize the levels of evaporation present in the developed prototype a brief study was launched into evaporation theory and possible methods to mitigate the extent of evaporation. Only the factors which could be of influence or controlled in the developed system are discussed.

Evaporation in a closed chamber reaches a state known as evaporative equilibrium. This occurs when the vapour in the air becomes saturated and no further increase in vapour pressure occurs [65]. Molecules which escape from the fluid as vapour often condense and return to vapour. The exchange from fluid to vapour and returning to fluid occurs with higher frequency as the density and pressure of the vapour increase. When this exchange reaches an equilibrium rate, evaporative equilibrium is said to be reached.

The following was identified as factors which play a role in the evaporation process in the developed prototype:

a) Flow rate of air
b) Pressure within the chamber
c) Exposed surface area of the fluid present
d) Temperature of the fluid

9.1.3 Flow Rate of Air

The flow rate of external air to the reaction was minimized by the use of thin hypodermic needles injected the fluids through the PDMS. Making such small perforations in the material causes it to fold back onto itself creating a light seal. The effects of external air sources were eliminated by the use of transparent adhesive tape across the perforations in the PDMS sealing it from the outer environment.

The only air which still plays a role is that trapped within the chamber. Blocking off any escape and renewal of air in the chamber promotes higher vapour content within the chamber causing evaporative equilibrium to occur quicker.

9.1.4 Pressure within the Chamber

Evaporation is known to occur faster at lower pressures since a smaller force exists on the surface of the fluid keeping the molecules from escaping to vapour. Slightly higher than normal atmospheric pressure are expected than in the chamber during normal operation with no practical way of increasing the pressure without stressing the PDMS seals against the glass. An attempt to increase the pressure in the well by any significant measure results in fluid breaking the seals between the glass and PDMS and expulsion of the fluid occurs.

9.1.5 Surface Area of the Fluid within the Chamber

The larger the exposed surface area of the fluid to the air the faster the evaporation occurs. One way to minimize the exposed surface area of the fluid to the air is to minimize the air present in the chamber and increase the levels of fluid (since some substance is required to take the place of the air). Smaller areas of air minimize the rate at evaporation which could potentially occur as well as minimizing the overall air pocket available to be filled with vapour.

9.1.6 Temperature of the Fluid

The higher the temperature of the fluid, the higher the kinetic energy present in the molecules. Higher kinetic energies allow molecules to escape to vapour form much quicker than those of lower kinetic energies. Hence the higher the kinetic energies, the faster evaporation occurs. Unfortunately, the temperature of the fluid in this application is required to be strictly controlled to 41°C.

9.2 Evaporation Testing

Due to the unforeseen evaporation levels present in the testing, further experiments were carried out in order to determine the levels of evaporation present in the PDMS chamber.

Initial volumes of food colouring mixed in water were injected using pediatric hypodermic needles into the chamber. Using such small hypodermic needles minimal structural damaged is caused to the PDMS housing of

the chamber and the PDMS re-seals itself. As an added precaution adhesive tape was also applied across the puncture in the PDMS in order to ensure complete sealing from the environment. The purpose of the food-coloured water is to measure the extent of evaporative loss in the system assuming that the water behaves in a similar manner to the isothermal amplification reagents under the same conditions. The evaporative study is carried out using the dyed water and eventually compared to the same response, under the same conditions to that of the isothermal reagents in order to verify whether or not the two substances respond similarly.

9.2.1 Evaporative Evaluation

Due to the high binding affinity of the liquid with the PDMS surface (being hydrophobic) there is a non-uniform spread of the liquid across the chamber (Fig. 60; below).



Figure 61 - Evaporative Evaluation - Non-Uniform Chamber Fill

This means that the liquid only partially fills a portion of the chamber, leaving the rest of the chamber filled with air. The pressure inside the chamber dictates that the fluid can only fill the chamber to an extent before air has to be removed for more fluid to enter the chamber. The air in the chamber is the point where the problem is introduced. Air has an exceptionally poor thermal conductivity of 0.024W/mK. This introduces a significant temperature difference across the chamber since the liquid is (ideally) in thermal equilibrium with the face of the glass which is kept at 41°C. The air being of a significantly reduced temperature to the rest of the chamber promotes higher levels of evaporation before the system reaches steady state.

During the testing, the formation of “pockets” of air within the fluid can be seen forming within 2 minutes (Fig. 61; below). These pockets are seen to be generated in areas where air has been trapped within the fluid.

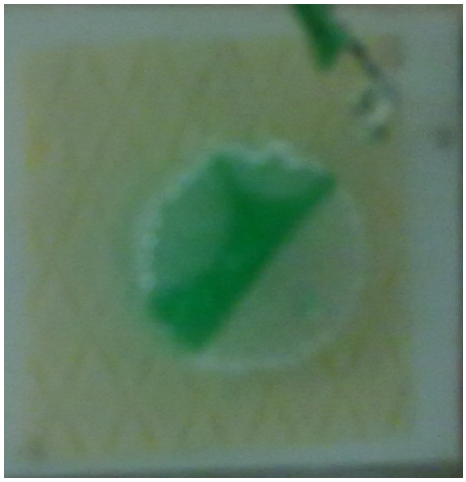

Figure 62 - Evaporative Evaluation - Air Pockets

Condensation is apparent within the chamber (due to evaporation) within 10 minutes of the experiment running (Fig. 62).

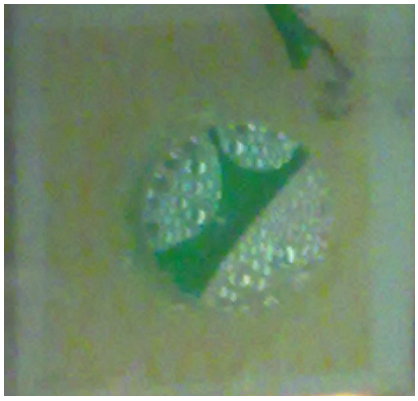

Figure 63 - Evaporative Evaluation - Condensation

The issue with the high binding affinity of the liquid to the PDMS plays a significant role in the evaporation process. Should the liquid, instead, spread over the glass rather than bind to a side of the chamber the same volume of air would remain in the chamber. The liquid spread over the base of the glass would provide a much higher surface area of exposure to the air and would likely increase the levels in evaporation.

9.2.2 Design Alternatives to Prevent Evaporation

A number of different design modifications to the developed prototype were considered in order to minimize the extent of evaporation present.

a) Adding PCR mineral oil to the fluid
b) Creating a “hot lid” device
c) Diluting the contents to fill the chamber whilst attempting to evacuate the air bubble

High evaporation levels within a sealed chamber have been known to occur with temperature differences as little as 2°C [66]. PDMS is known to be a porous substance which exacerbates the issue [67]. Ideally, the

optimal solution would be to have the chambers made with a maximum volume of 40µl, however, the CSIR were unable to achieve these dimensions using the laser ablation techniques.

9.2.3 Hot Lids

One of the common methods used in medical assays and PCR type devices to minimize evaporation levels are hot lids. In effect, the lid of the chamber is heated to the same temperature as the rest of the chamber in an attempt to minimize the levels of evaporation present. The evaporation is minimized since the lid is now heated to the same extent as the fluid lowering the overall possible surface available for condensation in an attempt to keep the vapor in the air and prevent further evaporative exchanges.

The effects of a hot lid in this implementation would, perhaps, minimize the levels of evaporation to an extent – but not noticeably. Due to the fact that the 'lid' is PDMS, this would require the inclusion of another heat source which would need to be able to sufficiently heat a purely PDMS surface. This would also not minimize the air volume in the chamber and the chamber walls would still be at a lower temperature than the liquid (albeit at a slightly higher temperature than without a heating lid) and a temperature difference would still be present. Including a heating element on the 'lid' of the chamber would also impede sample retrieval post-reaction as well add an additional source of possible contamination. The contamination may be introduced since an additional element is now being used to cover a small puncture in the PDMS which (is most likely not sterile) and in very close proximity (possible even in direct contact with) the PCR reagents and may cause inhibition in this current setup.

9.2.4 PCR Mineral Oil

Another commonly employed method to reduce evaporation levels is the use of PCR mineral oil. The oil forms a viscous layer in the solution. The mineral oil is intended to be immiscible and forms a layer at the top of the reagents. The temperature difference still exists within the chamber, however, the oil does not evaporate and any fluids underneath the oil are hindered from evaporating [12].

The problem in this implementation is the introduction of the mineral oil into the chamber. The oil is too viscous to be injected using a hypodermic needle and since the only other method for insertion would be to cut out the PDMS sealing lid. This method was not employed.

9.2.5 Dilution of Contents

The dilution of the contents of the chamber is an option, however, would negatively affect the fluorescent results. Dilution is required so as to minimize the amount of air in the reaction chamber thus lowering the levels of evaporation. Diluting the contents would minimize the fluorescence per square area of the contents as evaluated by the light-cycler and the risk of diluting the contents beyond detectable limits is high.

Ideally the chamber size should be reduced to the correct dimensions for a 40µl volume. This would minimize the amount of air in the chamber and significantly reduce the temperature difference as seen inside the well. This should also include a valve to allow the air to be forced out of the chamber so that the fluid would be able to fill the entire chamber. During initial experimentation the chamber could only be filled to approximately half its volume with water until the pressure inside the chamber (since no air could escape) forced any additional fluid out of the chamber. This was solved (to an extent) by using two syringes simultaneously – one to inject fluid, the other to suction air out of the chamber.

9.3 Implemented Evaporative Solution

From the above information, the possible design alternatives were identified as:

a) Developing a Hot Lid
b) Injecting PCR Mineral Oil, and
c) Increasing the volume of liquid in the chamber (dilution)

The design solution chosen was that of increasing the volume of the liquid within the chamber since neither the hot lid nor the PCR mineral oil could be successfully applied to this platform.

Testing was again conducted using food colouring in water in order to determine the evaporation levels present with the reaction chamber being filled to capacity.

9.3.1 Evaporative Evaluation – Maximum Capacity

Two syringes were used in order to get the fluid to fill the chamber as much as possible. One syringe injected the fluid whilst the other extracted air out of the chamber simultaneously. Some small air pockets and a small air bubble can be seen in the image below (Fig. 63). The chamber was filled with just under 100µl of fluid.

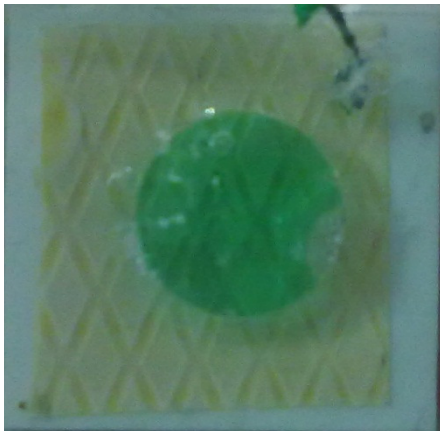

Figure 64 - Evaporative Evaluation - Maximum Capacity

The image above shows that most of the chamber was filled with the liquid barring minor air pockets. After allowing the system to run at 41°C for 1hour some condensation can be noted, as shown below. This indicates that evaporation in the chamber has not been eliminated, however, can be seen at significantly lower levels (Fig. 64).

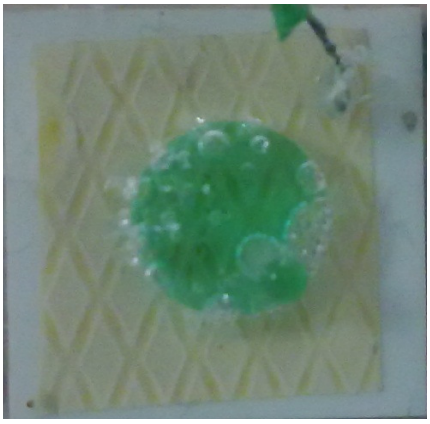

Figure 65 - Evaporative Evaluation - Maximum Capacity, Condensation

After allowing the system to run for a period of 4 hours the extent of the air bubbles and condensation were comparable to that seen after a 1 hour run time (Fig. 65). This experiment was repeated on 3 microfluidic cassettes each running three samples (total n = 9 experiments). The cassettes were limited to 3 runs due to the tearing of the PDMS lid from sample insertion and extraction).

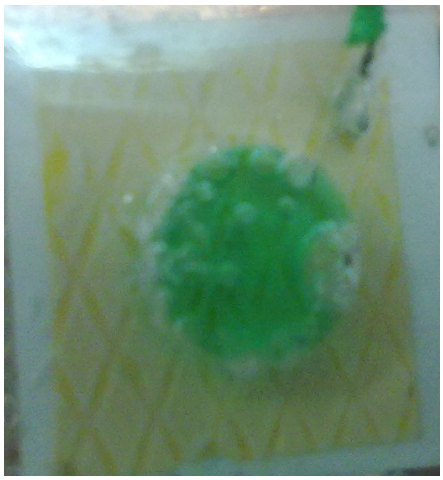

Figure 66 - Evaporative Equilibrium - Maximum Capacity, 4 Hours

After extracting the remaining fluid from the chamber more than 80µl was still present (in n=8 samples) indicating that the evaporation levels had decreased from 75% (as initially experience) to around 20% - which is manageable in this application since a minimum of 20µl is required for evaluation in the light-cycler.

9.3.2 Evaporation Testing – PCR Buffer

In order to determine whether the water with food colouring exhibited similar evaporation dynamics to that of the reagents used in the isothermal amplification system an evaluation of the evaporation levels of the PCR buffer used was conducted. This consisted of:

a) 30µl RNase free water
b) 40µl Primer
c) 10µl Enzyme

Which came to a total volume of 80µl. This was evaluated against 80µl of ordinary tap water coloured with green food colouring (Fig. 66) to verify whether or not the two fluids respond similarly in these conditions.

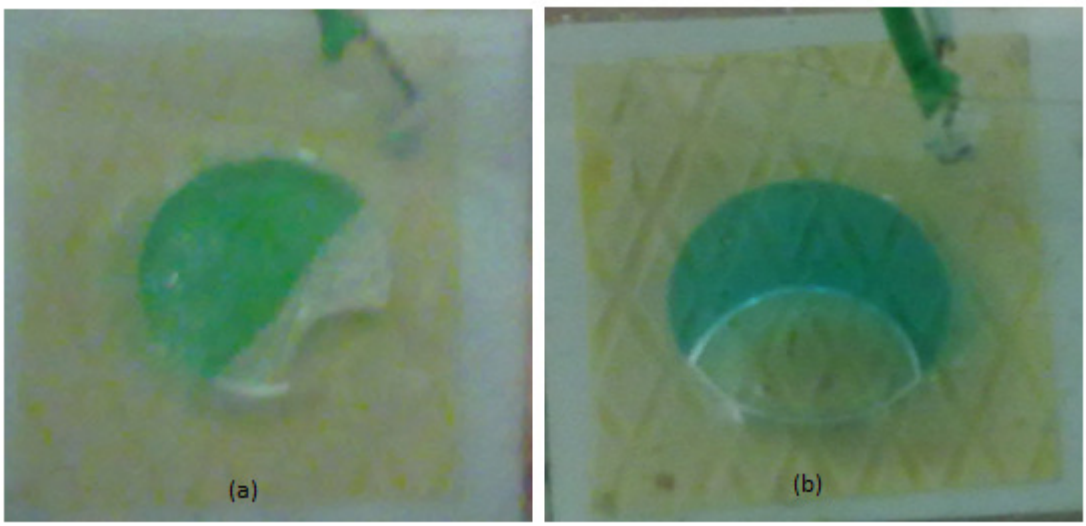

Figure 67 - Evaporative Evaluation; (a) 80µl of Water, (b) 80µl of PCR buffer

After allowing both tests to run for 4 hours the fluid remaining in the chamber from both the food coloured water and the PCR buffer were similar. The extracted PCR buffer fluid after the test is shown below (Fig. 67) and measured just over 30µl whilst the extracted water was around 35µl.



Figure 68 - Extracted PCR Buffer

This result, although confirming that both fluids respond similarly under the same conditions, showed high levels of evaporation- almost 60% fluid loss (n=1 experiment). Since both fluids exhibit similar levels of evaporation under the same conditions it can be assumed that the extent of evaporation when running the isothermal amplification reagents and samples would be of the same order as that of the food coloured water.

This experiment was only conducted once due to the costs and limited quantities of the PCR buffer.

9.4 Final Test

The final test completed with the BioMerieux NucliSENS EasyQ HIV-1 v2.0 on a sample containing HIV was conducted by combining two samples together in order to increase the overall fluid volume in the chamber in an attempt to minimize the overall evaporation. The test was conducted with a total fluid volume of 80µl and allowed to run for three hours instead of four.

The NucliSENS EasyQ HIV—1 v.20 recommends an allotted run time of at least two hours. Previous tests (n=1, viral RNA concentrations 350,000 copies/ml) were conducted allowing the sample to run for four hours in an attempt to get the highest possible yield out of each assay. The run-time was reduced in the final test (n=2) in an attempt to ensure that enough fluid remained (at least 20µl) for fluorescent evaluation. The reduced run-time may not have reduced the overall evaporation experienced, however, was hoped to minimize the effect of the porosity of the PDMS substrates.

After three hours the sample was extracted using a syringe and a micropipette measured the overall total volume to be just over 20µl indicating a slightly higher fluid loss to that of the regular PCR buffer. The additional loss, however, can be accounted for by residual fluid remaining in the syringe and needle. The sample must be extracted immediately and injected into a container and exposure to repeated extractions and syringing significantly increases the risk of contamination.

The two samples were run on the developed system and a PCR bench-top equivalent and the results were inserted into the light cycler for evaluation. The results from the light cycler print-out are shown below:

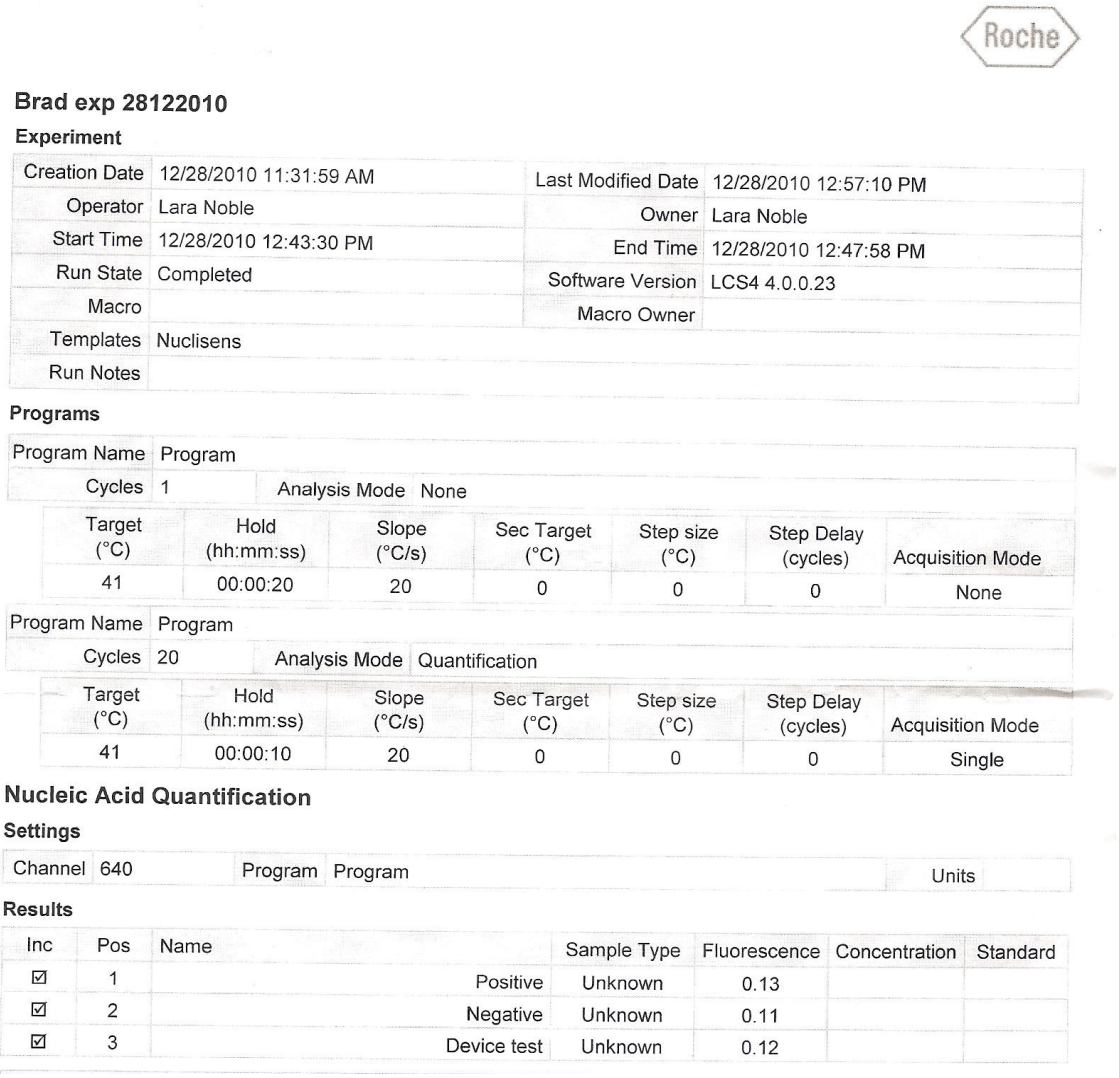

Roche

Brad exp 28122010

Experiment

Creation Date	12/28/2010 11:31:59 AM	Last Modified Date	12/28/2010 12:57:10 PM
Operator	Lara Noble	Owner	Lara Noble
Start Time	12/28/2010 12:43:30 PM	End Time	12/28/2010 12:47:58 PM
Run State	Completed	Software Version	LCS4 4.0.0.23
Macro		Macro Owner	
Templates	Nuclisens		
Run Notes			

Programs

Program Name	Program		
Cycles	1	Analysis Mode	None

Target (°C)	Hold (hh:mm:ss)	Slope (°C/s)	Sec Target (°C)	Step size (°C)	Step Delay (cycles)	Acquisition Mode
41	00:00:20	20	0	0	0	None

Program Name	Program		
Cycles	20	Analysis Mode	Quantification

Target (°C)	Hold (hh:mm:ss)	Slope (°C/s)	Sec Target (°C)	Step size (°C)	Step Delay (cycles)	Acquisition Mode
41	00:00:10	20	0	0	0	Single

Nucleic Acid Quantification

Settings

Channel	640	Program	Program	Units

Results

Inc	Pos	Name	Sample Type	Fluorescence	Concentration	Standard
☑	1	Positive	Unknown	0.13		
☑	2	Negative	Unknown	0.11		
☑	3	Device test	Unknown	0.12		

Figure 69 - Roche Light Cycler Test Result

The result obtained from the light cycler (Fig. 68) was a null result on both samples. The fluorescence measured on the bench-top sample was 0.13, the developed solution sample measured 0.12 and the negative control 0.11. The fluorescence measured was partially higher than that of the negative control, but not sufficiently high enough to indicate that the amplification occurred successfully, if at all. The expected results would be that the fluorescence should be at least double that of the negative control sample.

Neither the bench-top equivalent, nor the developed solution produced a measureable result using the NucliSENS EasyQ HIV-1 v2.0 assay. Possible reasons for this are that the intended use of the NucliSENS assay is in automated systems and any manual process in an environment which is not sealed increases the risk of contamination. A number of external sources introduced from a manual process could severely hamper the sensitive nucleic acid result.

No further samples or reagents were available for additional testing to verify the performance of the system.

10. FUTURE RECOMMENDATIONS

A number of recommendations can be made for future work concerning the project, most of which involve corrections or further developments towards the microfluidic chips which were developed.

10.1 Reaction Chamber Dimensions

The dimensions of the single chamber chips developed by the CSIR were created with dimensions which were more than double those of the actual designs. This significantly increased the amount of air present in the chamber during the reactions and adversely affected the performance of the system to crippling levels.

Recommendations for the evaluation of PDMS as a substrate for an isothermal nucleic acid amplification substrate would be to develop these chips to the correct dimensions and possibly incorporate another channel which would allow for the air to escape whilst the fluid is being injected into the well.

10.2 µTAS Prototype

Continuation of the developed µTAS chips which were discussed in *Chapter 3; 3.4 - µTAS Design Beginnings* would be recommended. These chips suffered from a number of issues which prevented them from being used in this evaluation even after extensive time investments. The issues suffered by these microfluidic substrates are summarized below:

1. Structural collapse is apparent on all of the developed prototypes which prevented the chips from being used as a functional evaluation platform for the isothermal amplification system.
2. Amplification and detection chambers do not fill uniformly – changing the chamber shape and the placement of the supportive structures to change the fill pattern need to be investigated.
3. The pressure in the chambers needs to be noted and an escape valve for the air present needs to be investigated.
4. Channel depths may need to be reduced to around 45µm in order for the sieve valves to seal correctly. This, however, has an effect on the overall volume capacity and the channels would need to be lengthened.
5. Sieve valves are far from ideal and require evaluation
6. The design of the chips must be altered to include the possibility of dimensions well above 5µl.

10.3 Evaluation of Isothermal Assay

An evaluation of the chosen isothermal nucleic acid amplification system needs to be conducted. The performance of the chosen NucliSENS assay needs to be verified being performed in a manual system to determine where the fault lies in obtaining a null result during the fluorescence evaluation. Should this system be found to give erroneous readings and consistent null results its application as a reliable platform for POC developments would need to be reconsidered.

Whichever the chosen isothermal amplification assay is, it would also be recommended that the system be able to function at known values in the sub-microlitres range. This not only eases the development constraints placed on the microfluidic technologies but allows for much shorter run times required for these systems.

10.4 PCB Developments

A dedicated voltage reference chip would be more accurate than the potentiometer used a reference voltage to increase the scaling present on the PIC18F452.

The inclusion of a system to program the run-time and the desired temperature would add a level of flexibility to the device. The thermal control algorithm is all soft-coded with variables which allow for a quick manipulation by simply re-assigning a variable value which would alter the set point for the current system.

The only additional implementation which would be required is that of an input device to truly make this a standalone system.

PWM does create additional noise due to the switching transients which are induced. One option is to stop any PWM switching during ADC operations; however, this was not considered necessary since the noise induced by the PWM was not sufficient to warrant this action. The required level of measurement sensitivity was obtained without this. This could be a future recommendation for further improve the signal to noise ratio of the PCB.

10.5 Fluorescent Detection Incorporation

A detection technique which makes use of fluorochrome filled liposomes bound to surface immobilized oligonucleotide probes. The advantage of using liposomes over using normal detection methods is that with standard fluorescent detection makes use of a single fluorochrome molecule per target [68]. Liposomes are able to be filled with thousands of fluorochrome molecules significantly increasing the fluorescence per target amplicon (Fig. 69).

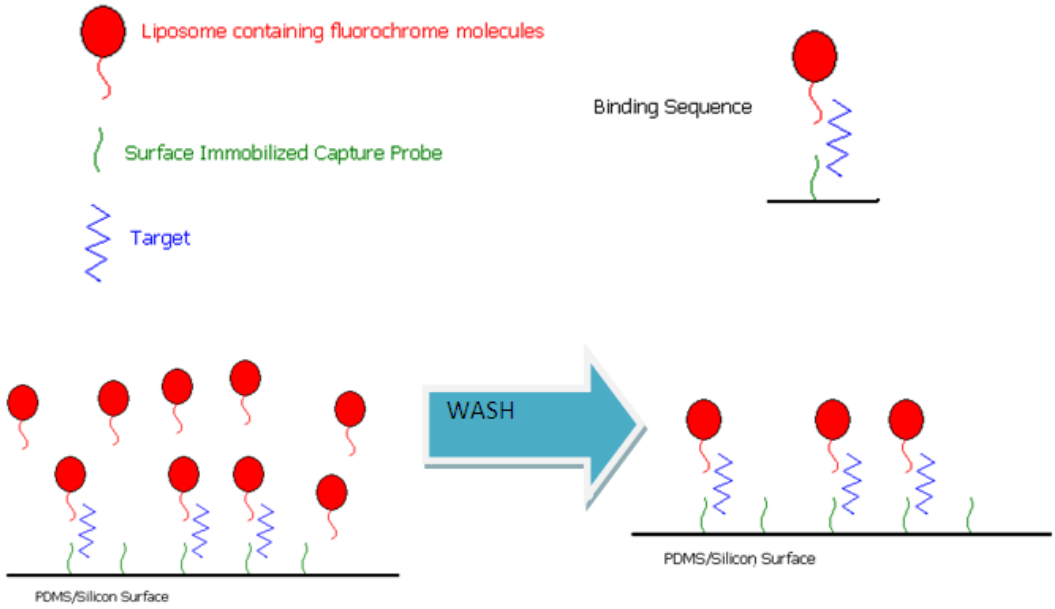

Figure 70 - Liposome Based detection

The detection stage would consist of the following process:

i. Introduce target into chamber containing liposomes and surface immobilized capture probes
ii. Liposomes and capture probes bind to the target
iii. Wash unbound liposomes out of the chamber
iv. Lyse the liposomes
v. Perform Fluorescent detection

Knowing the number of fluorochrome molecules per lipsome and fluorescence per fluorochrome molecule it would be possible to calculate the number of target amplicons present in – at least – a semi-quantitative manner.

11. CONCLUSION

The development of the point of care prototype device managed to achieve the initial goals as set out in the research proposal.

The temperature sensors selected were small enough to be able to measure a specified temperature of the device without interfering with either the functioning of the microfluidic substrates or the reaction occurring within the chamber. The initial developed µTAS system was an improvement on the functionality of the single chamber substrates; however, more work is required in order to allow these chips to be used as functional prototype platforms.

The entire device was developed using relatively low cost components in such a way which showed that expensive and customized components are not always necessary to develop accurate systems. The low noise characteristics of the developed PCB proved to be sufficient in eliminating both external and internal sources of noise and EMI with a significant reduction of 78.5% over that of using the PICDEM2+ development kit board. In this case the cost of the hardware was lower than that of the reagents used in the evaluation.

The poor thermal conductivity of PDMS was verified to be 0.21W/mK in this research. This low thermal conductivity did not, however, limit the accuracy of the control system. The implemented PI Controller managed to successfully manipulate the temperature of the PDMS to required values.

The thermal simulations conformed to the expected temperature profiles of the system and proved the validity of the assumptions which were developed for the successful implementation of the thermal control of the fluid. The assumption was that the fluid within the chamber reached thermal equilibrium with the glass face directly below it. This was proven to be that case both experimentally and in simulation. The second assumption was that the glass was uniform in temperature directly above the face of the peltier device which allowed for the insertion of a temperature probe anywhere within this area. This was also verified in the thermal simulations.

The accuracy and stability of the thermal controller were proven to be within acceptable limits as set out in the design constraints. The system was shown to be sensitive to within 1°C and stable over long periods of time. Any failure in amplification would not be a result of the thermal stability of the system. This was also shown in the Roche Light Cycler results with the developed system having a comparable yield to that of the bench-top equivalent; even though neither result was sufficient to prove successful amplification.

Exceptionally high levels of evaporation within a sealed environment were experienced in the attempted evaluations of the developed POC prototype system. Evaporation levels were initially minimized from 75% to 20% by increasing the volume of fluid within the chamber. Using this approach allowed for a high enough sample volume to remain at the end of the procedure for evaluation with the Roche Light Cycler. The lost evaporative vapour is assumed to be the cause of the porous nature of the PDMS absorbing the vapour and exacerbating the absorption levels. The initial cause of the extensively high evaporative levels are attributed to the manufacturing of the chips by the CSIR to dimensions which doubled the required design volume causing significant amounts of air to be present in the chamber.

The only evaluation which could not be performed was the comparison of the yield on the developed system against that of a bench-top equivalent. This is due to the repeated null result obtained from using the NucliSENS amplification system on both the bench-top and developed solution. Possible reasons for this are that the intended use of the NucliSENS assay is in automated systems and any manual process in an environment which is not sealed increases the risk of contamination. A number of external sources introduced from a manual process could severely hamper the sensitive nucleic acid result.

The BioMerieux NucliSENS EasyQ HIV-1 v2.0 needs to be evaluated as an assay which can be performed manually and possible replacement of this system in favour of a different isothermal nucleic acid amplification requires investigation. Due to the failure of the isothermal amplification system, the levels of protein fouling present in the PDMS developed substrates could not be evaluated. Protein fouling cannot be the cause of the failure of the amplification system since a null result was obtained in two out of the three tests using industry standard PCR sample containers on the bench-top equivalent device. These standard containers do not exhibit high levels of protein fouling.

The evaluation of the developed test platform obtaining a null result – which is most likely due to the performance of the chosen isothermal amplification system – poses the question of whether or not the novel RT-LDA should be evaluated on this platform. The recommendation is that a different isothermal amplification assay should first be evaluated on the platform and compared to a bench-top device (as with this experiment) before testing the novel amplification system's performance on an unproven testing platform.

12. Acknowledgements

The key personnel and research staff who played a role in the development along with their respective associations are shown below.

School of Electrical and Information Engineering:

i. Prof. D Rubin
ii. Prof. I Hofsajer

Department of Molecular Medicine and Haematology, School of Pathology, Wits Medical School:

i. Natasha Gous
ii. Prof. L. Scott
iii. Prof. W. Stevens

CSIR

i. K. Land
ii. Dr. S. Potgieter.

Special thanks to Dr. Lesley Scott for the hours of proposal writings in attempts to obtain funding for the extension of the project.

Thanks to Natasha Gous for taking time out of her research and preparing the viral samples, performing the required experiments and assisting where ever help was needed.

Special thanks to Prof. Ivan Hofsajer for the assistance in funding and all of the technical support throughout the process.

13. References

[1] S. Fiscus, B. Cheng, S. Crowe, L. Demeter, C. Jennings, V. Miller, and R. Respess, Stevens, "HIV-1 viral load assays for resource-limited settings.," *PLoS medicine*, vol. 3, Oct. 2006, p. e417.

[2] WHO, "HIV / AIDS Programme Antiretroviral Therapy for HIV Infection in Adults and Adolescents : Recommendations for a public health approach 2006 revision Addendum To 2006 WHO Guidlines On Antiretroviral Therapy for HIV Infection," *World Health - in Geneva*, 2006.

[3] S. Kasap, "THERMOELECTRIC EFFECTS IN METALS : THERMOCOUPLES," 2001, pp. 1-11.

[4] "AVERT International AIDS Charity," *World AIDS Statistics*, 2008.

[5] B. Faso, *Overview of the Global AIDS Epidemic*, 2006.

[6] C.F. Gilks, S. Crowley, R. Ekpini, S. Gove, J. Perriens, Y. Souteyrand, D. Sutherland, M. Vitoria, T. Guerma, and K. De Cock, "The WHO public-health approach to antiretroviral treatment against HIV in resource-limited settings.," *Lancet*, vol. 368, Aug. 2006, pp. 505-10.

[7] D. Morgan, C. Mahe, B. Okongo, R. Lubega, and J. Whitworth, "HIV-1 infection in rural Africa: is there a difference in median time to AIDS and survival compared with that in industrialized countries?," *AIDS*, vol. 16, 2002, pp. 597-603.

[8] D. Morgan, C. Mahe, B. Okongo, R. Lubega, and J. Whitworth, "HIV-1 infection in rural Africa: is there a difference in median time to AIDS and survival compared with that in industrialized countries?," *AIDS*, vol. 16, 2002, pp. 597-603.

[9] D. Ross, *Introduction to Molecular Medicine*, Springer-Verlag, 2002.

[10] P. Yager, G.J. Domingo, and J. Gerdes, "Point-of-care diagnostics for global health.," *Annual review of biomedical engineering*, vol. 10, Jan. 2008, pp. 107-44.

[11] C.D. Chin, V. Linder, and S.K. Sia, "Lab-on-a-chip devices for global health: past studies and future opportunities.," *Lab on a chip*, vol. 7, Jan. 2007, pp. 41-57.

[12] K.D. Spitzack and V.M. Ugaz, "Polymerase chain reaction in miniaturized systems: big progress in little devices.," *Methods in molecular biology (Clifton, N.J.)*, vol. 321, Jan. 2006, pp. 97-129.

[13] Y.S. Shin, K. Cho, S.H. Lim, S. Chung, S.-J. Park, C. Chung, D.-C. Han, and J.K. Chang, "PDMS-based micro PCR chip with Parylene coating," *Journal of Micromechanics and Microengineering*, vol. 13, Sep. 2003, pp. 768-774.

[14] H.-S. Chuang and S. Wereley, "Design, fabrication and characterization of a conducting PDMS for microheaters and temperature sensors," *Journal of Micromechanics and Microengineering*, vol. 19, Apr. 2009, p. 045010.

[15] J. Kim, J. Lee, S. Seong, S. Cha, S. Lee, and T. Park, "Fabrication and characterization of a PDMS–glass hybrid continuous-flow PCR chip," *Biochemical Engineering Journal*, vol. 29, Apr. 2006, pp. 91-97.

[16] M.A. Dineva, L. Mahilum-Tapay, and H. Lee, "Sample preparation: a challenge in the development of point-of-care nucleic acid-based assays for resource-limited settings," *The Analyst*, vol. 132, 2007, p. 1193.

[17] N. Gous, L. Scott, O. Perovic, F. Venter, and W. Stevens, "Should South Africa be performing Nucleic Acid testing on HIV ELISA negative samples?," *J. Clin Micro*, vol. 48, 2010.

[18] S. Franssila, "Introduction to Microfabrication," John Wiley and Sons, 2010, pp. 209-212.

[19] R. Chan and V. Chen, "Characterization of protein fouling on membranes : opportunities and challenges," *Journal of Membrane Science*, vol. 242, 2004, pp. 169-188.

[20] C. Velasco, M. Ouammou, J.I. Calvo, and A. Hernández, "Protein fouling in microfiltration : deposition mechanism as a function of pressure for different pH," *Journal of Colloid and Interface Science*, vol. 266, 2003, pp. 148-152.

[21] J. Johansson, H.K. Yasuda, and R.K. Bajpai, "Fouling and Protein Adsorption," *Applied Biochemistry And Biotechnology*, vol. 70, 1998.

[22] W.R. Bowen, T.A. Doneva, and J.A.G. Stoton, "Protein deposition during cross-flow membrane filtration : AFM studies and flux loss," *Colloids and Surfaces*, vol. 27, 2002, pp. 103-113.

[23] P. Gong and D.W. Grainger, "Nonfouling Surfaces - A Review of Principles and Applications for Microarray Capture Assay Designs," *Methods*, vol. 381, pp. 381-381.

[24] J.A. Koehler, M. Ulbricht, G. Belfort, and N. York, "Intermolecular Forces between a Protein and a Hydrophilic Modified Polysulfone Film with Relevance to Filtration," *Film*, 2000, pp. 10419-10427.

[25] J.-H. Han and J.-Y. Yoon, "Reusable, polyethylene glycol-structured microfluidic channel for particle immunoassays.," *Journal of biological engineering*, vol. 3, Jan. 2009, p. 6.

[26] A. Maartens and P. Swart, "Enzymatic cleaning of ultrafiltration membranes fouled in wool-scouring effluent," *WaterSA*, vol. 24, 1998, pp. 71-76.

[27] L. Chen, J. West, P.-A. Auroux, A. Manz, and P.J.R. Day, "Ultrasensitive PCR and real-time detection from human genomic samples using a bidirectional flow microreactor.," *Analytical chemistry*, vol. 79, Dec. 2007, pp. 9185-90.

[28] A. Gulliksen, "Microchips for Isothermal Amplification of RNA - Development of microsystems for analysis of bacteria , virii and cells," *Sciences-New York*, 2007.

[29] C.-H. Lin, G.-B. Lee, B.-W. Chang, and G.-L. Chang, "A new fabrication process for ultra-thick microfluidic microstructures utilizing SU-8 photoresist," *Journal of Micromechanics and Microengineering*, vol. 12, 2002, pp. 590-597.

[30] C. Hong, J. Choi, and C. Ahn, "A novel in-plane passive microfluidic mixer with modified Tesla structures," *Lab on a Chip*, 2004, pp. 109-113.

[31] T. Sakamoto, A. Kobori, and A. Murakami, "Microarray-based label-free detection of RNA using bispyrene-modified 2'-O-methyl oligoribonucleotide as capture and detection probe.," *Bioorganic & medicinal chemistry letters*, vol. 18, Apr. 2008, pp. 2590-3.

[32] K.H. Park, H.G. Park, J.-H. Kim, and K.H. Seong, "Poly(dimethyl siloxane)-based protein chip for simultaneous detection of multiple samples: use of glycidyl methacrylate photopolymer for site-specific protein immobilization.," *Biosensors & bioelectronics*, vol. 22, Dec. 2006, pp. 613-20.

[33] Y. Liu, "DNA probe attachment on plastic surfaces and microfluidic hybridization array channel devices with sample oscillation," *Analytical Biochemistry*, vol. 317, Jun. 2003, pp. 76-84.

[34] G. Zhang, "The immobilization of DNA on microstructured patterns fabricated by maskless lithography," *Sensors and Actuators B: Chemical*, vol. 97, Feb. 2004, pp. 243-248.

[35] C.J. Myatt, M. Delaney, K. Todorof, J. Heil, M. Givens, R.T. Schooley, and M.J. Lochhead, "Low-cost, multiplexed biosensor for disease diagnosis," *Proceedings of SPIE*, 2009, pp. 716703-716703-9.

[36] ASTM, *Manual on the Use of Thermocouples in Temperature Measurements*, 1974.

[37] Microchip Technology, *PIC18FXX2 Data Sheet*, 2002.

[38] T. Hubing, T.P. Van Doren, and R. Dubroff, "Identifying and Quantifying PCB Inductance," 1994.

[39] T.H. Hubing, J.L. Drewniak, T.P. Van Doren, and R.E. DuBroff, "Mitigating power bus noise with embedded capacitance in PCB designs," *2001 IEEE EMC International Symposium. Symposium Record. International Symposium on Electromagnetic Compatibility (Cat. No.01CH37161)*, pp. 496-500.

[40] A. Ricchiuti, A. Orlandi, and G. Antonini, “Buried Capacitance Technology for Power Bus Decoupling on High Speed Digital PCB’s,” *in Proc. 14th Int. Zurich Symp. Electromag. Compat.*, Zurich, Switzerland: 2001.

[41] J. Sisler, “Eliminating Capacitors from Multi-Layer PCB’s,” *Printer Circuit Design*, vol. 8, 2002, pp. 14-23.

[42] J.R. Howard, “Buried Capacitance Technology,” *in the Proceedings of the Technical Program, Surface Mount International*, Edina, MN: 1992, pp. 547-555.

[43] T.H. Hubing, “Estimating the power bus impedance of printed circuit boards with embedded capacitance,” *IEEE Transactions on Advanced Packaging*, vol. 25, Aug. 2002, pp. 424-432.

[44] T.H. Hubing, T.P. Van Doren, J.L. Drewniak, and R.E. DuBroff, “Power-bus decoupling with embedded capacitance in printed circuit board design,” *IEEE Transactions on Electromagnetic Compatibility*, vol. 45, Feb. 2003, pp. 22-30.

[45] T. Hubing, “Effective strategies for choosing and locating printed circuit board decoupling capacitors,” *2005 International Symposium on Electromagnetic Compatibility, 2005. EMC 2005.*, vol. 00, 2005, pp. 632-637.

[46] T. Hubing, “Effective strategies for choosing and locating printed circuit board decoupling capacitors,” *2005 International Symposium on Electromagnetic Compatibility, 2005. EMC 2005.*, vol. 00, 2005, pp. 632-637.

[47] T.H. Hubing, “Estimating the power bus impedance of printed circuit boards with embedded capacitance,” *IEEE Transactions on Advanced Packaging*, vol. 25, Aug. 2002, pp. 424-432.

[48] T. Hubing, J. Chen, J.L. Drewniak, Y. Ren, J. Fan, and R. Dubroff, “Power Bus Noise Reducution using Power Islands in PCBs.pdf.”

[49] “E2V - Design Considerations for a Mixed Signal PCB,” 2010.

[50] D. Mitrani, J.A. Tomé, J. Salazar, A. Turó, M.J. García, J.A. Chávez, and A. The, “Methodology for Extracting Thermoelectric Module Parameters,” *Instrumentation*, vol. 54, 2005, pp. 1548-1552.

[51] L. Chen, J. West, P.-A. Auroux, A. Manz, and P.J.R. Day, “Ultrasensitive PCR and real-time detection from human genomic samples using a bidirectional flow microreactor.,” *Analytical chemistry*, vol. 79, Dec. 2007, pp. 9185-90.

[52] J.-H. Han and J.-Y. Yoon, “Reusable, polyethylene glycol-structured microfluidic channel for particle immunoassays.,” *Journal of biological engineering*, vol. 3, Jan. 2009, p. 6.

[53] Y. Lin, S. Kang, and T. Wu, “Fabrication of polydimethylsiloxane (PDMS) pulsating heat pipe,” *Applied Thermal Engineering*, vol. 29, Feb. 2009, pp. 573-580.

[54] Y.S. Shin, K. Cho, S.H. Lim, S. Chung, S.-J. Park, C. Chung, D.-C. Han, and J.K. Chang, "PDMS-based micro PCR chip with Parylene coating," *Journal of Micromechanics and Microengineering*, vol. 13, Sep. 2003, pp. 768-774.

[55] S.C.J. J. Khandurina, T.E. McKnight, "Integrated System for Rapid PCR Based DNA Analysis in Microfluidic Devices," *Analytical Chemistry*, 2000, pp. 2995-3000.

[56] D. Pitts and L. Sissom, *Schaum's Outlines - Heat Transfer*, McGraw-Hill, 1997.

[57] N. Mohan, T. Undeland, and W. Robbins, *Power Electronics – Converters, Designs and Applications*, Wiley and Sons, 2003.

[58] S. Kutateladze and V. Borishankii, *A concise Encyclopedia of Heat Transfer*, Pergamon Press, 1966.

[59] T. Russel, A. Robinson, and N. Wagner, *Mass and Heat Transfer - Analysis of Mass Contractors and Heat Exchangers*, Cambridge University Press, 2008.

[60] D. Pitts and L. Sissom, *Schaum's Outlines - Heat Transfer*, McGraw-Hill, 1997.

[61] H.-S. Chuang and S. Wereley, "Design, fabrication and characterization of a conducting PDMS for microheaters and temperature sensors," *Journal of Micromechanics and Microengineering*, vol. 19, Apr. 2009, p. 045010.

[62] T. Zwinger, T. Sikanen, S. Tuomikoski, R.A. Ketola, R. Kostiainen, S. Franssila, T. Kotiaho, and A. Pursula, "Electrokinetically driven flows in Electrokinetically driven flows in," *Sensors And Actuators*, vol. 120, 2005, pp. 408-415.

[63] Y. Lin, S. Kang, and T. Wu, "Fabrication of polydimethylsiloxane (PDMS) pulsating heat pipe," *Applied Thermal Engineering*, vol. 29, Feb. 2009, pp. 573-580.

[64] M. Sen, "Principles of Thermal Control," 2004.

[65] M. Silberberg, *Chemistry*, New York: McGraw-Hill, 2006.

[66] L. Haff and J. Atwood, "No Title," *Amplifications*, 1989, pp. 15-16.

[67] S. Hirotaka, H. Onoeb, T. Osakia, R. Kawanoa, and S. Takeuch, "Parylene-coating in PDMS microfluidic channels prevents the absorption of fluorescent dyes," *Sensors and Actuators B: Chemical*, vol. 150, 2010, pp. 478-482.

[68] N.V. Zaytseva, V.N. Goral, A. Montagna, and A.J. Baeumner, "Development of a microfluidic biosensor module for pathogen detection," *Lab on a Chip*, 2005, pp. 805-811.

[69] National Health Laboratory Service (NHLS), "*NHLS SOP HAEM 1434*", 2011.

i. Bode Plot of Implemented RC Filter

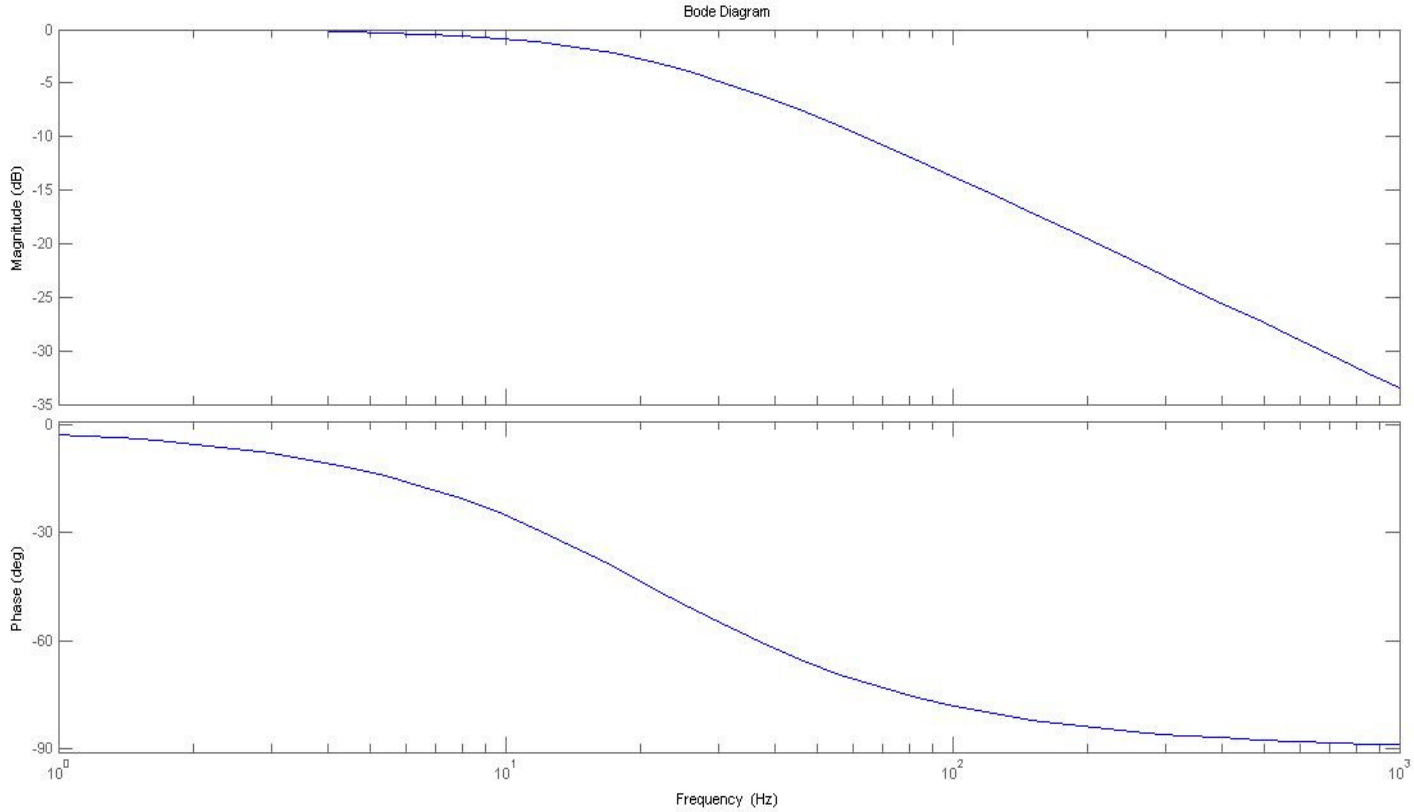

ii. Custom Developed PCB Circuit Diagram

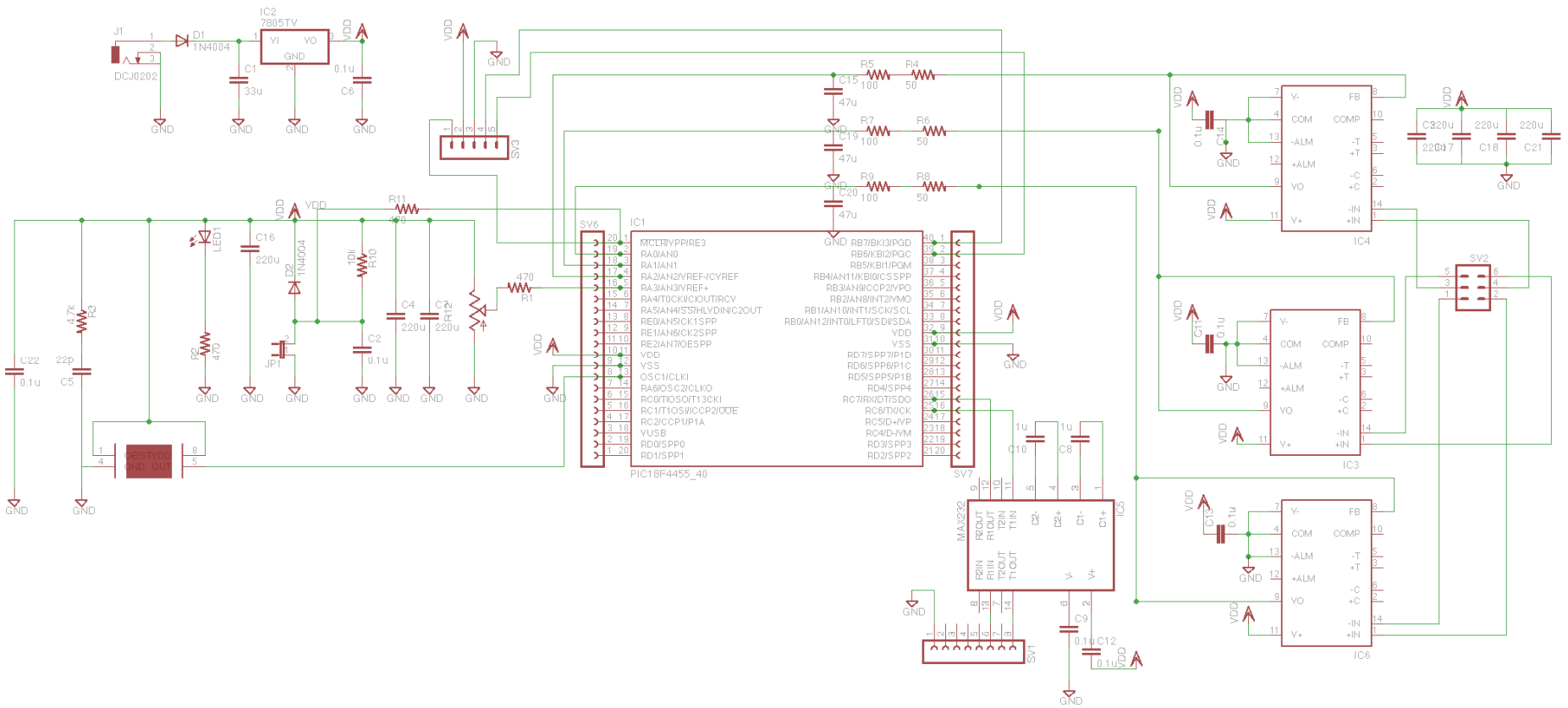

```
#include <spi.h>
#include <p18cxxx.h>
#include <timers.h>
#include <delays.h>
#include <stdlib.h>
#include <stdio.h>
/*****/
#include <usart.h>
#include <adc.h>
#include <pwm.h>
#include <timers.h>
#include <portb.h>
/*****/
#pragma config OSC  = HS
#pragma config PWRT = ON
#pragma config WDT  = OFF, WDTPS = 1
#pragma config LVP  = OFF
#pragma config DEBUG = OFF
#pragma config CP0  = OFF,CP1 = OFF,CP2 = OFF,CP3 = OFF,CPB = OFF,CPD =
OFF
#pragma config WRT0 = OFF,WRT1 = OFF,WRT2 = OFF,WRT3 = OFF,WRTB =
OFF,WRTC = OFF,WRTD = OFF
#pragma config EBTR0 = OFF,EBTR1 = OFF,EBTR2 = OFF,EBTR3 = OFF,EBTRB =
OFF
/*****/
#define TRUE 1
#define FALSE 0
/*****/
#define ModePressed !PORTBbits.RB0;
#define Laser_ON PORTBbits.RB1 = 1;
#define Laser_OFF PORTBbits.RB1 = 0
#define MOS_ON PORTBbits.RB2 = 1;
#define MOS_OFF PORTBbits.RB2 = 0;
#define MOS_TEST = PORTBbits.RB2;
#define Select !PORTAbits.RA4*/

#define HB1_OFF PORTBbits.RB0 = 0;
#define HB1_CHECK PORTBbits.RB0;

#define HB2_ON PORTBbits.RB1 = 1;
#define HB2_OFF PORTBbits.RB1 = 0;
#define HB2_CHECK PORTBbits.RB1;

#define HB3_ON PORTBbits.RB2 = 1;
#define HB3_OFF PORTBbits.RB2 = 0;
#define HB3_CHECK !PORTBbits.RB2;

#define HB4_ON PORTBbits.RB3 = 1;
#define HB4_OFF PORTBbits.RB3 = 0;
#define HB4_CHECK = PORTBbits.RB3;*/

//++++++++++++++++++++++++++++++++++++++++++++++++
// LED's
//++++++++++++++++++++++++++++++++++++++++++++++++
/*#define LED_ALARM_ON PORTBbits.RB4 = 1;
#define LED_ALARM_OFF PORTBbits.RB4 = 0;

#define LED_HEATING_ON PORTBbits.RB5 = 1;
```

```
#define LED_HEATING_OFF PORTBbits.RB5 = 0;

#define LED_CORRECT_TEMP_ON PORTBbits.RB6 = 1;
#define LED_CORRECT_TEMP_OFF PORTBbits.RB6 = 0;

#define LED_COOLING_ON PORTBbits.RB7 = 1;
#define LED_COOLING_OFF PORTBbits.RB7 = 0;*/
//++++++++++++++++++++++++++++++++++++++++++++++
#define CORRECT_TEMP 500
#define PWM_FREQ 128
#define PWM_DUTY 256
#define V_REF     0.6
#define POT_REF ADC_CH3
#define THERMO1 ADC_CH0
#define THERMO3 ADC_CH1
#define THERMO2 ADC_CH2
/*
#define GRAD1 10
#define C1 0
#define GRAD2 10
#define C2 0
#define GRAD3 10
#define C3 0 */
//#####################################################################

int SystemMode = -1;
static int STANDBY = 0;
static int GUIDED = 1;
static int FREE = 2;
static int REVIEW = 3;
int PWM_duty;
int totalPoints = 0;
int bias = 0;
int e_results[15];
int results_count = 0;
float shift = 0.00;

int flag = 0;
int hitCount = 0;
/*************************************************************/
// THERMAL CONTROL VARIABLES
//___________________________________________________________________
float ave;
int county = 0;
char global[5];
//float now = 0;
int last = 0;
float temp = 0;
/*********************************************************************/
//___________________________________________________________________
/*void ShortCircuitCheck()
{

      while(((PORTBbits.RB0 ==
1)&&(PORTBbits.RB1==1))||((PORTBbits.RB2==1)&&(PORTBbits.RB3==1)))
      {     //check for short
            LED_ALARM_ON;
            HB1_OFF;
```

```
            HB2_OFF;
            HB3_OFF;
            HB4_OFF;
      }
}

void CorrectTempLEDs()
{
      LED_CORRECT_TEMP_ON;
      LED_HEATING_OFF;
      LED_COOLING_OFF;
}

void UnderTempLEDs()
{
      LED_HEATING_ON;
      LED_COOLING_OFF;
      LED_CORRECT_TEMP_OFF;
}

void OverTempLEDs()
{
      LED_HEATING_ON;
      LED_COOLING_OFF;
      LED_CORRECT_TEMP_OFF;
}

void TurnOnHeating()
{
      HB2_OFF;
      HB3_OFF;
      ShortCircuitCheck();
      HB1_ON;
      HB4_ON;
      ShortCircuitCheck();
}

void TurnOnCooling()
{
      HB1_OFF;
      HB4_OFF;
      ShortCircuitCheck();
      HB2_ON;
      HB3_ON;
      ShortCircuitCheck();
}


void TempControlPWM(int temp)
//need to change which pwm is getting set for heating and cooling
//check the maximum duty cycle for the frequency being set
{
      int i = 0;
      int freq_count = 0;
      int updated_temp = temp;
      int new_freq = 0;

      if (temp > CORRECT_TEMP)
```

```
	{
		OverTempLEDs();
		TurnOnCooling();
		while (updated_temp != CORRECT_TEMP)
		{
			updated_temp = (int)ReadADPort(20,THERMO1);
			if (freq_count == PWM_FREQ)
			{
				if (PWM_duty > 1)
				{
					PWM_duty = PWM_duty-1;
				}
				else
				{
					PWM_duty = 1;
				}
				PWMDuty(PWM_duty,1);
			}
			freq_count++;
		}
	}

	if (temp == CORRECT_TEMP)
	{
		CorrectTempLEDs();
	}

	if (temp < CORRECT_TEMP)
	{
		UnderTempLEDs();
		TurnOnHeating();
		while (updated_temp != CORRECT_TEMP)
		{
			updated_temp = (int)ReadADPort(20,THERMO1);
			if (freq_count == PWM_FREQ)
			{
				if (PWM_duty < PWM_FREQ)
				{
					PWM_duty = PWM_duty+1;
				}
				else
				{
					PWM_duty = PWM_FREQ;
				}
				PWMDuty(PWM_duty,1);
			}
			freq_count++;
		}
	}
}

void TempControlIO(int temp)
{
	LED_ALARM_OFF;

	if (temp = CORRECT_TEMP)
	{
		CorrectTempLEDs();
```

```
	}
	if (temp < CORRECT_TEMP)
	{
		UnderTempLEDs();
		TurnOnHeating();
	}
	if (temp > CORRECT_TEMP)
	{
		OverTempLEDs();
		TurnOnCooling();
	}
}*/

void PWMDuty(int duty, int channel)
{
	if (channel == 1)
		SetDCPWM1(duty); //SET DUTY CYCLE
	else
		SetDCPWM2(duty);
}


void PWMFreq(int freq,int channel)
{
	if (freq < 0)
	{}
	else
	{
		if (channel == 1)
			OpenPWM1(freq); //SET FREQUENCY
		else
			OpenPWM2(freq);
	}
}

void SetPWM(int freq, int duty, int channel)
{
	PWMFreq(freq,channel); //SET FREQUENCY
	PWMDuty(duty,channel);// DT = 2F GIVES Approx. 50% DUTY CYCLE
}

int ConvertToVoltage(int ave, float vref)
/*-------------------------------------------------------------------
  - Converts a sample from the A/D port (18F4xx2: 10bit = 1024) to an
    actual voltage based on the reference voltage.
  - Reference voltage V_REF can be another A/D port or set in "V_REF"
    **** Add code to check whether using A/D port or hard-coded value
-------------------------------------------------------------------*/
{
	int max = 1023;
	float voltage = 0;
	voltage = ((float)ave/(float)max)*(float)vref*1000.00;
	return(voltage*10);
}


int ReadADPort(int readings, char port[])
/*-------------------------------------------------------------------
```

```
  - Readings: The number of samples on the given A/D port ("port")
      to convert and average.
  - Takes the samples, averages them and coverts them to a voltage
      based on the reference voltage "V_REF"
  - Returns an integer VOLTAGE which would represent the averaged,
      actual voltage measured on the port.
----------------------------------------------------------------------*/
{
      int i                  = 0;
      float result1    = 0.00;
      float average    = 0;
      //char port1 = ADC_CH5;

      SetChanADC(port); //set the a/d channel
      ConvertADC(); // Start conversion

      for (i = 0; i < readings; i++)
      {
            while( BusyADC() ); // Wait for completion
            result1 = result1 + ReadADC(); // Read result
      }
      average = result1/readings;
      return(ConvertToVoltage(average,(float)V_REF));
}

void WriteTo232(int val, char ref[])
/*----------------------------------------------------------------------
  - Takes a value (voltage averaged from A/D port and writes it to the
      serial port with a head "ref" indicating which port/device the
      value belongs to.
  - Use the Java App with the relevant header to separate all the
      measurements into separate files.
----------------------------------------------------------------------*/
{
      int i = 0;
      char string[5]="---";
      char spaces[2]=" ";

      //itoa(x1, string);
      sprintf(string, "%d", (int)val);

      while (BusyUSART()) //wait
      {}
      putrsUSART(ref);

      while (BusyUSART()) //wait
      {}
      putsUSART(string);


      while (BusyUSART()) //wait
      {}
      putsUSART(spaces);

}
//======================================================================
//                                PI CONTROL SECTION
//======================================================================
```

```
int I_Control(int setpoint, int current_val, int scaling)
/* USES
[global] int e_results[10]; * initialize to 0 in Init()
[global] results_count = 0; * initialize to 0 in Init()
                                        * Check range and reset in Main()
*/
{
      int i = 0;
      float e_ave = 0.00;
      int I_factor = 0;
      int aggregate = 0;

      if (results_count >= 10)
            results_count = 0;

      e_results[results_count] = setpoint - current_val;

      for (i = 0; i < 15; i++)
      {
            aggregate = aggregate + e_results[i];
      }
      e_ave = ((float)aggregate)/15;
      I_factor = e_ave*5*(float)scaling;

      results_count++;
      return(I_factor);
}

void P_Control(int current, int sp)
{
      int duty_k = 0;
      int initial = 200;
      //int setpoint = 480;
      int setpoint = sp;
      int cooling_threshold = 430;
      int error = 0;
      float scale_factor = 0;
      float temp;
      int current_val = current/10;

      scale_factor = 500/((float)setpoint-(float)initial);
      temp = ((float)setpoint/500)*112;
      bias = (int)temp;


      if (current_val > setpoint)
      {
            error = current_val-setpoint;
            // turn off heating - turn ON cooling;

            if (current_val >= cooling_threshold)
            {
                  error = current_val - setpoint;
                  duty_k = (int)((float)error*2*(float)scale_factor);
                  if (duty_k > 512)
                        duty_k = 512;
                  SetPWM(PWM_FREQ,0,2);
                  SetPWM(PWM_FREQ,duty_k,1);
```

```
            }
            else
            {
                  duty_k = bias -
2*(int)((float)error*(float)scale_factor);
                  SetPWM(PWM_FREQ,0,1);
                  SetPWM(PWM_FREQ,duty_k ,2);
            }
      }
      else
      {
            error = setpoint - current_val;
            // turn off cooling - turn ON heating
            //duty_k = (int)(error*scale_factor + bias);
            duty_k = (int)((float)error*5*(float)scale_factor +
0*(float)I_Control(setpoint, current_val,scale_factor))+bias;
            if (duty_k > 512)
                  duty_k = 512;
            SetPWM(PWM_FREQ,0,1);
            SetPWM(PWM_FREQ,duty_k,2);
      }

}
//=====================================================================
//                           PI CONTROL END
//=====================================================================
void CheckInternalTemp(char channel[])
{
      int  setpoint = 250;
      int ADVal = ((int)ReadADPort(20,THERMO1))/10;

      shift = (float)ADVal - setpoint;
}
void Checktemp(int current_val)
{
      int setpoint = 415;
      current_val = current_val/10;
      if ((current_val > (setpoint-5))&&(current_val < (setpoint + 5)))
      {
            PORTDbits.RD2 = 1;
      }
      else
      {
            PORTDbits.RD2 = 0;
      }
}
//=====================================================================

/*void SetupADC_NO_REF()
{
      OpenADC(ADC_FOSC_32 &
                        ADC_RIGHT_JUST &
                        ADC_8ANA_0REF ,
                        ADC_CH5 &
                        ADC_INT_OFF );

}*/
```

```
void SetupADC_1_REF()
{
	OpenADC(ADC_FOSC_32 &
			ADC_RIGHT_JUST &
			ADC_7ANA_1REF ,
			ADC_CH0 &
			ADC_INT_OFF );

	/*OpenADC(ADC_FOSC_32 &
			ADC_RIGHT_JUST &
			ADC_12_TAD,
			ADC_CH0 &
			ADC_INT_OFF &
			ADC_VREFPLUS_EXT, 15);*/

}
//=====================================================================

void Init()
{

	TRISC = 0b00000011; // SET RC2+1 as OUTPUT (PWM PIN)
	TRISD = 0b00110000;

	OpenUSART(USART_TX_INT_OFF &
				USART_RX_INT_OFF &
				USART_ASYNCH_MODE &
				USART_EIGHT_BIT &
				USART_CONT_RX &
				USART_BRGH_HIGH,
				25 );

	OpenTimer2( TIMER_INT_OFF &		// NEEDED FOR PWM - CCP1 (RC2)
			T2_PS_1_1 &
			T2_POST_1_1 );

	SetupADC_1_REF();

	results_count = 0;

	for (results_count = 0; results_count < 15; results_count++)
	{
		e_results[results_count] = 0;
	}

	results_count = 0;
}
//=====================================================================
void main (void)
{
	int ADVal = 0;
	int T1,T2,T3 = 0;
	float T1Scale, T2Scale, T3Scale = 0.0;
	int loopCount = 0;
	Init();


	while (1)
```

```
	{

		ADVal = (int)ReadADPort(20,THERMO1);
		T1 = ADVal +shift;
		//T1 = (int)((float)T1/(float)T1Scale);
		//WriteTo232(T1,"T1 ");
		//P_Control(ADVal);

		ADVal = (int)ReadADPort(20,THERMO2);
		T2 = ADVal +shift;
		//T2 = (int)((float)T2/(float)T2Scale);
		//WriteTo232(T2,"T2 ");

		ADVal = (int)ReadADPort(20,THERMO3);
		T3 = (float)(ADVal +shift)*(float)0.966981;
		//T3 = (int)((float)T3/(float)T3Scale);
		WriteTo232(T3,"T3 ");

		//Checktemp(T3);
		//CheckInternalTemp(CHANNEL);

			P_Control(T3, 415);

	}
		CloseADC();
		CloseUSART();
		ClosePWM1();
		ClosePWM2();
		CloseTimer2();
}
```